MICROCOPY RESOLUTION TEST CHART

NATIONAL BUREAU OF STANDARDS-1963-A

AD

BORONNITRIDE and SILICONNITRIDE SYSTEMS

First Annual Report

by

Peter Rogl
Julius C. Schuster

September 1985

United States Army

EUROPEAN RESEARCH OFFICE OF THE US ARMY
London England

CONTRACT NUMBER DAJA45-84-C-0038

Institut für Physikalische Chemie
der Universität Wien
Währingerstrasse 42, A-1090 Wien, Austria

Approved for Public Release; distribution unlimited

AD-A161 563

DTIC
ELECTE
NOV 25 1985
S   D
A

11 20-85 011

REPORT DOCUMENTATION PAGE	READ INSTRUCTIONS BEFORE COMPLETING FORM

1. REPORT NUMBER	2. GOVT ACCESSION NO. AD-A161 563	3. RECIPIENT'S CATALOG NUMBER

4. TITLE (and Subtitle) BORONNITRIDE AND SILICONNITRIDE SYSTEMS	5. TYPE OF REPORT & PERIOD COVERED First Annual Report Sept. 1984 to Sept. 1985
	6. PERFORMING ORG. REPORT NUMBER

7. AUTHOR(s) Peter Rogl Julius Schuster	8. CONTRACT OR GRANT NUMBER(s) DAJA45-84-C-0038

9. PERFORMING ORGANIZATION NAME AND ADDRESS Inst. f. Physikalische Chemie A-1090 Wien, Währingerstr. 42	10. PROGRAM ELEMENT, PROJECT, TASK AREA & WORK UNIT NUMBERS

11. CONTROLLING OFFICE NAME AND ADDRESS HQ. 47TH AREA SUPPORT GROUP, P.O. BOX 160, WARRINGTON, CHESHIRE, GB	12. REPORT DATE Sept. 1985
	13. NUMBER OF PAGES

14. MONITORING AGENCY NAME & ADDRESS(If different from Controlling Office)	15. SECURITY CLASS. (of this report)
	15a. DECLASSIFICATION/DOWNGRADING SCHEDULE

16. DISTRIBUTION STATEMENT (of this Report)

17. DISTRIBUTION STATEMENT (of the abstract entered in Block 20, if different from Report)

18. SUPPLEMENTARY NOTES

Differential Thermal Analysis

19. KEY WORDS (Continue on reverse side if necessary and identify by block number)

Ternary Systems
Phase Equilibria
Structural Chemistry
Thermodynamics
Nitriding Binary Borides

Iron-Boron-Nitrogen
Cobalt-Boron-Nitrogen
Nickel-Boron-Nitrogen

Literature Review

Titanium-Silicon-Nitrogen
Zirconium-Silicon-Nitrogen
Vanadium-Silicon-Nitrogen
Niobium-Silicon-Nitrogen
Tantalum-Silicon-Nitrogen

20. ABSTRACT (Continue on reverse side if necessary and identify by block number)

I. Transition Metal-Boron-Nitrogen Systems: The existing literature data regarding the systems Fe-B-N, Co-B-N and Ni-B-N were critically assessed including the binary boundary systems. The thermodynamic phase equilibria at 900°C were reinvestigated for the binary systems Fe-B, Co-B and Ni-B using different methods of preparation and analysis. A complete constitutional diagram Fe-B was established in the temperature range 600° < T < 1700°C using X-ray phase analysis, metallography, (DTA) and melting point analysis. Differential thermal analysis and melting point analysis revealed an eutectic

DD FORM 1473 EDITION OF 1 NOV 65 IS OBSOLETE
1 JAN 73

reaction $L \rightleftharpoons FeB + ss-\beta-rh(B,Fe)$ at $1450 \pm 3°C$. The congruent melting point of the compound FeB was measured to be $1588 \pm 8°C$. The phase diagram Fe-B was calculated thermodynamically with respect to the new experimental data established, and a complete set of parameters were obtained for the liquid phase. The phase equilibria in the ternary systems Fe-B-N, Co-B-N and Ni-B-N were established mainly from X-ray powder diffraction data, and isothermal sections at 900°C and 1 bar Ar have been constructed. In all three systems the binary transition metal borides form two-phase equilibria with hexagonal boronnitride with practically no mutual solubility. Melting in the concentrational sections M-BN, M= Fe,Co, occurs at ca. 1350°C. Up to these temperatures there is complete compatibility between metal, metal borides and BN; alloys M-BN, melted and quenched reveal the formation of metastable compounds $(Fe,Co,Ni)_{23}(B,N)_6$ with the $\tau-Cr_{23}C_6$-type of structure. Phase relations in the Fe-B-N system were also studied under technical conditions (900°C, technical argon, samples in a Mo-container within a graphite susceptor). Oxygen impurities via a gas phase transport reaction (carbonoxide) led to the formation of a ternary phase $Fe_3(B,N,C)$ with cementite-structure. The kinetic of nitriding was studied in all three systems from binary transition metal boride samples annealed at 900°C and 1200°C under 1 bar of high purity nitrogen.

II. Transition Metal-Silicon-Nitrogen Systems: The compilation and critical assessment of existing literature data as well as the experimental investigation in the ternary systems Ti-Si-N, Zr-Si-N, V-Si-N, Nb-Si-N and Ta-Si-N and the respective TM-N as well as TM-Si binary systems were completed. Silicon nitride reacts with each of these transition metals to form either binary silicides and nitrides or ternary phases of $D8_8$-type structure with the general formula $TM_5Si_3N_{1-x}$. These phases are commonly known as Nowotny phases and were described in the literature. No new ternary phase was observed.

Accesion For

NTIS CRA&I

A-1

QUALITY
INSPECTED
3

Part I   TRANSITION METAL-BORON-NITROGEN SYSTEMS

Part II   TRANSITION METAL-SILICON-NITROGEN SYSTEMS

SUMMARY

The existing literature data regarding the systems Fe-B-N, Co-B-N
and Ni-B-N were critically assessed including the binary boundary systems.
The thermodynamic phase equilibria at 900°C were reinvestigated for the
binary systems Fe-B, Co-B and Ni-B using different methods of preparation
and analysis. There were no indications for the existence of binary metal
diborides "MB_2"; compounds "$MB_{\sim 20}$", as earlier reported in literature
were successfully characterized with a rhombohedral unit cell and the
crystal structure of β-rhombohedral boron with the transition metal atoms
in the voids of the covalently bonded boron framework, i.e. ss-β-rh (B,M).
A complete constitutional diagram Fe-B was established in the temperature
range 600° < T < 1700°C using X-ray phase analysis, metallography, DTA and
melting point analysis (automatic computer controlled three-colour
pyrometry). Compounds "Fe_3B" with either the Ti_3P- or the Fe_3P-type as
recently postulated, were not confirmed as thermodynamic stable equilibrium
phases. Differential thermal analysis and melting point analysis revealed an
eutectic reaction L $\rightleftharpoons$ FeB + ss-β-rh(B,Fe) at 1450 ± 3°C. The congruent
melting point of the compound FeB was measured to be 1588 ± 8°C.

The phase diagram Fe-B was calculated thermodynamically with respect
to the new experimental data established, and a complete set of parameters
were obtained for the liquid phase.

The phase equilibria in the ternary systems Fe-B-N, Co-B-N and Ni-B-N
were established mainly from X-ray powder diffraction data, and isothermal
sections at 900°C and 1 bar Ar have been constructed. In all three systems
the binary transition metal borides form two-phase equilibria with
hexagonal boronnitride. There is practically no solubility of BN in the
binary metal borides and no ternary equilibrium phases were observed.
Melting in the concentrational sections M-BN, M= Fe,Co,occurs at ca. 1350°C;
for the corresponding nickel-alloys the temperatures are somewhat lower.
Up to these temperatures there is complete compatibility between metal,
metal borides and BN; Alloys M-BN, melted and quenched reveal the formation
of metastable compounds $(Fe,Co,Ni)_{23}(B,N)_6$ with the τ-$Cr_{23}C_6$-type of
structure. Phase relations in the Fe-B-N system were also studied under
technical conditions (900°C, technical argon, samples in a Mo-container
within a graphite susceptor). Oxygen impurities via a gas phase transport
reaction (carbonoxide) led to the formation of a ternary phase $Fe_3(B,N,C)$
with cementite-structure.
The kinetic of nitriding was studied in all three systems from binary
transition metal boride samples annealed at 900°C and 1200°C under
1 bar of high purity nitrogen.

II. Transition Metal-Silicon-Nitrogen Systems

The compilation and critical assessment of existing literature data
as well as the experimental investigation in the ternary systems Ti-Si-N,
Zr-Si-N, V-Si-N, Nb-Si-N and Ta-Si-N and the respective TM-N as well as TM-Si
binary systems were completed and are presented in part II of this report.
Silicon nitride reacts with each of these transition metals to form either
binary silicides and nitrides or ternary phases of $D8_8$-type structure with the
general formula $TM_5Si_3N_{1-x}$. These phases are commonly known as Nowotny phases
and were described in the literature (see part II for details). No new
ternary phase was observed.

The compilation of literature data for the binary systems (Cr,Mo,W,Mn,Re,
Fe,Co,Ni)-Si and (Cr,Mo,W,Mn,Re)-N as well as the ternary systems (Cr,Mo,W,Mn,
Re,Fe,Co,Ni)-Si-N are almost complete. Experimental investigations of these
systems are in progress. So far no unusual difficulties have been encountered.
The assessment of thermodynamic data for these systems has been started.

EXPERIMENTAL PROCEDURES

All samples each of a total amount of several grams were prepared using the starting materials listed below. Binary samples were mainly prepared by arc melting the elements together on a water cooled copper hearth using a nonconsumable 2%-thoriated tungsten electrode in a Zr-gettered high-purity argon atmosphere. To ensure homogeneity the alloy buttons were turned over and remelted several times; weight losses were checked to be within 2%.

Some of the binary alloys were also prepared by direct sintering techniques using a tungsten sheet-metal high vacuum furnace or a 500 kHz-HF furnace (high vacuum). In these cases the samples were placed on a molybdenum substrate (binary borides) or in a boronnitride crucible (ternary boron-nitrides) contained in a tungsten crucible (which acted as susceptor material in case of the HF-assembly). Temperatures were monitored by calibrated microoptical pyrometry. After heat treatment the samples were radiation cooled.

Various methods were employed for annealing the samples:

a) a part of each alloy button was wrapped in molybdenum foil, sealed in evacuated silica tubes and annealed at various temperatures $<$ 1200°C in a wire wound Al_2O_3-tube furnace for various annealing times Temperatures were monitored by Pt-(Pt,Rh) or Ni-NiCr thermocouples. After heat treatment the samples were finally quenched in water.

b) annealing treatment in a directly heated tungsten sheet-metal furnace or in the high frequency equipment under high vacuum or high purity argon using Mo- or BN-substrates.

c) nitriding experiments were performed in the high frequency furnace under high purity argon in crucibles machined from hex-BN.

For metallography the samples were mounted in epoxy resin, ground and polished with progressively finer diamond pastes down to 1 μm and examined under reflected and polarized light, in some cases SEM photographs were taken on a JEOL-equipment.

From each sample (powdered to a grain size $<$ 20 μm in a WC-Co morlar X-ray photographs have been taken, using CrKα or CuKα-radiation in a Debye-Scherrer or in a Guinier-Huber camera. 99.9999% pure Germanium was used as an internal calibration standard (a_0= 5.657906 Å). X-ray powder intensities were recorded by means of a KD-530 microdensitometer. Precise lattice parameters have been evaluated by means of a least squares extrapolation method (2). X-ray intensity calculations have been carried out

Differential thermal analytical investigations were performed on binary iron borides and iron boronnitrides only using a Netsch-type analyser for temperatures < 1500°C (Pt-Pt,Rh-thermocouples) in BN-crucibles under a stream of high purity argon. Usual rates were 2-5 K min^{-1}.

Melting points were determined by the Pirani technique under direct heating in high vacuum or high purity argon. Temperature measurements were carried out with the an automatic computer controlled three colour pyrometer; For those alloys unsuitable for direct heating, melting was performed in Al_2O_3-crucibles using the HF-frequency furnace in combination with the automatic pyrometer.

Table: Starting Materials

Boron	: crystalline powder, -60 mesh; purity: 99.9%, from Alpha Div., Ventron Corpor., USA
Boronnitride	: hex-BN powder, -325 mesh, 99.9%, from Alpha Div., Ventron Corpor., USA
Iron	: rod, purity: 99.99%, from Alpha Div., Ventron Corpor., USA, powder, -325 mesh, purity: 99.98%, from Alpha Div., Ventron Corpor., USA
Cobalt	: rod, purity: 99.99%, from Alpha Div., Ventron Corpor., USA, powder, purity: 99.8%, Fe+Ni 0.1%, from Alpha Div., Ventron Corpor., USA
Nickel	: rod, purity: 99.99%, from Alpha Div., Ventron Corpor., USA, powder, 1 μm, purity 99.9%, Alpha Div., Ventron Corpor., USA, powder, 40 μm, purity: 99.9%, from PRC, USA
Argon	: gas, purity 99.999%, from Air liquide, Vienna, Austria
Nitrogen	: gas, purity 99.999%, from Aga, Vienna, Austria

A) <u>BINARY BOUNDARY SYSTEMS</u>

I) <u>The Binary System: Iron-Boron</u>

a) <u>CRITICAL LITERATURE REVIEW</u>

The technical importance of borided steels has stimulated the early interest in the constitution of the iron-boron binary system; a more recent interest arose from the production of iron-boron-base alloy metal-glasses. Fig.I.1 represents a likely version of the binary iron-boron system according to a recent assessment work by O.Kubaschewski-von Goldbeck (14). This version furthermore corresponds to a thermodynamic optimization by Chart (34) (see also section thermodynamic data). A compilation of all binary-iron borides reported in the literature, including also metastable phases, is presented in Table I.1.

There is no doubt about the existence of two binary iron-borides i.e. congruently melting Fe_2B with the $CuAl_2$-type and the congruently melting iron-monoboride, which was earlier described with two "polymorphic" modifications: α,β-FeB. β-FeB is orthorhombic with the FeB-type of structure and exhibits a narrow range of homogeneity.

The socalled low temperature modifcation α-FeB (in the following denoted as T-FeB, see also section: RESULTS) was obtained from compacted powder mixtures after heat treatment at temperatures below 750°C with a socalled irreversible "transition" into the β-FeB high temperature form on heating (32,58). According to Fruchart (58), a mixture of both forms was observed for temperatures between 750 and 1200°C. X-ray powder data of T-FeB were said to derive from the FeB-type structure with the observed suppression of a series of reflections. It seemed that excess boron favours the formation of T-FeB and simultaneously retards the transition to the β-FeB-type (58), whereas the magnetic ordering (Curie-)temperature at T_c= 309°C(58) or 329°C(17) appeared to be independent of composition. From this observations a structural model containing two

Table : 1 Crystallographic Data (Literature) of Iron Borides Including Metastable Phases

Phase		Preparation and Heat Treatment	Structure type	Space group	Lattice Parameters (Å)			Ref.
					a	b	c	
α-Fe		stable below 910°C	W-Type	Im3m	2.8605	-	-	(26)
					2.8664	-	-	(27)
$Fe_{23}B_6$	(metastable)	amorphous foils rapidly quenched	$Cr_{23}C_6$	Fm3m	10.67	-	-	(28)
					10.69	-	-	(29)
$Fe_{80}B_{20}$	(metastable)	amorphous wires 1 sec. -15 min., 780°C	Ti_3P	$P4_2/n$	8.623(5)	-	4.294(5)	(30)
$Fe_{\sim3,5}B$	(metastable)	eutektoidal transform. $Fe_{80}B_{20}$(amorph) $\rightarrow$ Fe + $Fe_{\sim3,5}B$	(tetrag.)	?	8.62	-	4.28	(28,37)
Fe_3B	(metastable)	decompositon of "Fe_4B" by aging	(tetrag.)	?	8.64	-	4.28	(31)
$Fe_{80}B_{20}$	(metastable)	2 h, 380°C	Fe_3P	$I\bar{4}$	8.63	-	4.29	(34)
$Fe_{85}B_{15}$	(metastable)	477°C	Fe_3P	$I\bar{4}$	8.63	-	4.37	(35)
Fe - B	hypereut.	splat cooled	tetrag.		8.62	-	4.27	(29)
h-Fe_3B	(metastable)	3300 "revolutions"/min	Fe_3P	$I\bar{4}$	8.655	-	4.297	(23)
ℓ-Fe_3B	(metastable)	1600 "revolutions"/min	Ti_3P	$P4_2/n$	8.648	-	4.314	(23)
Fe_3B	(metastable)	2000 "revolutions"/min	Fe_3C	Pbnm	4.439	5.428	6.669	(23)
Fe_3B	(metastable)	"revolutions" quenching rate too slow for glass formation	Fe_3C	Pbnm	4.45	5.43	6.66	(28)
Fe_3B	(metastable)	splat cooled	Fe_3C	Pbnm	4.454	5.433	6.656	(36)
Fe_3B	(metastable)	splat cooled	Fe_3C	Pbnm	4.3311	5.468	6.726	(29)
"Fe_3B"		extrapolated from $Fe_3C_{1-x}B_x$ at 1000°C	Fe_3C	Pbnm	4.43	5.46	6.63	(38,see also 39)
"Fe_3B"		extrapolated from $Fe_xCo_{3-x}B$ at 1000°C	Fe_3C	Pbnm	4.456	5.462	6.635	(40)
Fe_2B			$CuAl_2$	I4/mcm	5.109	-	4.249	(26,28,32, 40,42)
FeB			FeB	Pbnm	4.061	5.506	2.952	(26,33,40,42)
FeB		HF sintering at 1000°C	FeB	Pbnm	4.057	5.502	2.948	(41)
(L)-FeB		hot pressed at ~700°C	FeB(*)	(*)	4.0577	5.495	2.9467	(17)
"FeB_2"		arc-melting	AlB_2	P6/mmm	3.045	-	3.035	(19)
$FeB_{\sim49}$		solid solution of iron in β-rh. boron	β-rh Bor	$R\bar{3}m$	a_{hex}=10.9514	c_{hex}=23.861		(22)
					a_{hex}=10.9718	c_{hex}=23.8705		(35)

(*) Dimensions of the basic unit cell; Intensity Calculation for a mixed stacking variant
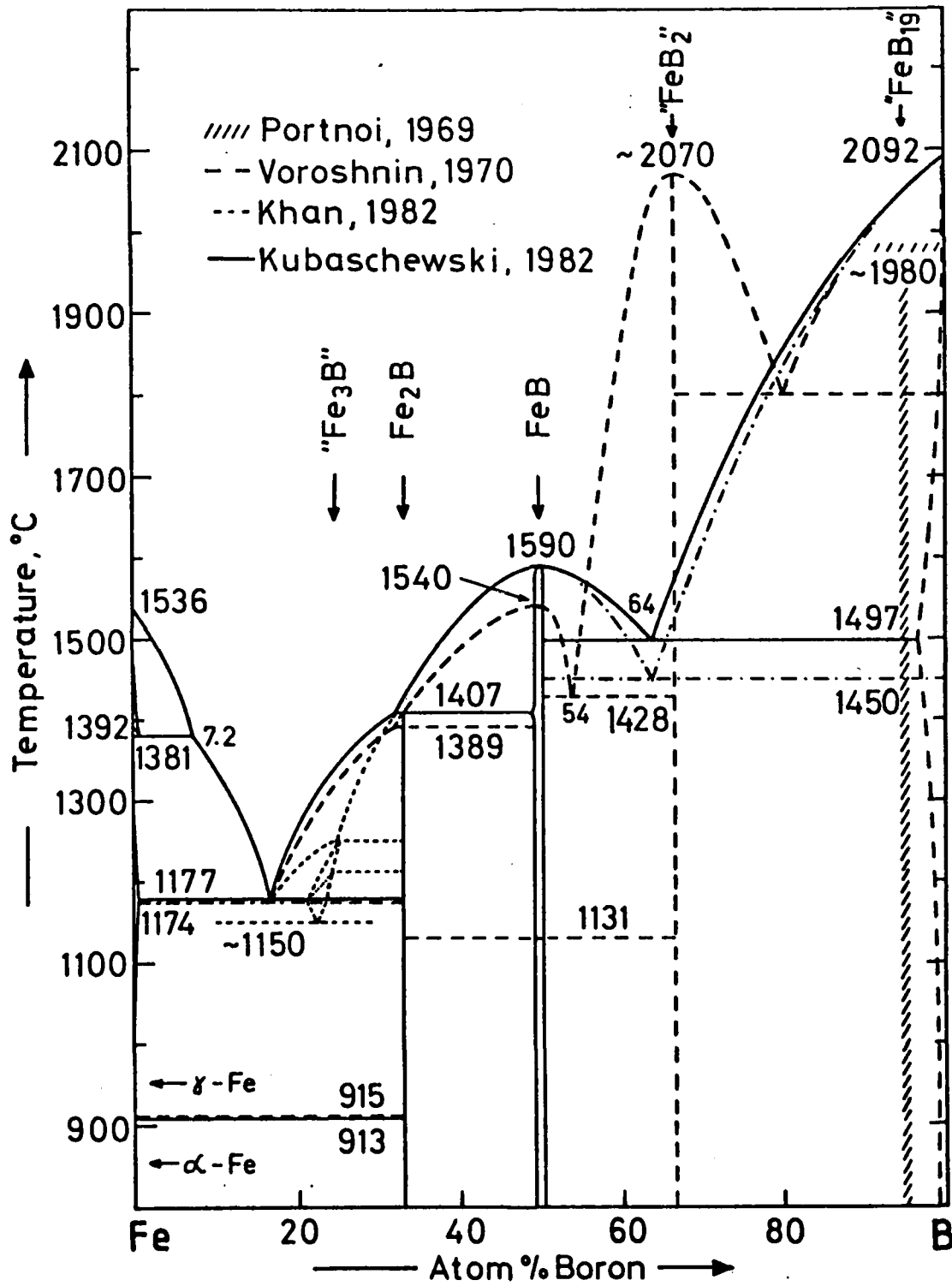
Fig.I.1 Constitutional diagram of the binary system Fe-B, comparison
of the different versions known in literature.

boron atoms per triangular metal prism was concluded with an exchange of atomic positions between an iron atom and a pair of boron atoms in adjacent triangular prisms so as not to affect the Fe-Fe distances responsible for the magnetic interactions (58). Fruchart's model however did not correspond to later experimental results on the magnetic properties of T-FeB, especially to recent Mössbauer data (17) which are quite different for both forms of FeB suggesting the existence of crystallographically inequivalent iron sites. According to Kanaizuka (17), a better crystallographic description the "low temperature modification" T-FeB in satisfactory agreement with X-ray-, phase diagram-,magnetic- and Mössbauer-data is found from a random stacking of slabs crystallizing with the FeB and the CrB-type structure respectively. Due to the slow diffusion rate below about 1000°C, the disordered intergrowth structure was said to appear as a nonequilibrium state (17).

Samples annealed by (17) below 650°C revealed an X-ray pattern of the Fe_2B-type suggesting a thermodynamic instability of FeB at T< 650°C according to an eutectoid reaction: T-FeB $\rightleftharpoons$ Fe_2B + ss-βrh Boron. These samples again converted to the normal FeB-type irreversibly above 740°C (17).

In contradiction to numerous investigations of the boron-rich region of the iron-boron system, which all seem to confirm a two phase equilibrium FeB + ss-βrh-Boron, the existence of an irondiboride "FeB_2" with AlB_2-structure and with congruent melting behavior was claimed by Russian authors (19). The dashed line in Fig.I.1 represents the liquidus and solidus lines for boron rich concentrations > 50 at%B, as proposed by the authors of (19). The observed melting point $T_M(FeB_2)$= 2070°C however is in close vicinity of the accepted melting point of pure β-rh Boron ($T_M(B)$= 2092°C, (64)). The crystallographic data as observed for "FeB_2" by (19) regarding both the d-values as well as the experimentally recorded intensities, do in no way

correspond with the AlB_2-type structure as proposed by (19) (see section RESULTS).Recent bandstructure-calculations of the isotypic transition metal diborides formed by the first row 3d-transition elements, reveal a decreasing stability with increasing atom number of the metal, and thereby suggest thermodynamic instability for the iron diboride, the corresponding "CoB_2" and "NiB_2" being unstable (20).

There are furthermore considerable doubts about the existence of a boron-rich compound $FeB_{\sim 19}$,(5 a/o Fe) as described by Portnoi (21) with a peritectic type of formation at 1980°C:

$$liquid + ss\text{-}\beta rh\text{-}Boron \rightleftharpoons FeB_{\sim 19} \; .$$

It would be more likely to assume a solid solution of 3-5 a/o iron in the voids of β-rhombohedral boron, as earlier discussed by Callmer (22) on the basis of a single crystal study of $FeB_{\sim 49}$ (see also section RESULTS).

A considerable interest in rapidly quenched iron-boron base alloys has lead to the discovery of a series of metastable binary iron-borides such as "$Fe_{23}B_6$" with the $Cr_{23}C_6$-type of structure, bct - "Fe_4B",and "Fe_3B" crystallizing with Ti_3P-, Fe_3P- or the Fe_3C-type of structure depending on duration and temperature of the annealing treatment of the quenched and recrystallizing amorphous foils (for a detailed compilation see Table I.1). While the above mentioned phases were generally considered to be metastable products, Khan et al. (23) interpreted his experimental results with the existence of two crystallographic modifications of a thermodynamically stable Fe_3B-phase (h-Fe_3B with the Fe_3P-type, and ℓ-Fe_3B with the Ti_3P-type). The dotted curves in Fig.I.1 represent the phase relations as suggested by (23). It was the sequence in which the various phases were obtained from quenching the liquid with decreasing cooling rate as well as the identical sequence in which the phases crystallize from the amorphous $Fe_{74}B_{26}$ alloy with increasing temperature, which caused the authors (23) to assume the

existence of ℓ,h-Fe$_3$B in thermodynamic equilibrium in the temperature range 1150°C<T< 1250°C. As a consequence a pertitectic formation was considered at $\sim$ 1250°C for h-Fe$_3$B according to the reaction:

$$\text{liquid} + \text{Fe}_2\text{B} \rightleftharpoons \text{h-Fe}_3\text{B} \quad (1250°C);$$
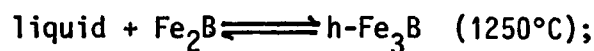
and ℓ-Fe$_3$B was said to decompose eutectoidically at $\sim$ 1150°C according to the reaction:

$$\ell\text{-Fe}_3\text{B} \rightleftharpoons \text{ss-}\gamma \text{ Fe} + \text{Fe}_2\text{B} \quad (1150°C).$$

Metastable "Fe$_3$B" with the cementite-type structure was obtained at even slower quenching rates by (28), and a metastable phase diagram (Fig.I.2) was constructued for the iron-rich region ($>$60 a/o Fe) integrating the two metastable phases "Fe$_{23}$B$_6$" and "Fe$_3$B" both with a peritectic mode of formation at $\sim$ 950°C and at $\sim$1250°C respectively.

According to the results obtained by Bashev et al. (29) on rapidly cooled alloys, orthorhombic (Fe$_3$C-type) metastable phases were observed to crystallize from hypoeutectic alloys, whereas the tetragonal metastable phases (Ti$_3$P-type and Fe$_3$P-type) crystallize from hypereutectic alloys.

The maximal solubility of boron in α-Fe is small ($<$ 0.01 a/o Boron, (62)) and detailed measurements of the electrical resistivity and the activity coefficients of boron in α,γ-Fe reveal a solubility of B in γ-Fe, which is about 2.7 times larger than that in α-Fe at the same temperature (24). While there seems to be no doubt that borons are solved interstitially in γ-Fe, a substitutional model Fe/B was discussed by Hayashi (25) for α-Fe.
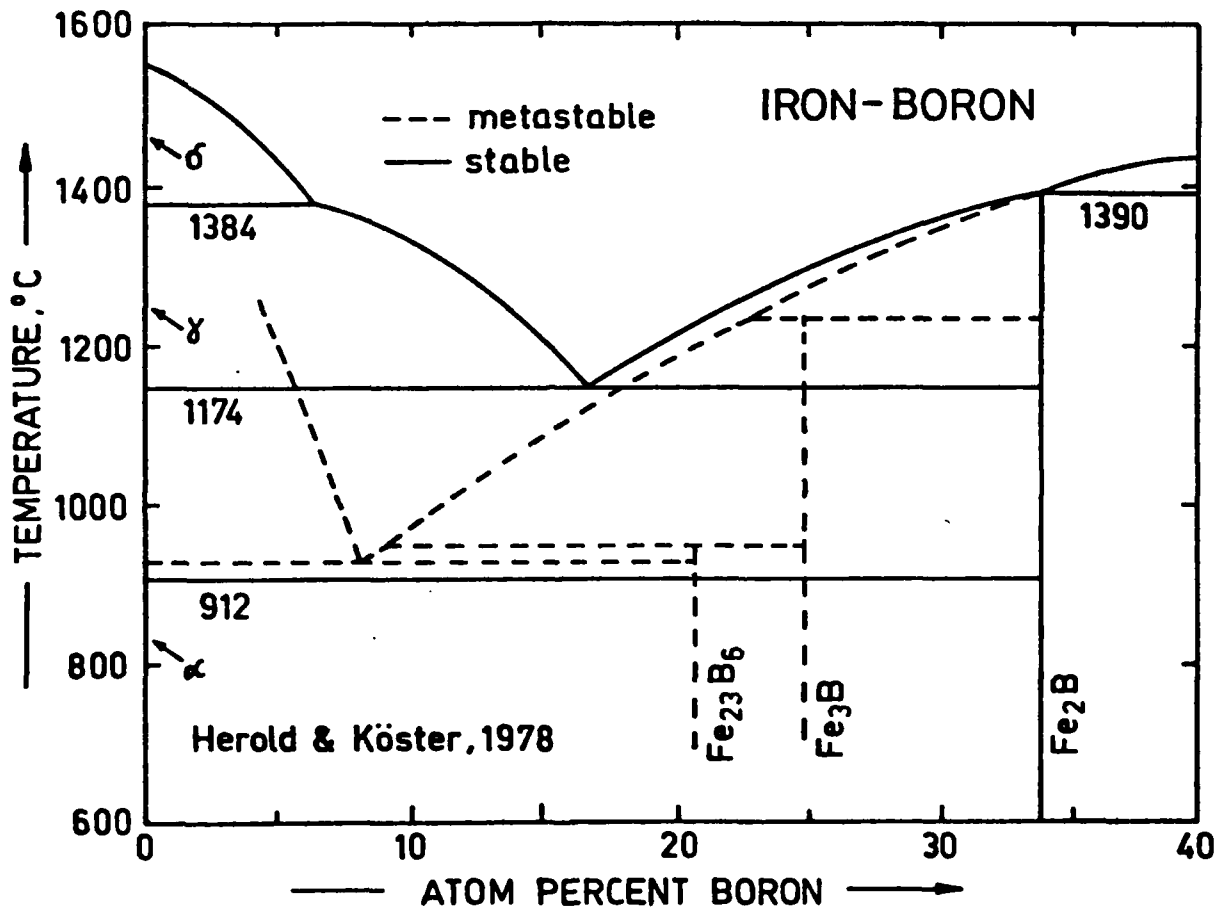
Fig.I.2 Iron-rich part of the equilibrium diagram Fe-B, showing
metastable equilibria including the metastable phases $Fe_{23}B_6$
and Fe_3B (after Herold and Köster (28)).

b) <u>RESULTS</u>

With respect to the confusing data obtained in the Fe-B binary system and described in literature, a reinvestigation of certain regions of the phase diagram seemed to be necessary with special emphasis on the following problems:

(i)   concerning the existence of "FeB_2" and "FeB_{19}"

(ii)   concerning the stability and 'polymorphism' of the compound FeB

(iii)   concerning the thermodynamic equilibrium around the composition "Fe_3B".

1. <u>Iron-Boron Constitutional Diagram</u>

A total of 20 binary alloys were prepared to investigate and check the thermodynamic phase equilibria. The analysis of the system was accomplished primarily by evaluation of X-ray powder diffraction patterns of the alloy material. Compositions and qualitative X-ray evaluation of the alloys is given in Fig.I.3 and Table I.2. A number of alloys were also arc melted and then equilibrated at 900°C for metallographic studies; in some cases SEM-analysis was employed.

X-ray data and metallography of samples annealed at 900°C confirm the extremely small solid solubility of boron in α-Fe (the unit cell dimensions remain unchanged !) and furthermore confirm the existence of three two-phase equilibria in the solid state such as: ss-αFe + Fe_2B, Fe_2B + FeB, and FeB + ss-βrh-Boron.

With only a few exceptions, the X-ray powder intensities and d-values of the "FeB_{19}"-phase earlier described by Portnoi (21) were found to correspond to the theoretical values, calculated for a solid solution of 3.5 a/o iron in β-rhombodedral boron, assuming a slightly altered atomic arrangement with respect to the crystal data as reported by Callmer (43) for a single crystal
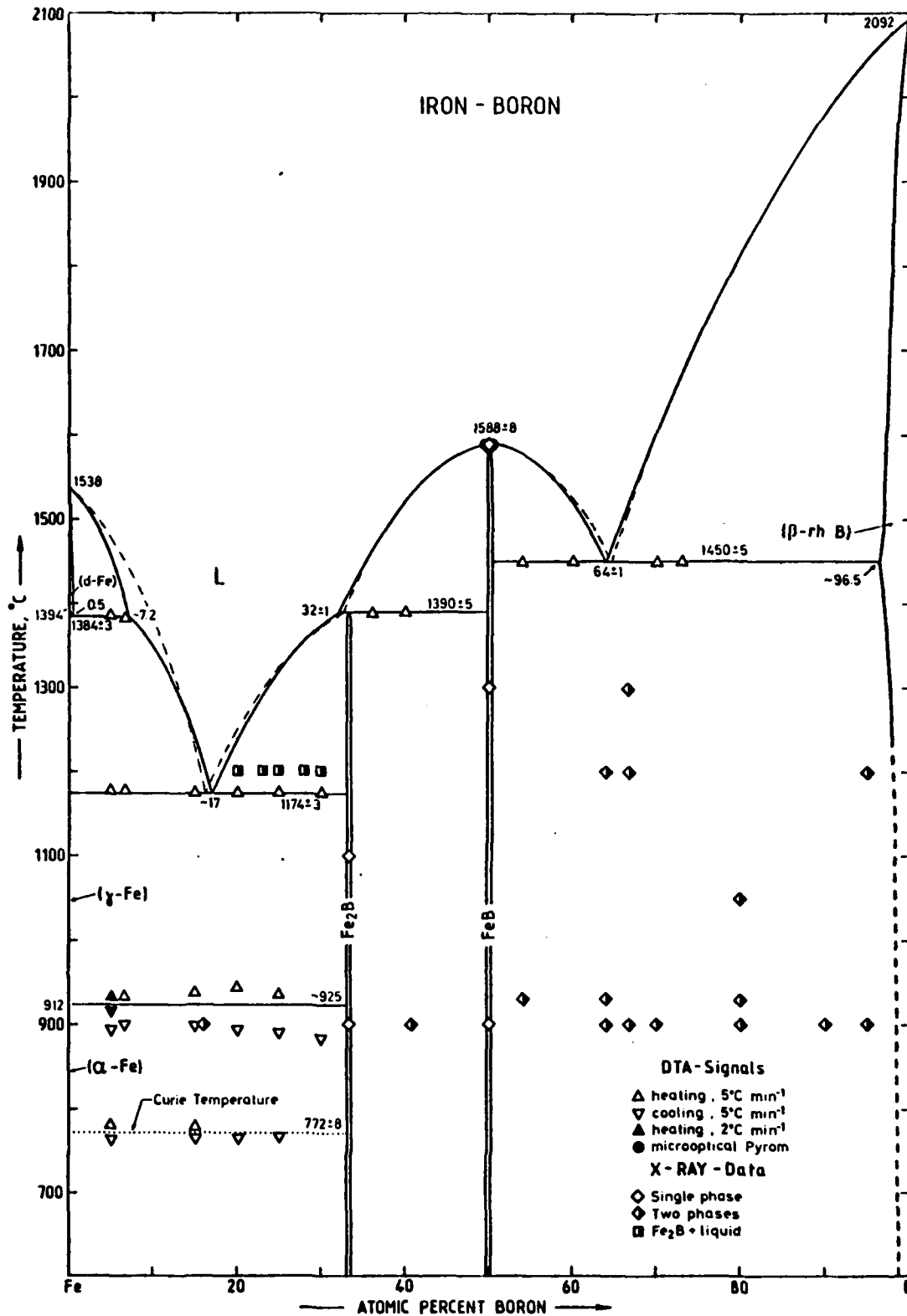
Fig.I.3 Constitutional equilibrium diagram of the system Fe-B (this work)
with experimental data points. The dashed curve represents the
thermodynamically calculated least squares fit (see also
section

Table I.2 Composition, Different Preparations Techniques and Crystal Data of Binary Iron-Borides

Nominal Composition in at% Fe - B	Preparation and Heat Treatment	X-ray Phase Analysis	Structure Type	Space Group	Lattice Parameters (Å) a	b	c	Volume (Å³)
84 - 16	cold compacted HF-heat./C-crucible Mo(Ar), 900°C, 48 h, B-amorph. (1)	α-Fe + Fe₂B	W-Type CuAl₂	Im3m I4/mcm	2.865(1) 5.105(2)	- -	- 4.248(4)	23.52(2) 110.72(14)
	cold compacted HF-heat./W-crucible Mo(Ar), 900°C, 72 h, B- amorph.(2)	α-Fe + Fe₂B	W-Type CuAl₂	Im3m I4/mcm	2.866(1) 5.106(1)	- -	- 4.248(1)	23.52(1) 110.74(5)
66.7 - 33.3	cold compacted HV-heat./W-crucible Mo(HV), 1100° 6 h, B-amorph. (3)	Fe₂B	CuAl₂	I4/mcm	5.104(1)	-	4.247(1)	110.62(5)
58 - 42	(1) Fe₂B + T-FeB(*)	CuAl₂ T-FeB	I4/mcm	5.106(2) 4.054(1)	- 5.504(3)	4.242(1) 2.946(1)	110.93(9) 65.74(4)
	(2) Fe₂B + T-FeB	CuAl₂ T-FeB	I4/mcm	5.106(1) 4.060(1)	- 5.497(3)	4.252(1) 2.947(1)	110.84(6) 65.77(4)
50 - 50	(3) + 12 h, 1300°C	FeB + traces Fe₂B	FeB	4.058(1) n.d.	5.500(2)	2.947(1)	65.78(3)

Table I.2   continued

42 - 58	(1) FeB (**)	FeB	Pbnm	4.056(1)	5.496(3)	2.948(1)	65.73(4)
	(2) T-FeB	T-FeB		4.058(2)	5.497(7)	2.945(1)	65.70(9)
33.3 - 66.7	(3) + 12 h, 1300°C	FeB + traces β-Boron	FeB	Pbnm	4.056(1)	5.498(2)	2.943(0)	65.64(3)
				n.d.			
20 - 84	cold compacted HF-heat./W-cruible Mo(Ar), 930°C 4 h, B-amorph.	T-FeB + β-Boron	T-FeB		4.060(2)	5.499(3)	2.949(1)	65.82(5)
				n.d.			
16 - 84	(1) T-FeB + β-Boron	T-FeB		4.061(2)	5.498(4)	2.946(1)	65.76(6)
				n.d.			
5 - 95	arc melted	FeB + (ss)β-rh.B β-Bor	FeB	Pbnm	4.060(2)	5.502(3)	2.947(1)	65.83(5)
			R3m	a_{hex}=10.973(2), c_{hex}=23.87(2)			2489 (2)

T-FeB-type denotes a transposition type of structure due to shift of unit cells (see text).

(**) uncontrolled heating (T>1100°C ?) by violent extherm reaction

n.d. not determined

Table I.3 : Powder Diffraction Data for Fe_5B_{95}

(hk l)	$10^4 \times \sin^2\theta$ obs.	calc.	Intensity obs.	calc.	d (Å) **	$10^4 \times \sin^2\theta$ **	Int. obs. **
(01 2)	106	107	20	25.6	–	–	–
					? 5.80	(176)	w/m
(11 0)	197	197	40	45.1	5.41	(203)	m
(10 4)	232	232	100	100.0	5.08	(230)	v st
(02 1)	*	273	*	8.5	4.64	(276)	m
(20 2)	*	304	*	6.0	4.44	(301)	w
(01 5)	*	326	*	3.7	4.27	(325)	w
					? 4.15	(345)	w
(00 6)	374	375	35	37.7	4.00	(371)	m
					? 3.82	(407)	vv w
					? 3.68	(438)	m/w
(21 1)	470	470	70	63.9	3.54	(473)	m
(20 5)	*	523	*	2.8	c 3.36	(526)	vv w
					? 3.30	(545)	vv w
(30 3)	684	685	10	9.9	2.95	(682)	vv w
(12 5)	720	720	10	13.5	2.86	(725)	w
(02 7)	770	773	30	28.3	2.77	(773)	w/m
(00 9)	*	844	*	2.7	2.65	(845)	w
(31 2)	*	895	*	6.1	2.57	(898)	vv w
(20 8)	*	929	*	2.8	2.52	(934)	vv w
(30 6)	965	966	10	11.6	2.47	(973)	m/w
(13 4)	1019	1020	40	32.3	2.41	(1022)	m/st
(04 2)	1090	1092	20	14.9	2.32	(1102)	w/m
(12 8)	*	1126	*	5.0	–	–	–
(22 6)	*	1163	*	1.0	2.25	(1172)	vv w
(40 4)	1218	1217	15	21.7	2.20	(1226)	m
(0210)	*	1305	*	6.9	–	–	–
(0111)	*	1326	*	7.7	2.11	(1333)	w/m
(32 4)	*	1414	*	6.0	2.04	(1426)	w/m
(03 9)	*	1435	*	8.0	–	–	–
(41 3)	*	1472	*	7.7	–	–	–
(23 5)	1508	1508	15	7.9	1.98	(1513)	vv w
(31 8)	1520	1520	10	4.3	1.96	(1544)	m/w
(33 0)	1775	1772	10	12.3	1.83	(1772)	w/m
(33 3)	1867	1866	15	11.6	–	–	–
(1310)	*	1895	*	4.6	–	–	–
(50 5)	*	1902	*	7.3	–	–	–
(23 8)	1914	1914	40	32.7	1.76	(1915)	w
					? 1.74	(1960)	st
(0213)	*	2024	*	10.4	1.71	(2029)	w/m
(3012)	*	2091	*	8.6 }	1.68	(2102)	m
(4010)	*	2092	*	5.4 }			

Table I.3 continued

(hk l)	$10^4 \times \sin^2\theta$ obs.	calc.	Intensity obs.	calc.	d (Å) **	$10^4 \times \sin^2\theta$ **	Int. obs. **
(3111)	*	2114	*	7.2	–	–	–
(51 4)	2202	2202	5	7.7	1.64	(2206)	w
(2212)	*	2288	*	1.7 }	1.61	(2289)	w
(3210)	*	2289	*	1.5]			
(06 3)	2456	2457	15	23.3	1.55	(2470)	st
(2311)	2510	2508	5	5.9	–	–	–
(43 4)	*	2595	*	3.8	1.51	(2602)	v w
(60 6)	*	2738	*	6.7	1.47	(2746)	w
(4013)	2813	2811	10	10.9	1.45	(2822)	w/m
(16 1)	*	2833	*	5.2	–	–	–
(2410)	2879	2880	10	13.9	–	–	–
(3114)	*	2896	*	8.5	1.43	(2902)	m/w
(0216)	*	2930	*	5.7	–	–	–
(0315)	*	2935	*	15.4 }	1.421	(2938)	m/st
(43 7)	*	2939	*	5.1]			
(61 5)	*	3083	*	7.4	–	–	–
(34 8)	3102	3096	10	14.5 }	1.382	(3107)	st
(4211)	*	3099	*	5.3]			
(44 0)	*	3151	*	6.8	1.368	(3170)	m
(44 3)	*	3245	*	10.1	–	–	–
(53 2)	*	3258	*	5.7	–	–	–
(3312)	3277	3273	5	6.0	1.347	(3270)	st
(1217)	*	3471	*	5.3	–	–	–
(07 5)	*	3477	*	4.4	–	–	–
(61 8)	*	3489	*	9.0	–	–	–
(2413)	*	3599	*	6.0	–	–	–
(35 7)	*	3727	*	4.3	–	–	–
(71 3)	*	3835	*	6.5	–	–	–

*: Not observed

**: Experimental data reported by Portnoi et al (21).

c: Correction made / old d-value: 3.56 Å.

?: Reflections not belonging to β- Boron.

Material: Fe_5B_{95}, arc melted.

Method: powder X-ray diffraction in a Guinier camera, $CuK_\alpha1$ radiation.

The intensity is normalized to the strongest reflection with I= 100.

Reflections with Int.(calc.)<4.0 % were omitted; exept: some reflections coresponding to those reported by (21).

(Space group: R$\bar{3}$m

Lattice parameters: a= 10.171 Å, Alpha= 65.33°.)

hexagonal setting: a= 10.978 Å, c= 23.86 Å.

Table I.4 : Powder Diffraction Data for Fe_2B

(hkℓ)	$10^4 \cdot \sin^2\theta$		Intensity	
	obs.	calc.	obs.	calc.
(110)	998	1007	10	7.9
(200)	2011	2015	20	17.9
(002)	2904	2910	20	23.3
(211)	3236	3246	100	100.0
(112)	3911	3918	5	6.3
(220)	4022	40$\measuredangle$9	2.5	3.0
(202)	4920	4925	15	15.3
(310)	5042	5037	15	14.9
(222)	6940	6940	2	1.5
(312)	7941	7947	20	18.2
(400)	8050	8059	5	4.6
(330) (213)	9055	$\left\{\begin{array}{l}9066\\9067\end{array}\right.$	100	$\left\{\begin{array}{l}29.8\\76.2\end{array}\right.$
(411)	9278	9290	90	87.3

Material: Fe_2B reacted for 6 h at 1100°C

Method: powder X-ray diffraction in a
   Debye-Scherrer camera, CrKα radiation

The intensity I is normalized to the
   strongest reflection with I= 100

Space group: I4/mcm

Lattice parameters: a= 5.104 Å, c= 4.247 Å

Table I.5: Powder Diffraction Data for FeB

(hkℓ)	$10^4 . \sin^2\theta$		Intensity	
	obs.	calc.	obs.	calc.
(110)	1224	1230	10	10.0
(020)	1730	1733	15	14.8
(101)	2302	2306	30	28.6
(120)	2528	2530	20	17.8
(111)	2736	2739	50	49.8
(200)	*	3186	*	0.2
(021)	3242	3243	35	33.5
(210)	3614	3619	30	33.4
(121)	4037	4039	15	15.9
(130)	4693	4697	15	16.8
(220)	*	4919	*	0.03
(211)	5129	5129	15	15.2
(002)	6039	6038	15	13.7
(131)	6209	6206	2	1.6
(221)	*	6429	*	0.2
(040)	*	6934	1	0.4
(230)	*	7086	1	0.3
(112)	7265	7268	2	2.6
(310)	7599	7602	1	1.0
(140)	7768	⎰ 7730	20	⎰ 12.4
(022)		⎱ 7771		⎱ 6.0
(041)	8437	8443	20	21.2
(122)	8561	8568	15	14.9
(231)	8594	8596	40	45.6
(301)	8670	8678	15	14.0
(320)	8893	8902	10	11.0
(311)	9105	9111	20	21.9
(202)	*	9224	*	0.2
(141)	9230	9240	5	4.2
(212)	9650	9657	100	100.0

*: Not observed or inaccurate

Material: FeB, reacted for 12 h at 1300°C

Method: powder X-ray diffraction in a
   Debye-Scherrer camera, CrKα radiation

The intensity I is normalized to the strongest
   reflections with I= 100

Space group: Pbnm

Lattice parameters: a= 4.0587 Å, b= 5.5024 Å
   c= 2.9483 Å

with composition $FeB_{\sim 49}$ (see Table I.3).

Samples with an iron to boron composition of 1:2 did not reveal any indications for the existence of a new compound "FeB_2" with the AlB_2-type; all alloys unambiguously revealed a stable two phase equilibrium FeB + ss-βrh Boron at all the different temperatures invesigated (900°C, 980°C, 1200°C, 1300°C, 1450°C). Metallography, SEM, and melting point samples in any case indicated a eutectic reaction isotherm according to

$$liquid \rightleftharpoons FeB(FeB\text{-type}) + ss\text{-}βrh\ Boron\ .$$
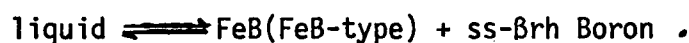
The eutectic point is located at 65 ± 1 a/o boron (see SEM-photograph, Fig.I.4). The precise eutectic temperature $T_E = 1450 \pm 3°C$ was obtained from DTA-experiments on arc melted as well as sintered alloy-specimens using Al_2O_3-crucibles. There was no attack of the Al_2O_3 crucibles visible after repeated heating and cooling.

The formation of a thermodynamically stable compound Fe_3B in the temperature region $1150°C \leqslant T \leqslant 1250°C$, as proposed by Khan, would be naturally connected with the existence of a two phase equilibrium Fe_3B + Fe_2B in the solid state. In order to reinvestigate this equilibrium condition, samples with compositions 20 at%B< x_{Boron}< 30 a/oB were arc melted and subsequently annealed for 48 hrs. at $1200 \pm 10°C$. After heat treatment however we found all alloys to be molten and thus confirm the two-phase equilibrium: liquid + Fe_2B earlier accepted in literature. Consequently "Fe_3B" is unstable or metastable at 1200°C (see also Fig.I.3).

Samples with a nominal composition Fe(50 a/o)B(50), prepared either by arc melting or by powder metallurgical sintering (>1200°C) of elemental powder compacts, confirm the existence of a compound with formula FeB. Lattice parameters and X-ray powder intensities show excellent agreement
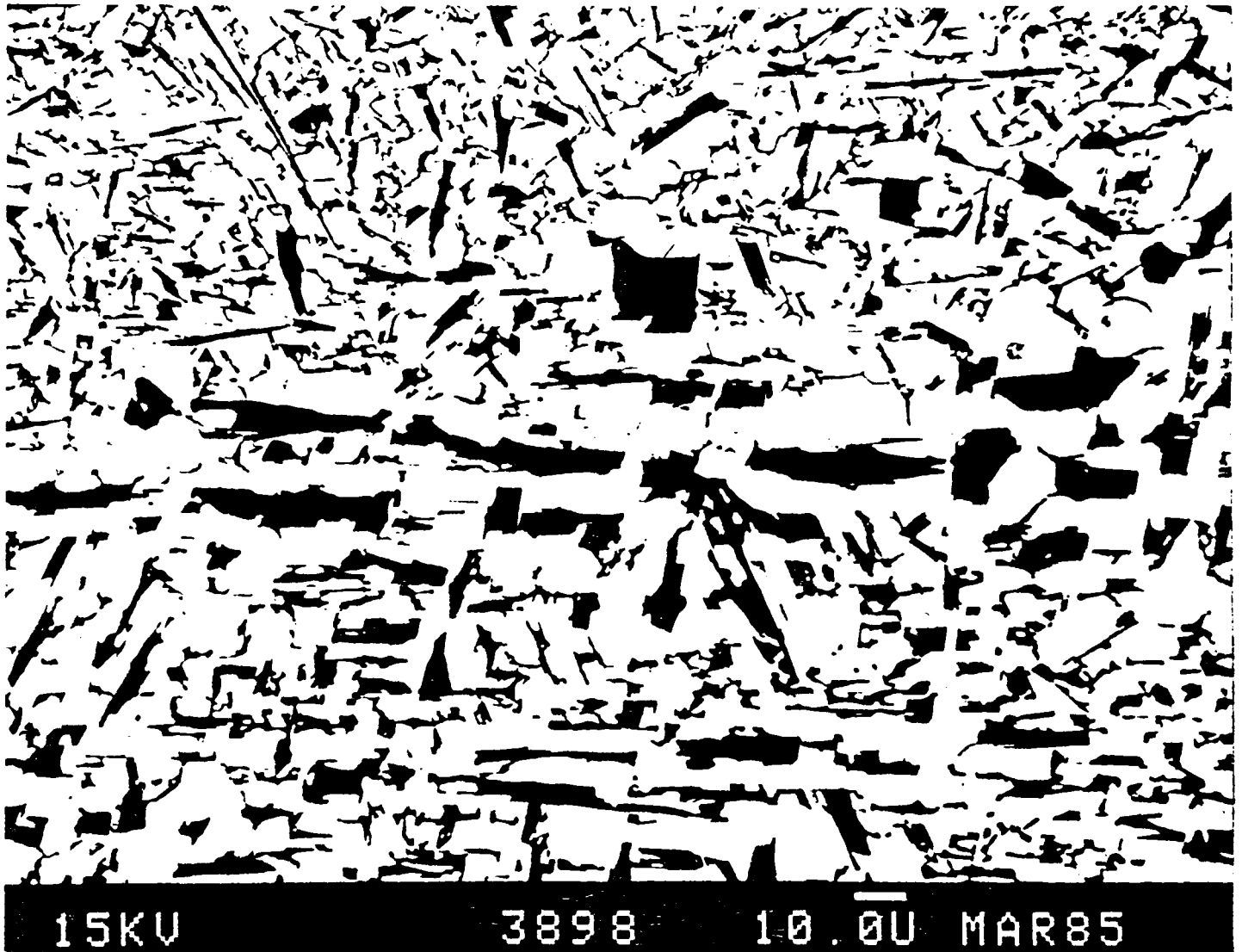
Fig.I.4 SEM-photograph of a Fe(35)B(65)-alloy in the as cast condition
(arc melting, quenched) revealing a binary eutectic FeB+ß-rh boron;
photographed as polished, 650 x.

with what is known as the β-FeB-type of structure in literature. Interestingly
there is no single crystal study available yet for this prototype of a
crystal structure. It is furthermore noteworthy that in some cases (without
any obvious systematics) an additional X-ray reflection was observed at
d= 2.33 $\overset{o}{A}$, which cannot be attributed to one of the neighbouring phases;
indexation however is possible (Miller's indices (111)) on the basis of a
doubling of the unit cell, according to a_o, b= $2b_o$ and c= c_o. In order to
unambiguously and crystallographically characterize the FeB-type, a single
crystal was grown, suitable for an X-ray diffraction study on a computer
controlled SIEMENS four-circle diffractometer with an ECLIPSE-computer system
attached. The single crystal was obtained by chemical vapour deposition
when a prereacted two-phase sample (FeB + ss-rh-Boron) with a nominal
composition of Fe(40)B(60) was annealed for two weeks at 900°C in an evacuated
silica tube, where small amounts of $FeC\ell_3$ where added as mineralisator.
The temperature gradient along the quartz tube of 15 cm length was 25°C,
the sample being at the hot end in an open Mo-container. The single crystal
was part of a whisker grown at the sample surface.

The obtained results of the structure determination are summarized in
Tables I6,7,8,9; For the first time the crystal structure of FeB has been
refined from single crystal data; the reliability factor R=$\sum |\Delta F| / |F_o|$ = 0.06
confirmes the crystal symmetry and atom order of the socalled β-FeB-type,
and due to the metal/boron ratio ≈ 1 the crystal structure of FeB is
correctly classified (65) as a typical boron-chain type monoboride. The
crystal specimen investigated did not reveal any deviations from the
FeB-type symmetry ("high temperature form") as earlier accepted in literature
from X-ray powder data.

Table I.6

Atomic and thermal parameters for FeB (Pbnm, No.62; origin at I); standard deviations are in parentheses; R= 0.06. isotropic temperature factors are expressed as $T= \exp[-2\ell\ell^2 . 10^{-2} U(2\sin\theta/\lambda)^2]$, anisotropic thermal factors are of the form: $T = \exp[-2\ell\ell^2(U_{11}h^2a^{*2} + U_{22}k^2b^{*2} + U_{33}\ell^2c^{*2} + 2U_{12}hka^*b^* + \ldots).10^{-2}]$;

Atom	Site	x	y	z	occ.	$U(Å^2)$	U_{11}	U_{22}	U_{33}	U_{12}
Fe	4c	0.1194(3)	0.1770(3)	1/4	1.0	0.0010	0.0005	0.0005	0.0020	0.0002
B	4c	0.6159(28)	0.0349(31)	1/4	1.0	0.0005	-	-	-	-

By symmetry $U_{13}=U_{23}=0$

Table I.7

| Crystallographic Data for FeB |
| Space Group Pbnm (D_{2h}^{16}-No.62), Z= 4 |

$$a = 4.0587(5)$$
$$b = 5.5024(5)$$
$$c = 2.9483(2)$$
$$V = 65.84 \quad (6)$$
$$D_x = 6.73 \text{ Mgm}^{-3}$$
$$\mu(\text{MoK}_\alpha) = 20.59 \text{ nm}^{-1}$$

Table I.8

Interatomic Distances in FeB ($<$ 4.0 Å)			
Fe - 4 Fe	2.948(1)	B - 1 Fe	2.188(12)
4 Fe	2.634(1)	4 Fe	2.165(11)
2 Fe	2.628(2)	1 Fe	2.162(12)
1 B	2.162(12)	B - 2 B	1.790(10)
4 B	2.165(11)		
1 B	2.188(16)		

Table I.9 Comparison of Fo and Fc-data for FeB

h	k	l	10F$_o$	10F$_c$	h	k	l	10F$_o$	10F$_c$	h	k	l	10F$_o$	10F$_c$	h	k	l	10F$_o$	10F$_c$	h	k	l	10F$_o$	10F$_c$
4	0	0	69	63	6	0	0	80	-83	6	1	0	190	186	2	1	0	404	-512
4	1	0	124	-121	5	1	0	90	-92	4	2	0	255	239	0	2	0	321	-348
2	2	0	330	-344	3	2	0	282	-277	3	3	0	210	198	5	2	0	152	148
2	3	0	417	-401	3	3	0	306	285	3	4	0	14	2	5	3	0	276	261
1	4	0	128	-109	2	4	0	9	-7	3	5	0	322	303	4	4	0	63	65
1	4	0	182	-183	2	5	0	244	213	4	6	0	175	-165	4	5	0	29	25
2	6	0	359	303	2	6	0	34	28	3	8	0	65	-65	1	6	0	275	-248
3	7	0	32	17	5	7	0	26	-11	0	0	1	262	-232	2	8	0	79	-79
4	0	1	337	-410	5	0	1	181	173	1	2	1	355	-419	1	1	1	297	-322
3	1	1	273	263	4	1	1	231	225	1	3	1	388	-488	0	2	1	282	309
3	2	1	39	-38	4	3	1	307	291	1	4	1	143	-140	5	3	1	133	118
3	3	1	380	382	3	4	1	44	46	4	5	1	73	-80	0	4	1	350	391
2	4	1	131	119	3	5	1	118	115	5	6	1	277	-261	2	6	1	51	-61
2	5	1	245	228	3	6	1	173	-172	5	7	1	41	-40	4	7	1	191	-194
2	6	1	218	-215	0	8	1	216	-208	4	0	2	143	152	0	0	2	198	-196
3	7	1	8	-25	2	1	2	175	-104	0	1	2	420	-508	2	2	2	46	-45
0	1	2	350	330	1	2	2	363	376	2	2	2	94	91	4	3	2	45	51
5	2	2	79	79	1	3	2	263	244	2	3	2	19	14	3	3	2	227	222
5	2	2	166	-167	0	3	2	343	311	2	4	2	61	-53	3	5	2	253	-241
3	3	2	15	-1	1	4	2	81	80	2	5	2	294	-266	2	6	2	18	5
4	4	2	269	-264	0	5	2	194	-181	2	6	2	190	-181	3	1	3	136	144
5	5	2	6	-22	1	6	2	63	61	3	0	3	33	-25	2	5	3	56	57
7	7	2	20	-16	1	0	3	214	211	2	2	3	249	239	2	6	3	212	204
0	0	3	185	-181	3	1	3	297	290	3	3	3	196	-186	1	0	3	0	25
1	1	3	186	-187	0	2	3	81	-79	3	4	3	276	-256	2	2	3	61	60
2	2	3	275	-251	2	3	3	25	-19	3	6	3	81	-90	3	5	3	176	-173
5	4	4	233	218	4	6	3	168	167	4	0	4	298	301	4	2	4	27	28
1	6	4	64	70	2	2	4	136	-143	2	2	4	145	-148	4			9	-8
3	1	4	214	-209															

The powdermetallurgical reaction of FeB by use of elemental iron and amorphous boron powder is extremely exothermal, and for compositions Fe:B = 1 it is hardly possible to avoid short-term superheating of the samplespecimens above 1100°C. This is the likely explanation why in all these cases the socalled high temperature form with the FeB-type was obtained. Control of the exotherm reaction however is easily attained in sinter alloys with a considerable amount of excess boron i.e. for compositions with a boron content of more than 55 a/o B. In these samples (prepared at 900°C) the X-ray powder analysis confirmed the type of powder pattern, which was earlier described (16,17) as due to a socalled "low temperature modification" of FeB (T-FeB).

The X-ray powder diffractogram of T-FeB obviously derives from the one characteristic for the high temperature alloys: the main difference is found in the existence of a "sharp" and a "diffuse" subset of reflections observed at those d-values characteristic for the β-FeB-type unit cell dimensions. Position (d-values) and intensities of the "sharp" subset of X-ray reflections thus correspond to the "high temperature" FeB-type and in no case were possibly indexed on the base of an orthogonal CrB-type unit cell.

The dissappearance of a subset of reflections out of the general set of X-ray reflections of the β-FeB type shows striking similarity with the existence of a socalled "transposition-type" as observed in case of the tungsten monoboride with a CrB-type high-temperature phase and a MoB-type low-temperature modification (66).

A direct comparison of the X-ray powder data for T-FeB (alloy Fe(20)B(80) sintered at 900°C and FeB (alloy Fe(50)B(50) annealed at 1300°C) is presented in Fig.I.5). Indeed in T-FeB the subset of diffuse reflections (hkℓ) obeys
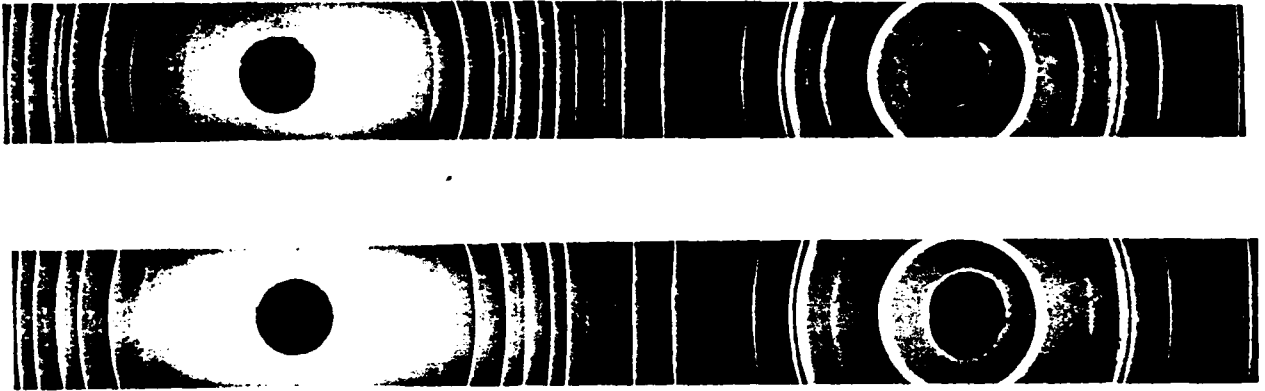
Fig.I.5 Comparision of X-ray diffractograms of h,1-FeB.

Fe B   Cr B
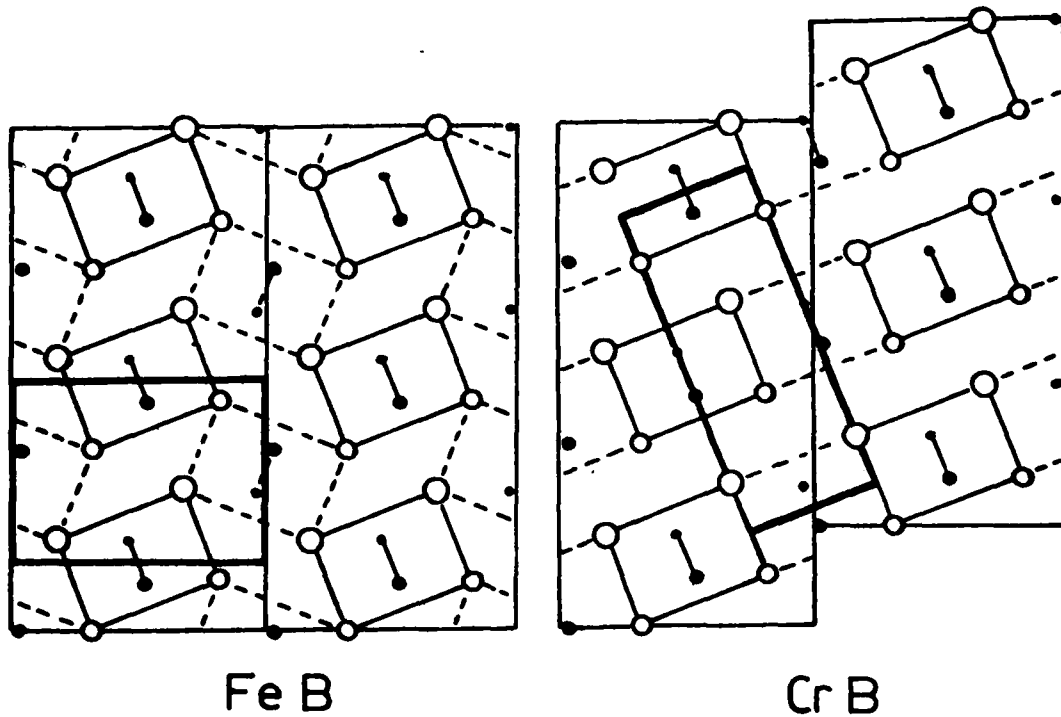
Fig.I.6 On the crystallographic relation between the two structure
         types of FeB and CrB. Both structures are simply related by
         a shift of slabs of FeB by the vector $\frac{1}{2}$ a_o (FeB) (after Hohnke
         and Parthé, ref.18.) The unit cells are outlined by heavy lines.
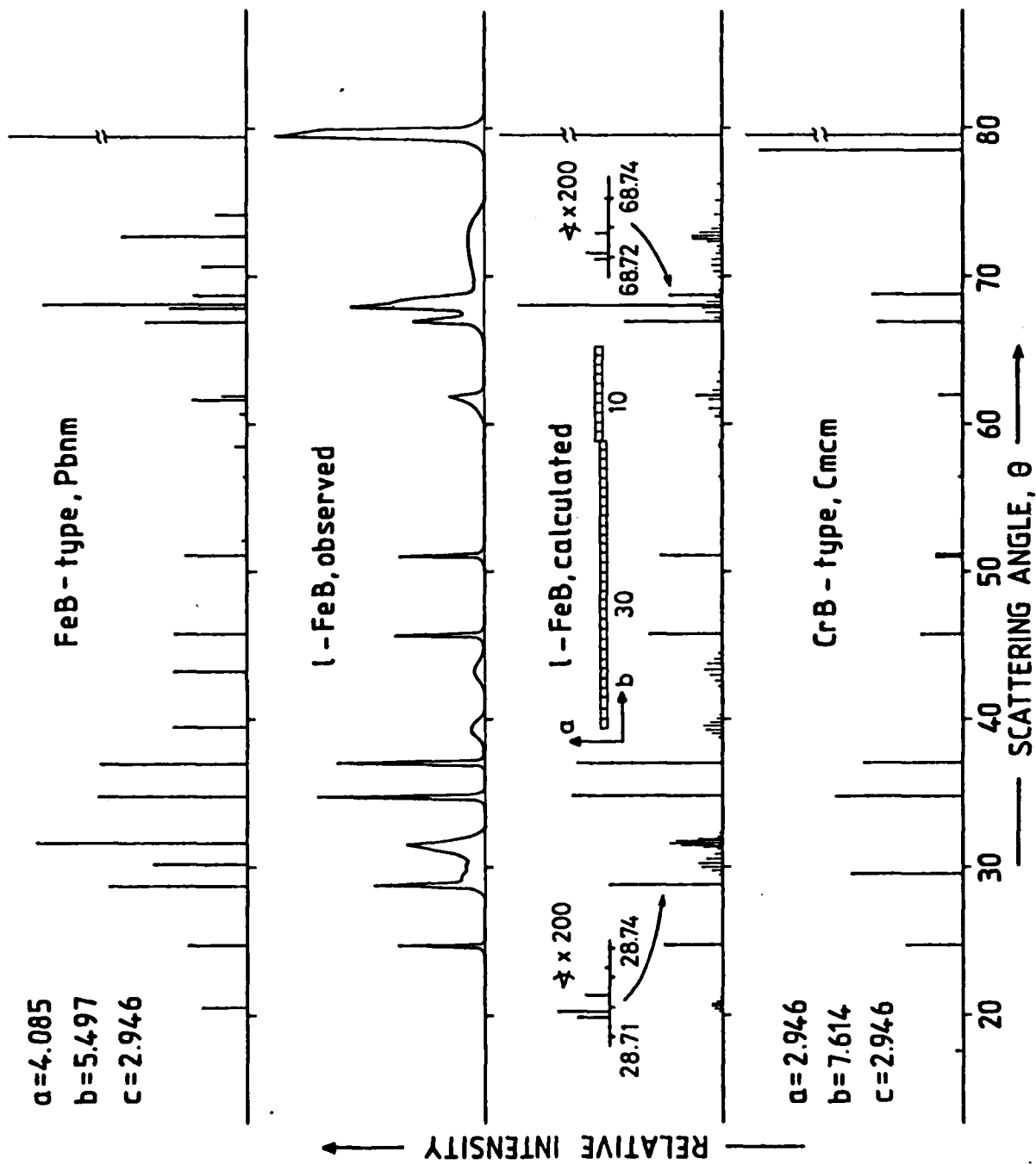
Fig.I.7 X-ray powder diagram of iron monoboride; observed and calculated
         intensities and comparison with the calculated patterns for the
         FeB-type and CrB-type structure (for details see text).

the condition h= 2n + 1 and thus follows the proposed shift-mode for the
pair of related structure types CrB-FeB as earlier discussed by Hohnke and
Parthé (18). Fig.I.6 explains how the structure type of CrB is generated
by a simple shift of slabs of the FeB-type by a vector of $\frac{1}{2} a_{FeB}$ (18).
The socalled low temperature modification T-FeB thus merely represents an
irregular arrangement of FeB-type slabs in shifted and unshifted position,
and without long range order with respect to the shift operation. Applying
Scherrer's formula usually employed for the determination of particle sizes:
$\beta_{1/2} = \frac{K. \lambda.57.3}{D.cos\theta}$ we arrive at a size of $\sim$ 80 $\overset{o}{A}$ for the undisturbed FeB-type
regions. Based on this transposition type and refering to an average cell
size of 80 $\overset{o}{A}$ it is easy to calculate the X-ray powder pattern of T-FeB in
fine agreement with the observed data (see Fig.I.7). The calculation further-
more and directly reveals the two subsets of sharp and diffuse reflections
according to the shift operation FeB - CrB.

Applying a pressure of $\sim$ 2 bar while sintering a prereacted T-FeB at 700°C
for about 20 min in a hotpress with BN-lined graphite dies easily converts
the T-FeB condition into a well crystallized sample corresponding to the
β-FeB-type.

With respect to the presented results obtained on samples annealed at
different temperatures 500°C < T < 1300°C and in contradiction to literature
there is no defined transition temperature between α-FeB and β-FeB.
The socalled "irreversible transition" is thus merely the transition of an
irregular shifted arrangement without long-range order into a crystallo-
graphically defined arrangement of FeB-type unit cells without shifted slabs.

Characteristic X-ray powder diagrams for easy identification of all binary
equilibrium phases are presented in Table I.3,4,5.

II. THE BINARY SYSTEM COBALT-BORON

a) CRITICAL LITERATURE REVIEW

A detailed investigation (temperature versus concentration) of the cobalt-boron binary system is due to a report by Schöbel and Stadelmaier (45) which also contains a review on the older literature data. According to (45) three stable binary cobalt borides exist i.e. Co_3B formed by a peritectic reaction at 1110°C, congruently melting Co_2B, and congruently melting CoB.

The formation of the binary phase Co_3B appears to be kinetically retarded and its formation is thus frequently suppressed. Especially in ternary samples Co_3B is usually obtained after long term heat treatment only (45,46). The suppression of the Co_3B-precipitation or-crystallization in rapidly cooled melts yields a metastable eutectic reaction isotherm at 1095°C:

liquid $\rightleftharpoons$ ss-Co + Co_2B.

There are considerable doubts about the existence of a compound "FeB_2" earlier described by Kolomytsev (47) (see also RESULTS).

There are furthermore doubts about the formation of a boron-rich compound "$CoB_{\sim 12}$" for which X-ray powder data were reported by Avlokhashvili (48) (see also RESULTS). X-ray analysis of these data favor a solid solution of 3-5 a/o cobalt in the voids of the boron framework of β-rh boron, rather than the existence of a new compound (see i.e. also section iron-boron, concerning FeB_{19}).

The solubility of boron in cobalt was reported to be 3 a/o B (29) at 1000° or 5.2 a/o boron at 1100°C (63) respectively.

A detailed compilation of the crystal data of all binary cobalt borides is presented in Table II.1, including the metastable phase "$Co_{23}B_6$", which forms during recrystallization of rapidly quenched foils (29).

The complete phase diagram (T-X-diagram according to (45)) is presented in Fig.II.1.
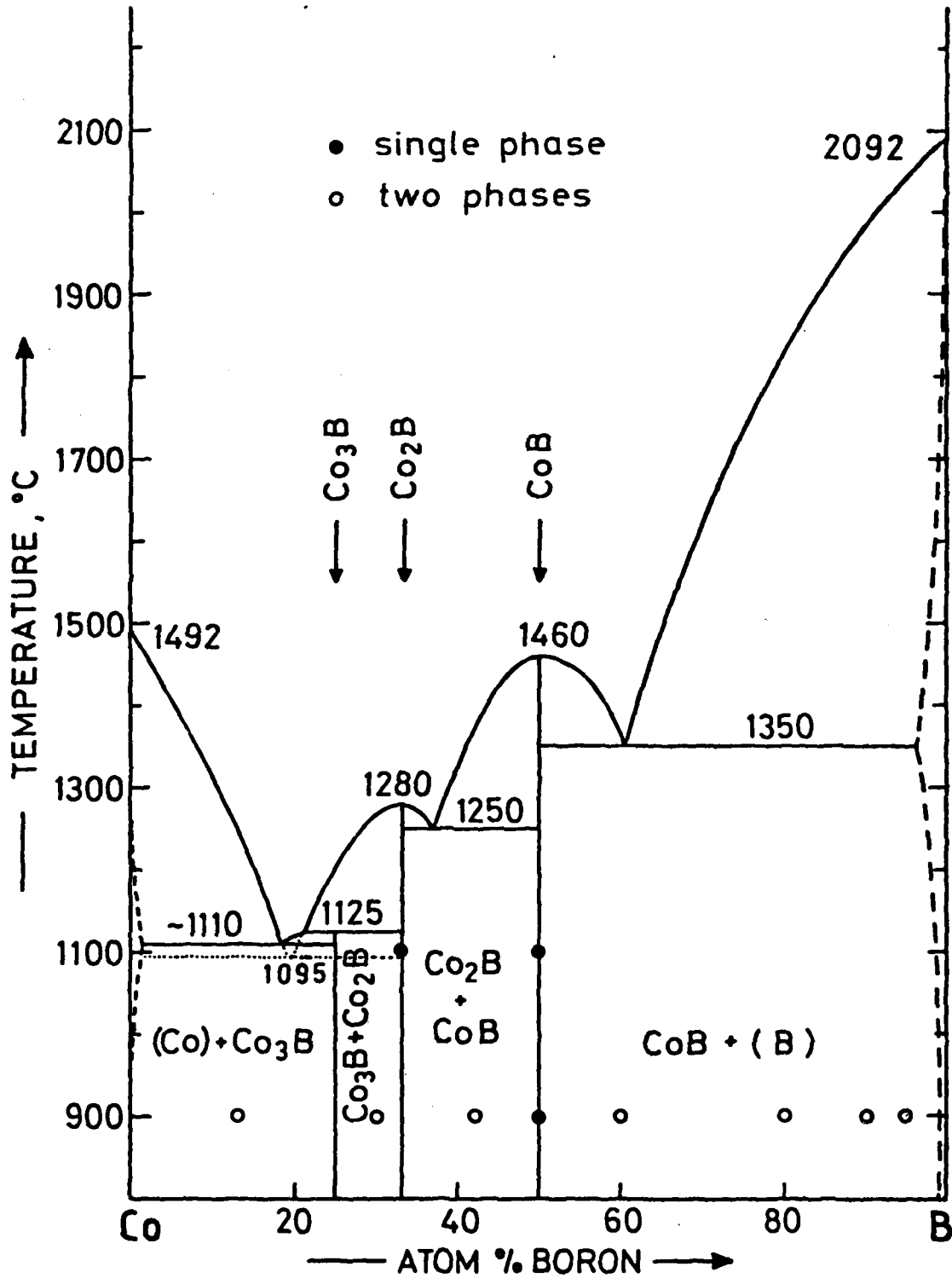
Fig.II.1 Constitutional diagram of the binary system cobalt-boron
and experimental data points (this work); phase equilibria
based on Schoebel and Stadelmaier (1966), ref.45.

Table II.1: Crystallographic Data (Literature) of Cobalt-Borides

Phase	Structure Type	Space Group	Lattice Parameters (Å)			References
			a	b	c	
$Co_{23}B_6$ (metastable)	$Cr_{23}C_6$	Fm3m	11.05			(29)
Co_3B boron poor boron rich	Fe_3C	Pbnm	4.408– -4.411	5.255– -5.235	6.629– -6.634	(40,50,51)
Co_2B	$CuAl_2$	I4/mcm	5.016	–	4.220	(33,40,42,52)
CoB	FeB	Pbnm	3.956	5.253	3.043	(33,40,42)
CoB_x (x > 20)	ß-rh Boron	R$\bar{3}$m	a_{hex}=10.9459	c_{hex}=23.8397		(44)

b) EXPERIMENTS AND RESULTS

X-ray analysis and metallography of about 10 binary alloys prepared by
arc melting and annealed at 900°C and 1100°C respectively, undoubtedly
confirm the phase relations reported by Schöbel et al. (45). According to
their data, thermodynamic equilibrium was rather slowly attained for Co_3B
which finally appeared after prolonged heat treatment (2 x 72 hrs at 900°C).
The unit cell dimensions of ss-β Cobalt remained practically unchanged
with respect to pure cobalt, indicating a rather small solubility of less
than 1 atomic percent of boron.

Detailed X-ray analysis did not reveal any indications for the existence
of binary boron-rich compounds such as "CoB_2" or "CoB_{12}" respectively. A
comparision of the X-ray-powder data reported by (48) for "CoB_{12}" with an
intensity diagram calculated on the basis of the crystal symmetry and atom
order as derived for the β-rhombohedral solid solution MnB_{23} by (49) shows
satisfactory agreement, which gives proof to the fact, that "CoB_{12}" is rather
a solid solution of Co in β-rh B than a new binary compound.

A compilation of all crystallographic and phase diagram data obtained
on our samples annealed at 900°C is represented in Table II.2 and confirms
the phase relationships in the binary cobalt-boron system as published
by (45); Fig.II.1.

Characteristic X-ray powder diagrams for easy identification of all binary
equilibrium phases are presented in Tables II, 3-6.

Table II.2 Composition, Preparation Techniques and Crystal Data of Binary Cobalt Borides

Nominal Composition in at%	Preparation and Heat Treatment	X-ray Phase Analysis	Structure Type	Space group	Lattice Parameters (Å) a	b	c	Volume (Å³)
Co - B								
87 - 13	cold compacted HF-heat/W-crucible Mo(Ar), 900°C, 72 h, B-amorph.	Cu(cubic)+	Cu-Type	Fm3m	3.540(3)	-	-	44.36(7)
		Co₃B	Fe₃C	Pbnm	4.406(2)	5.210(3)	6.628(3)	152.13(13)
70 - 30	"	Co₃B +	Fe₃C	Pbnm	4.406(5)	5.227(4)	6.621(2)	152.48(21)
		Co₂B	CuAl₂	I4/mcm	5.014(1)	-	4.217(2)	106.00(5)
58 - 42	"	Co₂B +	CuAl₂	I4/mcm	5.011(2)	-	4.217(3)	105.89(11)
		CoB	FeB	Pbnm	3.954(0)	5.245(2)	3.043(1)	63.11(2)
40 - 60	"	CoB	FeB	Pbnm	3.954(1)	5.248(3)	3.041(1)	63.10(5)
20 - 80	"	CoB +	FeB	Pbnm	3.955(1)	5.261(2)	3.037(0)	63.18(4)
		traces B			n.d.			
10 - 90	"	CoB +	FeB	Pbnm	3.955(2)	5.256(4)	3.037(1)	63.12(5)
		B (diffuse)						
5 - 95	arc melted, 14d 900°C, Mo (Quartz) B-Cristalline	CoB +	FeB	Pbnm	3.951(1)	5.253(3)	3.044(1)	63.15(4)
		(ss)β-rh.B β-Boron	β-Boron	R3m	a_hex=10.940(4)		c_hex=23.81(6)	2467(6)

Table II.3: Powder Diffraction Data for Co_3B

(hkℓ)	$10^4 \cdot \sin^2\theta$ obs.	calc.	Intensity obs.	calc.
(011)	*	975	*	0.2
(101)	*	1159	*	0.1
(020)	*	1195	*	1.1
(111)	1460	1458	5	4.7
(200)	*	1934	*	0.5
(210)	2230	2232	10	11.1
(121)	2355	2354	15	15.5
(201)	2605	2610	10	9.0
(002)	*	2704	2	2.1
(211)	2903	2908	15	15.2
(220)	3125	3129	20	19.9
(102)	3176	3187	20	20.7
(031)	3355	3364	25	25.2
(112)	3485	3486	20	17.8
(221)	3795	3804	10	11.2
(131)	3842	3848	10	8.3
(022)	*	3898	*	0.8
(122)	4382	4382	10	6.9
(230)	4612	4622	5	3.2
(202)	*	4638	*	0.3
(040)	*	4779	3	2.2
(212)	*	4936	*	0.2
(301)	5025	5027	10	8.9
(231)	*	5298	*	0.3
(311)	*	5326	*	0.6
(222)	*	5832	*	0.9
(132)	*	5875	*	0.4
(141)	*	5938	1	1.6
(321)	*	6222	*	0.2
(013)	*	6382	*	0.2
(240)	*	6713	2	2.1

Table II.3 continued

(hkℓ)	$10^4 . \sin^2\theta$ obs.	calc.	Intensity obs.	calc.
(113)	*	6866	1	1.2
(302)	*·	7055	*	0.1
(232)	*	7326	1	1.4
(312)	*	7354	*	0.1
(241)	*	7389	*	0.1
(123)	7754	7762	10	12.1
(142)	*	7966	*	0.5
(203)	*	8017	*	0.3
(051)	*	8143	2	2.1
(322)	*	8250	5	4.6
(213)	*	8316	2	2.4
(401)	Co(220)	8411	c	13.9
(151)	*	8626	5	5.9
(411)	*	8710	4	4.2
(033)	*	8772	3	3.0
(420)	*	8930	4	3.9
(223)	*	9212	1	1.2
(133)	9245	9255	30	29.2
(250)	9390	9401	20	19.8
(242)	*	9416	*	0.1
(421)	*	9606	5	6.0
(332)	9734	9743	100	100.0
(341)	*	9806	*	8.1

*: Not observed or inaccurate

c: Coincidence with Co-reflections

Material: Co_3B, reacted for 72 h at 900°C

Mathod: powder X-ray diffraction in a
Debye-Scherrer camera, CrKα radiation

The intensity is normalized to the strongest
reflection with I= 100

Space group: Pbnm

Lattice parameters: a= 5.210 Å, b= 6.628 Å
c= 4.406 Å

Table II.4: Powder Diffraction Data for Co_2B

(hkl)	$10^4 \cdot \sin^2\theta$		Intensity	
	obs.	calc.	obs.	calc.
(110)	1036	1044	10	6.5
(200)	2083	2088	15	14.4
(002)	2953	2951	20	19.2
(211)	3348	3347	80	79.7
(112)	3989	3995	5	5.1
(220)	4164	4175	2	2.4
(202)	5031	5039	15	12.4
(310)	5211	5219	15	12.0
(222)	*	7127	1	1.3
(312)	8158	8170	20	16.4
(400)	8350	8350	5	4.3
(213)	9243	9250	70	72.0
(330)	9385	9394	30	31.6
(411)	9594	9610	100	100.0

*: Inaccurate

Material: Co_2B, reacted for 72 h at 900°C

Method: powder X-ray diffraction in a
Debye-Scherrer camera, CrKα radiation

The intensity is normalized to the
strongest reflection with I= 100

Space group: I4/mcm

Lattice parameters: a= 5.014 Å, c= 4.217 Å

Table II.5: Powder Diffraction Data for CoB

(hkℓ)	$10^4 \cdot \sin^2\theta$ obs.	calc.	Intensity obs.	calc.
(110)	1309	1316	10	9.5
(020)	1894	1908	15	15.4
(101)	2260	2259	40	39.2
(111)	2722	2736	60	56.4
(120)	2728	2747	20	20.6
(021)	3317	3328	40	37.3
(200)	*	3357	*	0.1
(210)	3827	3834	30	36.1
(121)	4158	4167	20	18.3
(130)	5120	5132	20	17.7
(211)	5252	5254	20	17.3
(220)	*	5265	*	0.01
(002)	5680	5679	20	16.8
(131)	6538	6552	1	1.8
(221)	*	6684	*	0.02
(112)	6982	6995	3	2.7
(022)	7565	7587	10	7.1
(040)	*	7631	*	0.4
(230)	*	7649	*	0.5
(310)	8010	8030	2	2.2
(122)	8404	8426	20	19.0
(140)	8453	8470	20	17.7
(301)	8962	8973	15	15.4
(202)	*	9036	*	0.1
(041)	9043	9051	30	33.6
(231)	9060	9069	70	67.5
(311)	9432	9450	40	42.2
(320)	9445	9461	20	16.1
(212)	9497	9513	100	100.0
(141)	*	9890	*	14.0

*: Not observed

Material: CoB, reacted at 1100°C for 24 h

Method: powder X-ray diffraction in a
  Debye-Scherrer camera, CrKα radiation

The intensity is normalized to the strongest
  reflection with I= 100

Space group: Pbnm

Lattice parameters: a= 3.954 Å, b= 5.245 Å
                    c= 3.040 Å

Table II.6   continued

Table II.6 Powder Diffraction Data for Co_5B_{95}

(hk l)	10^4 x $\sin^2\theta$ obs.	calc.	Intensity obs.	calc.
(01 2)	109	108	30	26.0
(11 0)	200	198	50	46.4
(10 4)	234	234	100	100.0
(02 1)	276	275	10	7.1
(11 3)	294	293	5	3.2
(20 2)	307	307	5	5.5
(01 5)	329	328	5	3.0
(00 6)	377	377	40	38.7
(21 1)	475	474	70	65.4
(30 0)	596	595	5	3.1
(21 4)	*	631	*	3.4
(30 3)	688	690	2	12.7
(12 5)	*	725	*	13.3
(02 7)	778	777	15	29.5
(13 1)	*	871	*	3.1
(31 2)	898	902	5	5.9
(30 6)	972	972	15	11.0
(13 4)	1026	1028	39	32.9
(04 2)	1104	1100	10	14.8
(12 8)	1138	1133	5	5.1
(40 4)	CoB	1226	c	22.2
(0210)	*	1311	*	7.2
(0111)	*	1332	*	8.1
(41 0)	*	1389	*	3.2
(32 4)	*	1425	*	5.7
(30 9)	*	1443	*	8.3
(41 3)	*	1484	*	8.1
(23 5)	*	1519	*	8.5
(31 8)	*	1530	*	4.6
(40 7)	*	1571	*	3.9
(14 6)	*	1766	*	3.3
(33 0)	*	1786	*	12.7
(24 1)	*	1863	*	3.7
(33 3)	1880	1881	10	12.2
(1310)	*	1906	*	4.7
(50 5)	*	1916	*	7.2
(23 8)	1928	1927	20	33.5
(24 4)	*	2020	*	3.3
(0213)	*	2033	*	10.5
(3012)	*	2102	*	9.0
(4010)	*	2105	*	5.6
(42 5)	*	2114	*	3.4
(3111)	2125	2126	5	7.6
(51 4)	*	2219	*	8.1
(43 1)	*	2459	*	3.5
(06 3)	2478	2476	20	23.1
(2311)	*	2523	*	6.4
(51 7)	2558	2564	2	3.1
(43 4)	*	2615	*	4.0
(60 6)	*	2759	*	6.6
(4013)	2826	2827	10	10.5
(16 1)	2854	2856	5	5.3
(2410)	2890	2899	5	13.3
(3114)	*	2911	*	8.6
(0216)	2939	2943	5	5.5
(3015)	*	2949	*	15.8
(43 7)	2957	2961	5	5.3
(61 5)	3102	3107	5	7.0
(0414)		3109		3.3
(34 8)	3120	3118	15	14.4
(4211)		3118		5.5
(44 0)	*	3176	*	6.8
(60 9)	3227	3229	2	3.2
(44 3)	3273	3270	5	9.6
(53 2)	3286	3284	5	5.4
(3312)	*	3293	*	5.9
(35 4)	*	3409	*	6.7
(1217)	*	3486	*	5.1

*: Not observed
c: Coincidence with CoB reflrctions
Material: Co_5B_{95} , arc melted
Method: powder X-ray diffraction in
  a Guinier camera, $CuK_\alpha 1$ radiation
The intensity is normalized to the
  strongest reflection with I= 100.
Reflections with Int.(calc.)< 3.0 %
  were omitted.
(Space group: $R\bar{3}m$
  Lattice parameters: a= 10.143 Å,
              Alpha= 65.24°.   )
  hexagonal setting: a= 10.935 Å,
              c= 23.82 Å.

III. <u>THE BINARY SYSTEM NICKEL-BORON</u>

a) <u>CRITICAL LITERATURE REVIEW</u>

The binary system Ni-B is characterized by relatively low melting temperatures in the region of 40 to 50 at% boron and by a much smaller thermodynamic stability of the incongruently melting nickelmonoboride as compared to the corresponding CoB.

Earlier data in literature (53,54) confirm the existence of five binary nickel-borides i.e. Ni_3B, Ni_2B, orthorhombic $o-Ni_4B_{3-x}$ and monoclinic $m-Ni_4B_3$ (all congruently melting), and incongruently melting NiB (peritectic reaction). A detailed listing of phase diagram and crystal data reported in literature is presented in Table III.1.

Acccording to Schöbel et al. (53) orthorhombic and monoclinic nickelborides were observed without narrow homogeneous regions at 41.4 and 43.6 a/o boron respectively. The variation of unit cell parameters as observed by (54) for orthorhombic $o-Ni_4B_3$ indicates however a small homogeneity range for $o-Ni_4B_3$.

Thermodynamic equilibrium in the range of the Ni_4B_3-borides is rather slowly attained as reported by (54), and accordingly alloys tend to loose small quantities of boron into the metal container material during the prolonged annealing procedures.

The cooling characteristic of melting-point alloys in the range between $o-Ni_4B_3$ and $m-Ni_4B_3$ was observed to deviate from the normal behavior, and was interpreted by (53) as the inversion of primary and secondary solidification. Due to undercooling $o-Ni_4B_3$ is precipitating first, and thus triggers spontaneous formation of stable $m-Ni_4B_3$.

Table III.1 Crystallographic Data (Literature) of Nickel-Borides

Phase	Structure Type	Space Group	Lattice Parameters (Å)				Ref.
			a	b	c	β	
Ni$_3$B	Fe$_3$B	Pbnm	4.390(4)	5.2105(5)	6.6174(6)		(55)
			4.389	5.211	6.619		(57)
			4.392	5.223	6.615		(58)
Ni$_2$B	CuAl$_2$	I4/mcm	4.991	–	4.247		(52)
			4.990	–	4.245		(33)
			4.989	–	4.246		(54)
o-Ni$_4$B$_3$ Ni-rich	o-Ni$_4$B$_3$	Pnma	11.9540(8)	2.9815(3)	6.5684(5)		(55)
B-rich			11.973	2.985	6.584		(54)
m-Ni$_4$B$_3$	m-Ni$_4$B$_3$	C2/c	6.430	4.882	7.818	β=103.30°	(54)
			6.4282(5)	4.8795(4)	7.8190(6)	β=103.315(8)°	(55)
NiB	CrB	Cmcm	2.936	7.38	2.968		(61)
			2.925	7.396	2.966		(60)
			2.928	7.391	2.964		(60)
NiB$_x$ (x> 20)	β-rh Boron	R$\bar{3}$m	a$_{hex}$=10.9584	c$_{hex}$=23.8546			(44)

Table III.2 Composition, Preparation Techniques and Crystal Data of Binary Nickel Borides

Nominal Composition in at%	Preparation and Heat Treatment	X-ray Phase Analysis	Structure Type	Space Group	Lattice Parameters (Å) a	b	c	β	Volume(Å³)
Ni - B									
87 - 13	cold compacted HF-heat/W-crucible Mo(Ar), 900°C 72 h, B-amorph.	Ni +	Cu-Type	Fm3m	3.5228(7)	-	-		43.720(16)
		Ni₃B	Fe₃C	Pbnm	4.3918(16)	5.2208(21)	6.618 (4)		151.74 (12)
70 - 30	"	Ni₃B +	Fe₃C	Pbnm	4.3920(9)	5.2236(10)	6.616 (1)		151.78 (5)
		Ni₂B	CuAl₂	I4/mcm	4.9917(3)	-	4.2468(5)		105.82 (2)
62 - 38	"	Ni₂B +	CuAl₂	I4/mcm	4.9892(7)	-	4.2449(7)		105.67 (3)
		o-Ni₄B₃	o-Ni₄B₃	Pnma	11.959 (5)	2.9825(4)	6.575 (4)		234.52 (17)
50 - 50 (**)	arc melting HF-heat./W-crucible Al₂O₃(Ar), 900°C 48 h, B-crist.	o-Ni₄B₃ +	o-Ni₄B₃	Pnma	11.987 (6)	2.9915(3)	6.603 (3)		236.77 (15)
		m-Ni₄B₃ +	m-Ni₄B₃	C2/c	6.431 (1)	4.8822(9)	7.820 (2)	103.29(1)	239.0 (8)
		NiB	CrB	Cmcm	2.9288(5)	7.390 (4)	2.9664(9)		64.208(40)
10 - 90	"	NiB +	CrB	Cmcm	2.9318(6)	7.391 (3)	2.9678(9)		64.308(37)
5 - 95	arc melting, 14d 900°C, Mo (Quartz) B-Cristalline	NiB + (ss)β-rh.B	CrB β-Boron	Cmcm R3̄m	2.9334(5) a_hex=10.954(3)	7.393 (4)	2.9697(7) c_hex= 23.85 (3)		64.401(39) 2479(3)

$a_{hex}=10.954(3)$

$c_{hex}=23.85(3)$

(**) after heat treatment (72 h, 900°C) the composition appears to be shifted by ca. 4 at%B towards the nickel side; (loss of boron) thermodynamic equilibrium was not attained
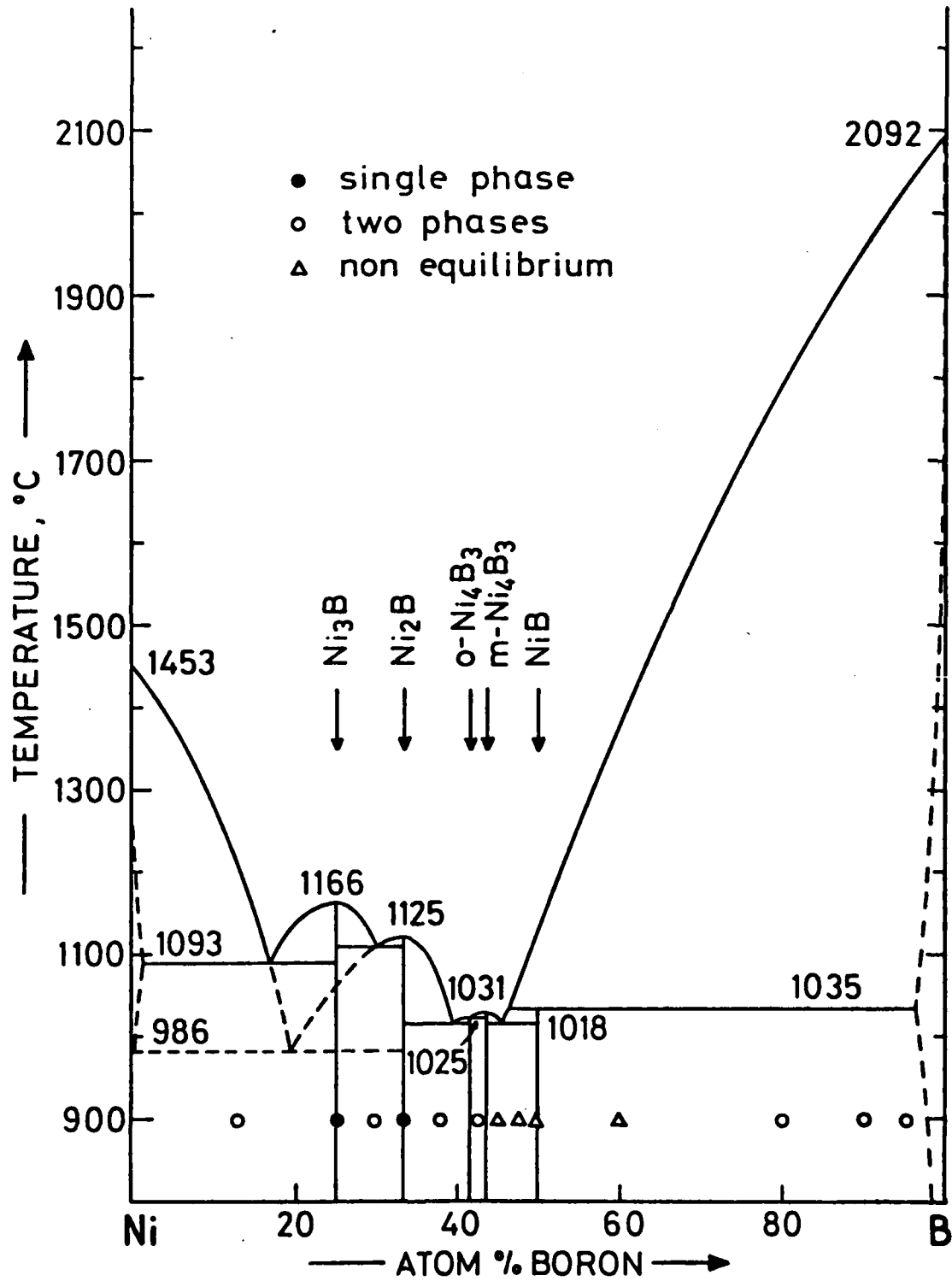
Fig.III.1 Constitutional diagram of the binary system Ni-B and
experimental X-ray phase analysis. Phase equilibria are
based on Schoebel and Stadelmaier (1965), ref.53.

Rapid quenching of liquids nickel-rich suppresses the formation of Ni_3B due to the existence of a metastable eutectic reaction isotherm at 986°C: liquid $\rightleftharpoons$ Ni + Ni_2B. This metastable equilibrium is represented by a dotted curve in Fig.III.1.

Severe doubts exist with respect to the existence of binary compounds such as "Ni_3B_2" and "NiB_2". Both were claimed to exist according to data by (56), however were not confirmed by (53). It is likely that "Ni_3B_2" in fact is identical with one of the Ni_4B_3-phases.

A solubility of 0.3 a/o boron in nickel at 1085°C was accepted in the literature (53).

b) EXPERIMENTS AND RESULTS

Phase equilibria in the nickel-boron binary system have been reinvestigated on a series of 17 binary samples prepared by arc melting as well as by powdermetallurgical sintering and subsequent annealing at 900°C. The experimental results as summarized in Table III.2 confirm the phase relations reported by (53,54). In excellent agreement to the findings of (54) we also conclude a small homogeneous region for o-Ni_4B_3 observed from a small variation of the unit cell dimensions (see Tables III.1,2).

Alloys with compositions between m-Ni_4B_3 and NiB even afer prolonged heat treatment contain o-Ni_4B_3 as tertiary phase in a nonequilibrium state. This behavior results from the kinetically retarded formation of m-Ni_4B_3 and is likewise found within the ternary system Ni-B-N (see below).

X-ray powder analysis and metallography did not reveal any indications of a binary compound "NiB_2". Instead a two phase equilibrium is observed: nickelmonoboride plus a solid solution of small amounts of nickel (< 3 a/o Ni) in β-rhombodral boron.

Considering the variation of the unit cell dimensions of the ss-βrh boron for Fe,Co,Ni at the metal-rich boundary at 900°C, the following sequence is observed $V(Co)<V(Ni)<V(Fe)$, which does not correspond to the normal variation of the metal Goldschmidt radii $R_{Fe}>R_{Co}>R_{Ni}$, suggesting a slightly smaller extent of the solid solubility in case of cobalt. The rhombodhedral symmetry however remains unchanged in all three cases, so does the rhombohedral angle $\alpha_R = 65.3°$.

Characteristic X-ray powder diagrams for easy identification of all binary equilibrium phases are presented in Tables III.3-7.

Table III.3 Powder Diffraction Data for Ni_3B				
(hkℓ)	$10^4 \cdot \sin^2\theta$ obs.	calc.	Intensity obs.	calc.
(011)	*	443	*	0.8
(101)	*	525	*	0.2
(020)	539	542	5	4.0
(111)	660	661	15	15.9
(200)	868	870	2	1.7
(210)	1005	1005	40	41.3
(121)	1066	1067	60	59.1
(201)	1175	1177	30	34.7
(002)	1230	1230	10	8.0
(211)	1313	1313	60	59.7
(220)	1412	1412	80	78.9
(102)	1449	1448	80	81.5
(031)	1528	1528	100	100.0
(112)	1584	1583	70	70.3
(221)	1720	1720	45	45.1
(131)	1745	1745	30	33.1
(022)	1772	1773		3.0
(122)	1001	1990	25	27.0
(230)	2089	2090	15	12.4
(202)	*	2100	*	1.2
(040)	2169	2169	10	8.3
(212)	*	2236	*	0.8
(301)	2265	2265	35	33.5
(231)	*	{ 2398	*	{ 1.1
(311)		2400		2.3
(222)	*	2642	3	3.1
(132)	2669	2668	2	1.4
(141)	2694	2694	5	5.2
(321)	*	2807	*	0.6
(013)	*	2904	*	0.5
(240)	3041	3039	5	5.7
(113)	3121	3121	3	3.1
(302)	*	3187	*	0.2
(232)	3320	3320	3	3.2
(312)	*	3323	*	0.2
(241)	3345	3346	*	0.3
(042)	*	3399	*	0.1
(400)	*	3479	*	0.1
(331)	*	3485	*	0.01
(123)	Ge(331)	3528	c	22.9
(410)	*	3615	*	0.01
(142)	*	3617	*	0.9
(203)	*	3638	*	0.5
(051)	3697	3697	3	3.5
(322)	3730	3730	5	7.2
(213)	3773	3774	3	3.6

Table III.3   continued

(hkℓ)	$10^4 \cdot \sin^2\theta$ obs.	calc.	Intensity obs.	calc.
(410)	3789	3787	20	20.5
(151)	*	⎰ 3914	10	⎰ 7.6
(411)		⎱ 3922		⎱ 5.3
(033)	3988	3988	5	3.6
(420)	4020	4021	5	4.4
(223)	*	4180	*	1.2
(133)	4206	4206	25	25.0
(250)	4259	4259	15	14.8
(242)	*	4269	*	0.1
(421)	*	4329	2	3.5
(332)	4407	4408	40	46.7
(341)	Ge(422)	4434	c	3.2
(251)	4565	4567	20	19.5
(430)	4701	4699	20	20.7
(303)	4723	4725	20	22.9
(152)	*	4837	20	21.5
(412)	*	4845	*	0.2
(233)	*	4858	*	0.3
(313)	*	4861	2	2.4
(060)	4881	4880	10	9.7
(004)	4922	4921	10	10.0

*: Not observed or inaccurate

c: Coincidence with Ge-reflections

Material: Ni_3B, reacted for 72 h at 900°C

Method: powder X-ray diffraction in a
   Guinier camera, $CrK\alpha_1$ radiation

The intensity is normalized to the
   strongest reflection with I= 100.

Space group: Pbnm

Lattice parameters: a= 5.2236 Å, b= 6.6156 Å,
   c= 4.3920 Å

Table III.4 Powder Diffraction Data for Ni_2B

(hkℓ)	$10^4 \cdot \sin^2\theta$ obs.	calc.	Intensity obs.	calc.
(110)	477	476	10	6.8
(200)	952	952	20	16.7
(002)	1313	1316	30	24.4
(211)	1520	1520	100	100.0
(112)	1793	1792	10	6.5
(220)	1905	1905	5	2.9
(202)	2269	2268	20	14.6
(310)	2382	2381	20	13.5
(222)	3222	3221	1	1.0
(312)	3697	3697	10	8.3
(400)	3808	3810	3	2.0
(213)	4151	4151	25	19.7
(330)	4288	4286	10	7.4
(411)	4376	4377	20	18.1
(420)	4763	4762	2	1.4
(402)	5124	5126	5	4.0
(004)	5265	5264	5	3.5
(332)	5602	5602	15	12.9

Material: Ni_2B, reacted for 24 h at 900°C

Method: powder X-ray diffraction in a
Guinier camera, CuKα_1 radiation

The intensity is normalized to the
strongest reflection with I= 100

Space group: I4/mcm

Lattice parameters: a= 4.9917 Å, c= 4.2468 Å

Table III.5 : Powder Diffraction Data for Ni_4B_3

ortho. (hkl)	monocl. (hk l)	$10^4 \times \sin^2 \theta$ obs.	calc.	Intensity obs.	ortho. calc.	monocl. calc.
	(11 0)	401	400	8		8.6
	(00 2)	410	410	5		7.7
	(11-1)	444	446	12		10.9
	(11 1)	Ge(111)	560	c		10.0
(102)		*	587	*	1.1	
(400)		662	661	5	3.5	
	(11-2)	696	696	40		45.4
(202)		711	711	5	5.3	
	(20-2)	787	787	70		67.1
(011)		*	800	*	1.3	
(111)		*	841	*	1.5	
(302)		917	917	5	4.8	
(211)		965	965	15	12.8	
	(02 0)	995	996	3		2.5
	(02 1)	1098	1098	40		37.6
	(11-3)	1151	1150	50		51.9
(311)		1173	1172	10	8.0	
(402)		*	1207	*	1.0	
	(20 2)	1245	1245	95		98.7
(112)		1249	1250	5	5.7	
(103)		1267	1269	6	6.7	
(410)		1325	1325	20	18.2	
(212)		1375	1374	25	25.0	
	(02 2)	1406	1405	100		100.0
(411)		1462	1461	5	4.7	
	(31-1)	1544	1543	50		47.9
(312)		1580	1581	12	11.8	
	(22-1)	1590	1590	10		10.0
(303)		1602	1599	80	10.9	
	(22 0)		1602			73.3
	(31 0)	1613	1613	20		19.3
(601)		1624	1624	15	13.8	
	(00 4)	1640	1639	40		43.6
	(31-2)	1679	1679	20		22.6
	(22-2)	1782	1782	8		5.6
	(20-4)		1787			4.7
	(11-4)	1810	1810	25		24.7

Table III.5 continued

ortho. (hkl)	monocl. (hk l)	$10^4 \times \sin^2\theta$ obs.	calc.	Intensity obs.	ortho. calc.	monocl. calc.
	(22 1)	1819	1819	20		17.5
(511)		1833	1833	10	8.5	
	(31 1)		1887			3.5
(403)		1888	1889	15	4.6	
(013)			1891		5.2	
	(02 3)	1919	1918	7		6.8
(113)		1933	1932	2	2.1	
	(31-3)	2019	2019	5		5.2
(602)		Ge(311)	2034	c	2.5	
(701)		2161	2162	2	2.0	
(104)		2224	2223	1	1.3	
	(22 2)	2242	2241	2		1.9
(313)		2270	2263	10	2.4	
	(11 4)		2269			9.7
(611)		*	2288	*	1.0	
(204)		2345	2347	2	2.5	
	(31 2)	2365	2367	5		3.6
	(40-2)	*	2376	2		2.8
	(40 0)	2423	2425	10		9.2
	(13-1)	2437	2437	10		11.1
(413)		*	2552	*	1.2	
	(31-4)	2564	2564	20		18.0
(702)			2571		2.3	
	(02 4)	2638	2635	5		4.0
(020)		2654	2654	10	9.5	
	(11-5)	*	2675	*		1.5
	(22-4)	2781	2782	5		5.2
(711)		*	2825	*	1.0	
	(22 3)	2869	2868	5		6.5
	(31 3)	3052	3051	5		4.1
	(13-3)	3140	3142	2		1.2
	(11 5)	3246	3248	5		4.4
	(31-5)	3316	3314	20		21.0
(222)		*	3365	*	1.1	
(811)		*	3445	*	1.4	
	(13 3)	*	3486	*		2.2
	(02 5)	*	3557	*		1.6
(322)		*	3572	*	1.2	
	(00 6)	*	3688	*		1.9
	(22 4)	3699	3700	25		24.6

Table III.5 continued

ortho. (hkl)	monocl. (hk l)	$10^4 \times \sin^2\theta$ obs.	calc.	Intensity obs.	ortho. calc.	monocl. calc.
	(11-6)	3744	3745	5		7.4
	(42 1)	*	3752	*		2.4
(305)		*	3781	*	1.0	
	(51-1)	*	3853	*		3.8
(812)		*	3854	*	2.2	
	(51-2)	3879	3874	20		7.0
	(33 1)		3878			16.0
(902)		*	3894	*	1.1	
(713)		*	3916	*	1.4	
(123)		*	3923	*	2.3	
	(04 0)	*	3982	*		2.6
	(33-3)	4010	4010	30		32.8
	(51 0)	4038	4038	5		5.6
(405)		*	4071	*	1.5	
(015)		*	4073	*	3.2	
	(04 1)	4083	4085	5		8.4
	(51-3)	4098	4100	15		16.0
(115)		*	4114	*	3.2	
	(42-4)	*	4142	*		1.1
(911)		*	4148	*	2.7	
(323)		*	4254	*	4.5	
	(31-6)	*	4269	*		2.3
(621)		*	4279	*	5.8	
	(42 2)	*	4289	*		9.3
(614)		*	4334	*	7.6	
	(04 2)	4394	4392	10		7.9
	(51 1)	4428	4427	15		14.1
	(11 6)	*	4433	*		3.6
	(51-4)	*	4530	*		2.7
(813)		*	4536	*	2.0	
(423)		*	4543	*	2.2	
	(24-1)	*	4576	*		3.2
	(24 0)	4587	4588	5		7.3
	(22-6)	*	4602	*		2.5
	(13-5)	4665	4666	20		19.8
	(02 6)	4684	4684	5		5.8
(622)		*	4688	*	1.3	
	(22 5)	*	4736	*		3.5
	(40-6)	*	4737	*		1.9
	(24-2)	*	4769	*		3.3

Table III.5 continued

ortho. (hkl)	monocl. (hk l)	$10^4 \times \sin^2\theta$ obs.	calc.	obs.	Intensity ortho. calc.	monocl. calc.
	(24 1)	*	4805	5		6.3
(721)		*	4816	*	1.1	
	(42-5)	*	4835	*		1.3
	(04 3)	*	4904	*		3.0
(1011)		*	4933	*	2.6	
	(40 4)	4981	4982	20		9.8
	(20 6)		4983			10.7

*: Not observed or inaccurate
c: Coincidence with Ge-reflections
Material: $Ni_{45}B_{55}$, arc melted
Method: powder X-ray diffraction in a Guinier camera,
    $CuK_\alpha 1$ radiation.
The intensity I is normalized to the strongest reflection
    with: I= 25.0 for ortho. – Ni_4B_3 and
            I= 100.0 for monocl. – Ni_4B_3 .
Reflections weaker than 1% were omitted.
Space groups: Pnma for ortho. – Ni_4B_3
         and C2/c for monocl. – Ni_4B_3.
Lattice parameters: ortho. – Ni_4B_3 : a= 11.981 Å,
                                          b= 2.9902 Å,
                                          c= 6.5962 Å;

    monocl. – Ni_4B_3 :   a= 6.4295 Å,
                            b= 4.8826 Å,
                            c= 7.8199 Å,
                     Beta= 103.30°.

Table III.6 Powder Diffraction Data for NiB

(hkℓ)	$10^4 \cdot \sin^2\theta$ obs.	calc.	Intensity obs.	calc.
(020)	*	435	*	4.6
(110)	800	800	40	41.2
(021)	1108	1109	80	85.3
(111)	1475	1474	100	100.0
(130)	1668	1669	50	56.2
(040)	1736	1738	20	20.6
(131)	2343	2343	15	15.8
(041)	2413	2412	10	12.3
(002)	2698	2697	20	17.0
(200)	2765	2765	15	16.3
(022)	*	3131	*	0.7
(220)	*	3199	*	0.7
(150)	*	3407	*	0.2
(112)	3497	3496	10	9.4
(221)	3874	3874	20	24.4
(060)	*	3911	*	3.1
(151)	4080	4081	20	22.3
(132)	4365	4365	20	24.0
(042)	Ge(422)	4435	c	9.1
(240)	4504	4503	10	8.9
(061)	4586	4585	5	7.3
(241)	5178	5177	5	7.5
(202)	5459	5461	10	11.5

*: Not observed

c: Coincidence with Ge-reflections

Material: NiB, reacted at 900°C for 72 h

Method: powder X-ray diffraction in a
Guinier camera, CuKα_1 radiation

The intensity is normalized to the
strongest reflection with I= 100.

Space group: Cmcm

Lattice parameters: a= 2.9298 Å, b= 7.3906 Å
c= 2.9667 Å

Table III.7 Powder Diffraction Data for Ni_5B_{95}

(hk l)	$10^4 \times \sin^2\theta$		Intensity	
	obs.	calc.	obs.	calc.
(10 1)	*	76	*	1.8
(00 3)	*	94	*	1.7
(01 2)	106	108	20	26.5
(11 0)	197	198	50	47.9
(10 4)	233	233	100	100.0
(02 1)	274	274	5	6.0
(11 3)	292	292	1	1.8
(20 2)	305	306	5	5.0
(01 5)	*	327	*	2.5
(00 6)	375	376	40	39.6
(21 1)	472	472	70	67.3
(12 2)	*	503	*	1.0
(20 5)	525	525	2	2.8
(11 6)	*	573	*	2.6
(10 7)	577	577	3	2.8
(30 0)	594	594	2	3.3
(21 4)	628	629	3	4.1
(30 3)	687	687	10	13.0
(12 5)	721	722	15	13.1
(02 7)	773	775	30	30.8
(00 9)	*	845	*	2.3
(13 1)	868	868	2	2.8
(22 3)	889	889	2	2.1
(31 2)	898	899	5	5.8
(20 8)	*	931	*	2.2
(30 6)	968	969	10	10.8
(13 4)	1023	1024	30	33.7
(11 9)	1044	1043	3	2.7
(40 1)	1066	1066	2	1.3
(04 2)	1098	1097	15	14.9
(12 8)	1129	1129	5	5.2

Table III.7 continued

(hk l)	$10^4 \times \sin^2\theta$ obs.	calc.	Intensity obs.	calc.
(40 4)	1223	1222	20	22.9
(32 1)	1265	1264	1	2.4
(0210)	1309	1307	5	7.7
(0111)	1328	1328	10	8.6
(41 0)	*	1385	*	3.6
(32 4)	1420	1420	5	5.6
(30 9)	1439	1439	10	8.7
(41 3)	NiB	1479	c	9.6
(0012)	*	1502	*	1.1
(2110)	*	1505	*	2.2
(23 5)	*	1514	*	9.1
(31 8)	*	1525	*	5.0
(2011)	*	1526	*	3.2
(40 7)	1565	1566	3	4.2
(05 1)	*	1659	*	2.4
(1112)	*	1700	*	1.5
(1211)	*	1724	*	1.3
(41 6)	1762	1761	2	3.4
(33 0)	1781	1781	10	13.2
(05 4)	*	1816	*	2.5
(1013)	*	1829	*	1.9
(24 1)	*	1857	*	3.8
(33 3)	1875	1875	10	12.9
(1310)	1900	1901	5	4.9
(50 5)	1910	1910	10	7.2
(23 8)	1921	1921	30	34.7
(24 4)	*	2014	*	3.5
(0213)	2028	2027	10	10.6
(15 2)	*	2086	*	2.4
(3012)	2095	2096	10	9.4
(4010)	*	2098	*	5.7
(42 5)	*	2107	*	3.6
(3111)	2117	2120	10	7.9
(51 4)	2210	2211	5	8.6

Table III.7 continued

(hk l)	$10^4 \times \sin^2\theta$ obs.	calc.	Intensity obs.	calc.
(2212)	*	2294	*	1.7
(0411)	*	2317	*	1.2
(24 7)	*	2358	*	2.5
(43 1)	*	2451	*	3.7
(60 3)	2470	2468	20	23.2
(42 8)	*	2514	*	1.3
(2311)	2513	2515	3	6.9
(1115)	*	2545	*	3.0
(51 7)	*	2556	*	3.4
(43 4)	*	2607	*	4.2
(1016)	*	2736	*	1.8
(60 6)	*	2750	*	6.5
(4013)	2819	2818	10	10.2
(16 1)	2845	2846	2	5.4
(2410)	2888	2890	10	12.8
(3114)	*	2902	*	8.9
(5011)	*	2911	*	1.1
(0216)	2934	2934	5	5.4
(3015)	2940	2941	10	16.2
(52 6)	*	2948	*	2.9
(43 7)	*	2951	*	5.5
(5110)	*	3088	*	2.1
(61 5)	*	3097	*	6.7
(0414)	*	3100	*	3.4
(34 8)	3106	3108	10	14.4
(4211)	*	3109	*	5.8
(44 0)	3165	3166	5	6.9
(60 9)	*	3219	*	3.0
(35 1)	*	3242	*	2.3
(44 3)	3262	3260	5	9.2
(54 2)	*	3273	*	5.2
(3312)	*	3283	*	5.8
(1511)	*	3307	*	2.7
(16 7)	*	3347	*	1.2

Table III.7   continued

(hk l)	$10^4 \times \sin^2\theta$		Intensity	
	obs.	calc.	obs.	calc.
(35 4)	*	3399	*	3.6
(70 4)	*	3399	*	3.4
(25 9)	*	3417	*	2.4
(1217)	3478	3476	5	5.0
(07 5)	*	3492	*	4.6
(61 8)	*	3504	*	9.2
(1316)	*	3528	*	3.5
(1118)	*	3578	*	1.1
(2413)	3608	3610	5	5.7
(5014)	*	3693	*	1.0
(3411)	*	3702	*	2.1
(4016)	*	3726	*	1.7
(35 7)	3735	3743	2	4.8
(1019)	3832	3832	2	2.2
(71 3)	*	3853	*	7.1
(6012)	*	3876	*	2.1
(62 7)	3947	3941	2	1.9
(3018)	*	3973	*	1.9
(4419)	*	4011	*	1.0

*: Not observed
c: Coincidence with Nib reflections
Material: Ni_5B_{95}, arc melted.
Method: powder X-ray diffraction in
 a Guinier camera, $CuK\alpha1$ radiation.
The intensity is normalized to the
 strongest reflection with I= 100.
Reflections with Int.(calc.) $<$ 1.0 %
 were omitted.
(Space group: $R\bar{3}m$
 Lattice parameters: a= 10.158 Å,
 Alpha= 65.25°.   )
 hexagonal setting: a= 10.952 Å,
 c= 23.85 Å.

IV THE BINARY SYSTEM: IRON - NITROGEN

LITERATURE

A partial metastable phase diagram of the system Fe-N was recently critically assessed by O.Kubaschewski-von Goldbeck (14) and is presented in Fig.IV.1. Three binary nitrides have been characterized: $Fe_{16}N_2$, Fe_4N (19.6 to 19.95 a/o N) and ε, ζ-Fe_2N. As far as the nitrogen solubility in α, γ, δ and liquid iron is concerned, the following equations have been assembled (71,72) for the reaction $1/2\ N_2 = [N]$ Fe:

N in α, δ-Fe (25-1536°C): $\log c(\text{at\%N}) = -1700\ T^{-1} - 0.30$

N in γ-Fe (590 to 1050°C): $\log c = 155\ T^{-1} - 1.1$

N in ℓ-Fe   : $\log c = -457\ T^{-1} - 0.5$

A detailed compilation of the solubility data in combination with thermo-dynamic data is presented by (71).
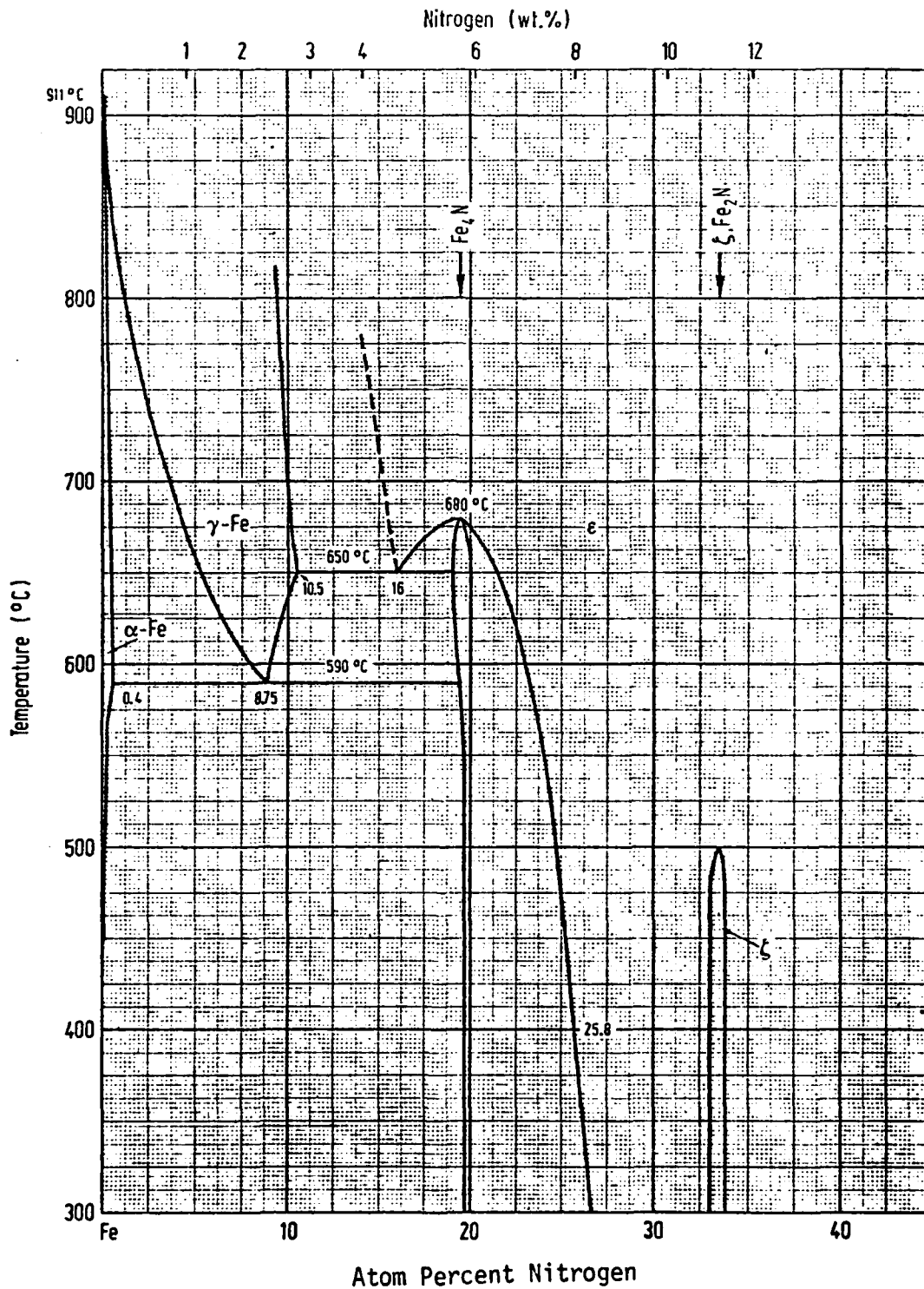
Fig.VI.1. Phase relations (metastable) in the binary system: Fe-N
(after Kubaschewskii-von Goldbeck, ref.14)

V THE BINARY SYSTEM: COBALT - NITROGEN

LITERATURE

No binary phase diagram Co-N is available in the literature, however the existence of five cobalt-nitrides has been reported (69): Co_4N, hexagonal Co_3N (stable from 7.7 to 8 wt%N; a= 2.663, c= 4.360), orthorhombic Co_2N (stable at 10.71 wt%N), Co_2C-type, a= 2.848, b= 4.636 and c= 4.339), CoN and Co_3Ni_2 (12). All cobalt nitrides easily decompose on heating at 276°C in vacuum (12). At pressures p < 760 Torr and up to 1200°C N was found to be practically insoluble (71) in Co. The solubility of N in liquid cobalt is rather small and within the temperature range of 1550°C to 1700°C obeys the equation (70):

$$\log c = 1/2 \log p - 2.0 - 2190/T \ .$$

Thermodynamic data for the solubility of N in liquid Co are presented by the same authors (70) as follows: (1550°C-1700°C)

$$1/2 \ N_2 = N \ in \ \ell\text{-Co} : \Delta G° = 10.000 + 11.7 \ T$$

VI THE BINARY SYSTEM NICKEL - NITROGEN

LITERATURE

No binary phase diagram Ni-N has been prepared yet.

The early literature on nickel-nitrides mentiones the preparation of nickel-azides such as Ni_3Ni_2 and $Ni(N_3)_2$ (ref.69).

Juza and Sachsze (12) reported about the formation of hexagonal Ni_3N (a= 2.66, c= 4.34 $\overset{o}{A}$); thermodynamic decomposition of this compound to normal Ni was said to start at 480°C on heating in vacuum.

From electron diffraction data it was concluded that the dilated fcc-ss(Ni,N) with a= 3.72 $\overset{o}{A}$ in fact is Ni_4N (69). However Ni_4N formed at 230-240°C was later reported to be tetragonal with a= 3.72 and c= 7.28 $\overset{o}{A}$ (69).

The solubility of nitrogen in nickel at 445°C amounts to less than 0.3 a/o Ni(12). The solubility of N in liquid Ni is rather small and within the temperature region 1550-1700°C follows the equation:

$$\log c = 1/2 \log p - 2.45 - 2340/T \quad (70).$$

Thermodynamic data available for the solubility of N in Ni are given by the same authors (70) as follows 1550°C-1700°C

$$1/2 \; N_2 = N \text{ in } \ell\text{-Ni} : \Delta G° = 10700 + 13.7 \; T$$

B) TERNARY SYSTEMS M-B-N

I) THE TERNARY SYSTEM IRON-BORON-NITROGEN

a) CRITICAL LITERATURE REVIEW

Kiessling (59) investigated the thermal stability of binary iron borides in a stream of dry ammonia at temperatures below 768°C.

His results are presented in Table I.1 and show the decomposition of the binary iron-borides Fe_2B, FeB into the various iron-nitrides and boronnitride according to the formation of stable two-phase equilibria between the ironnitrides and boronnitride, as well as between the ironborides and boron-nitride. No ternary iron-boronnitrides were encountered, but great differences were observed among the iron-borides in their stability against attach by ammonia, the resistance being higher for the higher boride. The lattice parameters obtained, indicate that no B is in solution in the nitrides nor nitrogen in the borides.

Fountain (67) determined the solubility of nitrogen in iron-rich iron-boron alloys (0.001 to 0.91 % B) by the Sievert's technique in the temperature range from 950°C to 1150°C. Partial phase diagrams of the iron-rich corner of the Fe-B-N system were established at 950°C, 1050°C and at 1150°C under 1 atm N gas and are presented in Fig. B1a,b,c. At all temperatures employed a stable two-phase equilibrium was observed between ss-(Fe) and hexagonal boronnitride.

An electron microscopic study of the ss-hex-BN particles (thin flakes extracted from the alloy in a solution of 5 pct HNO_3-25 pct HCℓ-70 pct alcohol) revealed a lack of threedimensional perfection due to stacking faults and random displacement of the graphite layers perpendicular to the c-axis, but with unaffected intensities of the (hk0) reflections (see also (68)).

The lattice parameters of ss-h-BN (a= 2.504, c= 6.68 Å), at 1050°C indicate a small solubility of Fe in BN as compared to pure BN with a= 2.504, and c= 6.661 Å. Similarly the solubility of nitrogen in Fe_2B was small as can be judged from the unit cell dimensions presented by Fountain (a= 5.103, c= 4.244)
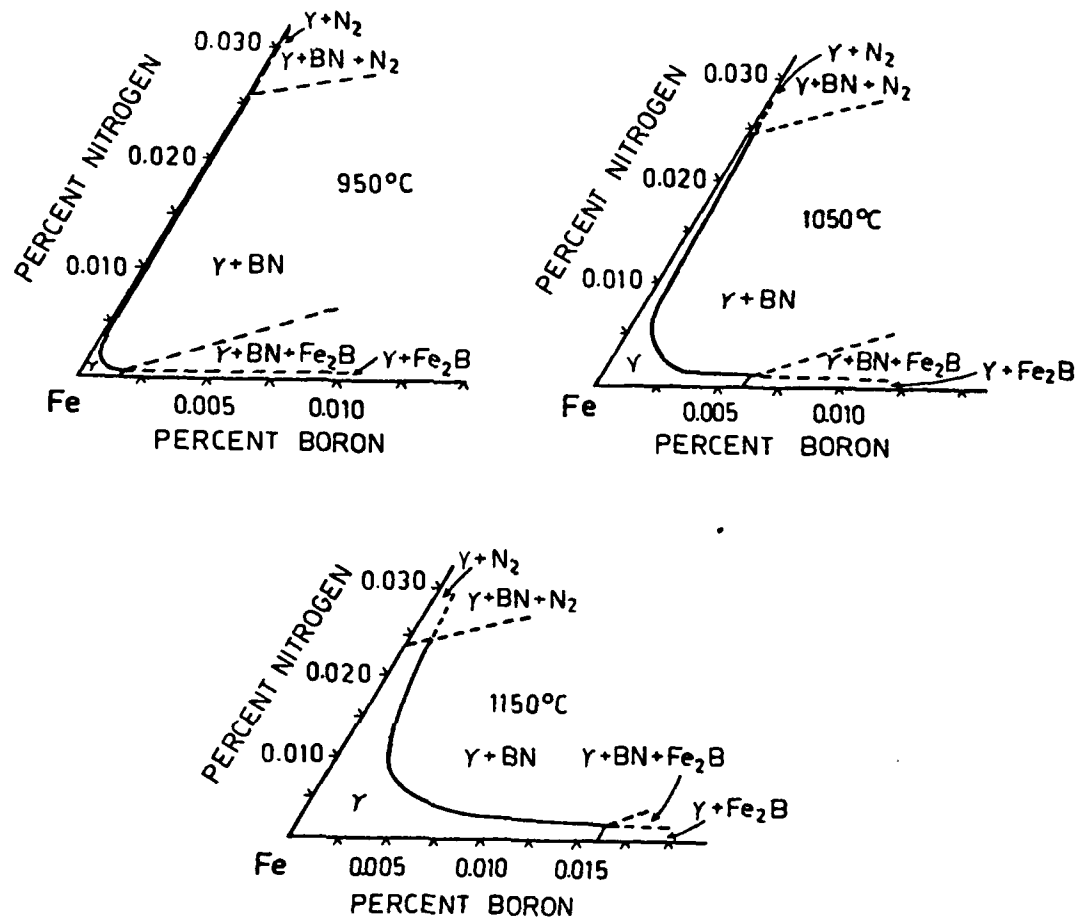
Fig.B.I.1 Phase equilibria in the iron rich corner of the ternary
system Fe-B-N at different temperatures: a) 950°C,
b) 1050°C and c) at 1150°C; after Fountain et al., ref.67.

Table B.I.1   Phases present after nitriding Fe borides in a dry ammonia
stream; 10 h; specimens quenched from reaction temperature
(After Kiessling and Liu (59)).

Fe-B-N* initial boride	Fe_2B	FeB
Temperature, °C	Products	
352	Fe_2B	FeB
400	ζ + BN	FeB + ζ + BN(?)
448	ε + BN	-
505	ε + μ' + BN	-
550	μ' + ε + BN	μ' + ε + BN
602	α-Fe + μ' + (ε) + BN	μ' + ε + α-Fe + BN
702	α-Fe + BN	-
768	α-Fe + BN	α-Fe + BN

* Phases stated in order of decreasing amount but BN always last; lattice
  dimensions indicate that no B is in solution in the nitrides, nor N in
  the borides; Greek letters under Fe-B-N denote the known iron nitrides.

in comparison to his data for binary iron-rich Fe_2B (a= 5.099, c= 4.240 Å).

b) EXPERIMENTS AND RESULTS

Phase equilibria in the ternary system Fe-B-N at 900°C (see Fig.B.I.2) were determined by X-ray diffraction analysis of about 15 ternary cold-compacted powder mixtures (Fe + B + BN) which subsequently were heat treated in a HF-furnace with a tungsten crucible as susceptor material under 1 atm of high purity 6N-argon on molybdenum or BN-substrates. Annealing for 48 hrs was generally sufficient to obtain thermodynamic equilibrium. The results of the X-ray phase analysis for a series of characteristic samples are presented in Table B.I.2.

According to the phase relations obtained in Fig.B.I.2, iron and all binary iron-borides at 900°C are in stable thermodynamic equilibrium with hexagonal BN. Iron monoborides in all samples revealed the powder pattern of T-FeB (see section: the binary system Fe-B).

The unit cell dimensions of the boundary phases in multiphase alloys obviously correspond to the binary data within the error bars of the least squares extrapolation. It is thus concluded that practically no nitrogen (< 0.5 a/o N) is soluble in the binary iron borides.

The crystallographic data of the hex-ss-BN (see Table B.I.2) as compared to pure BN (a= 2.505, c= 6.680 Å) however indicate a small but significant solubility of iron between the covalently bonded graphite layers; Phase equilibria at 1250°C remain unchanged except for the appearance of an extended liquid region adjacent to the low melting binary iron-boron eutectic (Fe + Fe_2B). Thus from the above mentioned data, compatibility is observed between iron, the iron-borides, and hexagonalboronnitride with only a very limited mutual solid solubility. Alloys along the isopleth Fe - BN from 20 to 50 mol% BN appear to be melted at 1250°C under 1 atm Ar. The reguli show a phase separation
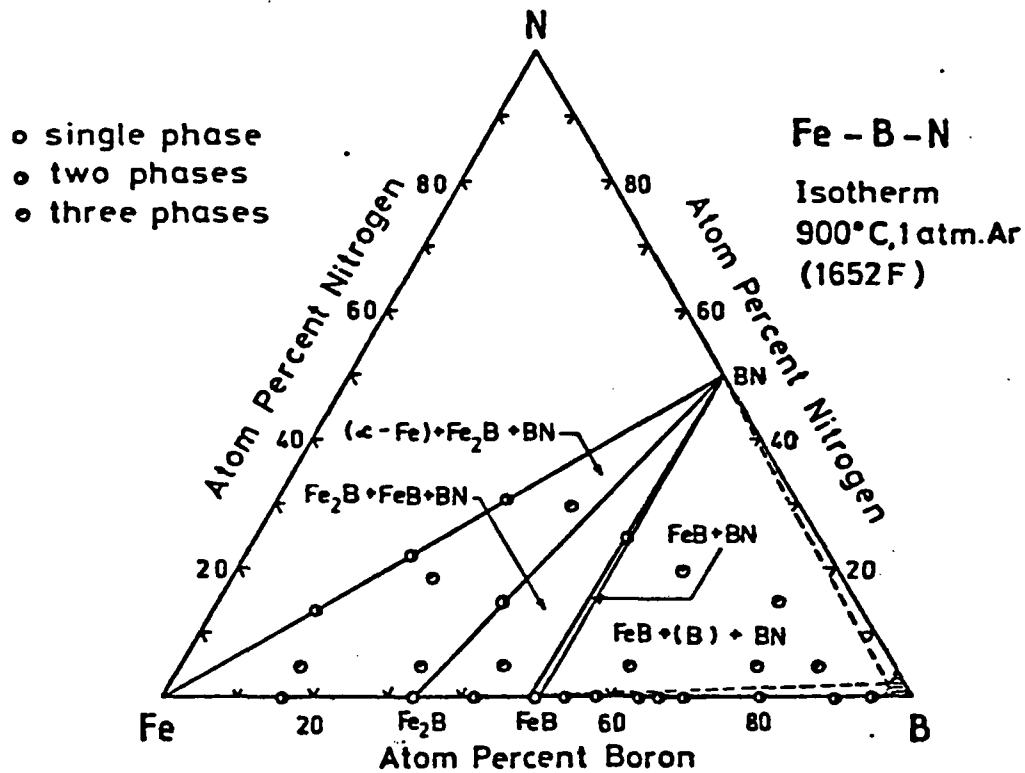
Fig.B.I.2 Phase Equilibria in the ternary system Fe-B-N, isothermal section at 900°C and 1 atm. argon.

Table B.I.2 Composition, Preparation Techniques and Crystal Data of Ternary Alloys Fe-B-N

Nominal Composition in at%	Preparation and Heat Treatment	X-ray Phase Analysis (*)	Structure Type	Space group	Lattice Parameters (Å)			Volume (Å³)
					a	b	c	
Fe - B - N								
79 - 16 - 5	cold compacted HF-heat/W-crucible Mo(Ar), 900°C, 72 h, B-amorph.	Fe + Fe₂B	W-Type CuAl₂	Im3m I4/mcm	2.865(1) 5.107(2)	– –	– 4.249(2)	23.52(2) 110.81(9)
63 - 32 - 5	. .	Fe₂B + traces Fe	CuAl₂	I4/mcm	5.107(2) n.d.	–	4.249(2)	110.80(8)
52 - 43 - 5	. .	Fe₂B + T-FeB	CuAl₂ T-FeB	I4/mcm	5.107(2) 4.059(1)	– 5.500(2)	4.246(2) 2.948(1)	110.75(11) 65.81(3)
35 - 60 - 5	. .	T-FeB	T-FeB		4.059(2)	5.497(3)	2.948(1)	65.78(5)
18 - 77 - 5	. .	T-FeB + traces B	T-FeB		4.058(1) n.d.	5.498(3)	2.948(1)	65.76(4)
10 - 85 - 5	. .	T-FeB + β-Boron	T-FeB		4.060(1) n.d.	5.498(4)	2.946(1)	65.75(5)
10 - 75 -15	. .	T-FeB + β-Boron	T-FeB		4.062(1) n.d.	5.500(1)	2.948(1)	65.86(3)

(*) All samples contained small amounts of hex.-BN in thermodynamic equilibrium (a= 2.504, c= 6.671)

n.d. not determined

of a metal rich liquid and a porous body of ss-hex BN. Due to a rather high

surface tension, the metal-rich part is found to adopt almost spherical

shape when above the soft and porous substrate of light colour. X-ray

analysis of the powdered spherical droplets interestingly revealed the

existence of a cubic phase whose lattice parameters, X-ray intensities and

extinctions prove isotypism with the structure type of $Cr_{23}C_6$ (tau phase).

An X-ray powder intensity calculation (see Table B.I.3) confirmed the crystal

symmetry and atom arrangement suggesting a formula $Fe_{23}(B,N)_6$. The new compound

however is probably metastable as heat treatments at different temperatures

do not produce this compound in solid state equilibrium. Due to the metastable

character the new phase is never encountered in single-phase condition but

accompanied by varying amounts of α-Fe and BN. The unit cell dimensions of

m-$Fe_{23}(B,N)_6$ are significantly larger than binary metastable $Fe_{23}B_6$ (for

comparison see Table B.I.4) and suggest a boron/nitrogen ratio of $B/N > 4$.

Table B.I.3 Powder Diffraction Data for
$Fe_{23}(B,N)_6$

(hkl)	$10^4 \times \sin^2\theta$		Intensity	
	obs.	calc.	obs.	calc.
(111)	*	343	*	2.9
(200)	*	457	*	0.1
(220)	*	915	*	0.4
(311)	1258	1258	3.4	2.6
(222)	1370	1372	9.6	1.3
(400)	1826	1829	12.5	10.6
(331)	2172	2172	4.8	1.8
(420)	2287	2287	36.9	40.1
(422)	2745	2744	44.3	48.3
(333)	3091	3087	170.0	100.0
(511)		3087		69.8
(440)	3656	3659	42.3	36.7
(531)	4006	4002	46.3	46.1
(442)	4114	4116	27.2	6.7
(600)		4116		18.1
(620)	4570	4573	6.2	4.9
(533)	4912	4916	5.1	8.0
(622)	5032	5031	16.5	14.7
(444)	*	5488	*	0.2
(551)	*	5831	*	0.2
(711)	*	5831	*	2.5
(640)	5946	5945	1.7	1.2
(642)	*	6403	*	0.0
(553)	*	6745	*	0.7
(731)	*	6745	*	0.0
(800)	7319	7317	11.1	17.5
(733)	*	7660	*	0.0
(644)	7778	7774	14.8	19.7
(820)		7774		6.5
(660)	8228	8232	57.3	80.2
(822)		8232		21.5
(555)	8575	8575	36.0	16.9
(751)		8575		58.1
(662)	*	8689	*	2.0
(840)	9146	9146	24.4	43.6
(753)	c	9489	c	33.4
(911)	c	9489	c	50.2
(842)	*	9604	*	5.8

*: Not observed or inaccurate
c: Coincidence with Fe and BN reflections
Material: $Fe_{94}BN_{19}$, reacted for
    15 h at 1300° C
Method: powder X-ray diffraction in a
    Powder-Diffractometer, CrK_α radiation
The intensity is normalized to the
    strongest reflection with I= 170.0
Space group: Fm3m
Lattice parameter: 10.7070 Å.

Table BI4 TERNARY BORONNITRIDES WITH $Cr_{23}C_6$-TYPE, Fm3m, Z= 4

$Fe_{23}B_6$ (extr.)	10.69 Å	$Co_{23}B_6$ (extr.)	10.493	$Ni_{23}B_6$ (extr.)	10.48
$m-Fe_{23}B_6$	10.67-9	$m-Co_{23}B_6$	11.05		
$Fe_{23}(B_{.5}C_{.5})_6$	10.617	"$Co_{11}B_2C$"	10.47(1)		
$m-Fe_{23}(B,N)_6$	10.707(1)	$m-Co_{23}(B,N)_6$	10.483(2)	$m-Ni_{23}(B,N)_6$	10.448(2)

c) PHASE RELATIONS IN THE TERNARY SYSTEM IRON-BORON-NITROGEN

UNDER TECHNICAL CONDITIONS

The phase relations in the ternary system Fe-B-N have been also checked under technical conditions i.e. graphite as technical crucible material under 1 atm of technical argon containing 0.01% O_2 and 0.02% N_2.

X-ray analysis of samples annealed at 900°C for 48 hrs under the above mentioned conditions gave evidence for the existence of a ternary compound especially in the region Fe - Fe_2B - BN, Lattice parameters, X-ray powder intensities and the observed extinctions indicate structural analogy with the structure type of Fe_3C. A second series of samples independently annealed in graphite crucibles however under high purity 6N argon failed to produce a cementite phase. The stabilization of this compound is thus likely to be caused by the small oxygen-content of the technical argon via a gasphase-transport reaction where oxygen reacts first with the hot graphite crucible material to form carbonoxide which in turn is cracked at the hot sample surface and by this traces of carbon are likely to be effective in stabilizing a metastable ternary-compound with a suggested formula of $Fe_3(B,C,N)$. Due to the extremely small differences in the scattering factors of the nonmetal atoms, the X-ray analysis is incapable of determining the relative amounts of B,N and C. A comparison of the unit cell dimensions of the new compound (a= 4.459(1), b= 5.347(3), c= 6.664(3), V= 158.90(11)) with those obtained by Borlera (38) from the solid solution range $Fe_3B_xC_{1-x}$ allows for a rough estimate of a B/C ratio equal to 5:1, not taking into account the amount of lattice expansion due to the larger nitrogen atoms.

The phase equilibria resulting under technical conditions are represented in Fig.B.I.3 and samples in the encircled area denoted as $\emptyset$ were observed to contain the $Fe_3(B,C,N)$-phase as the bulk material.

The crystallographic data of these binary compounds prepared under
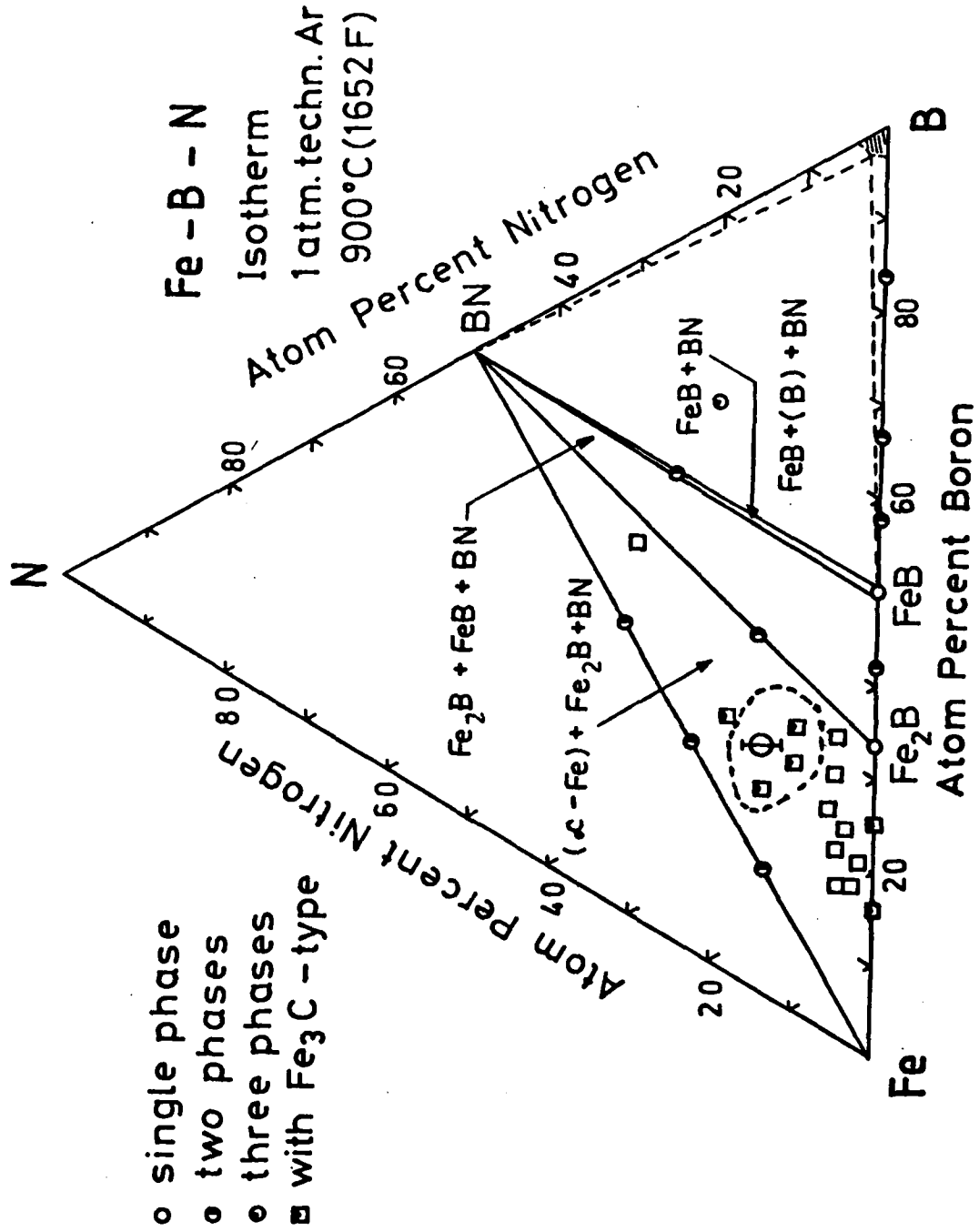
Fig.B.I.3 Phase equilibria in the ternary system Fe–B–N, under technical conditions, isothermal section at 900°C and 1 atm. technical argon, graphite susceptor material.

Table B.I.5 continued

(hkl)	$10^4 \times \sin^2 \theta$ obs.	calc.	Intensity obs.	calc.
(312)	*	7065	*	0.1
(232)	7129	7134	1	2.2
(241)	*	7223	*	0.2
(400)	*	7342	*	0.1
(123)	7570	7579	20	17.6
(203)	*	7774	*	0.4
(142)	*	7826	*	0.7
(322)	7941	7951	5	6.6
(401)		8002		18.9
(051)	8030	8047	25	3.1
(213)		8070		3.3
(411)	8286	8297	5	5.6
(151)	8495	8506	10	8.6
(420)		8524		5.0
(033)	8585	8598	3	4.2
(223)	8948	8956	2	1.6
(133)	9048	9057	40	38.9
(421)	9177	9184	5	6.2
(242)	*	9202	*	0.1
(250)	9215	9222	20	26.2
(332)	9415	9428	100	100.0
(341)	9506	9517	10	7.8

*: Not observed
Material: $Fe_{67}B_{18}N_5$, reacted for 120 h
   at 900° C in a graphite crucible.
Method: powder X-ray diffraction in a
   Debye-Scherrer camera, CrKa radiation.
The intensity I is normalized to the
   strongest reflection with I= 100.0
Space group: Pbnm
Lattice parameters: a= 5.347 Å,
   b= 6.664 Å, c= 4.459 Å.

Table B.I.5 Powder Diffraction Data for Fe₃(B,C,N)

(hkl)	$10^4 \times \sin^2 \theta$ obs.	calc.	Intensity obs.	calc.
(011)	*	955	*	0.3
(101)	*	1119	*	0.1
(020)	1181	1182	5	1.7
(111)	1413	1414	1	7.7
(200)	*	1835	*	0.8
(210)	2126	2131	3	18.4
(121)	2295	2301	30	24.3
(201)	2496	2495	10	14.8
(002)	2640	2639	2	3.2
(211)	2791	2791	20	24.6
(220)	3018	3017	30	32.1
(102)	3092	3098	30	33.0
(031)	3316	3319	30	38.9
(112)	3389	3394	30	28.3
(221)	3672	3677	25	17.8
(131)	3780	3778	15	12.8
(022)	*	3821	*	1.2
(122)	4278	4280	15	10.7
(202)	*	4475	*	0.5
(230)	4491	4495	10	4.9
(040)	4718	4728	5	3.4
(212)	*	4770	*	0.3
(301)	4788	4790	10	14.3
(311)	*	5085	*	1.0
(231)	*	5155	*	0.4
(222)	5641	5657	1	1.4
(132)	5753	5758	1	0.7
(141)	5836	5846	2	2.4
(321)	*	5972	*	0.3
(013)	*	6234	*	0.2
(240)	6555	6563	2	3.2
(113)	6691	6693	2	1.8
(302)	*	6769	*	0.1

technical conditions are also presented in Table B.I.5 in comparison

... ... synthesized under "pure" conditions.
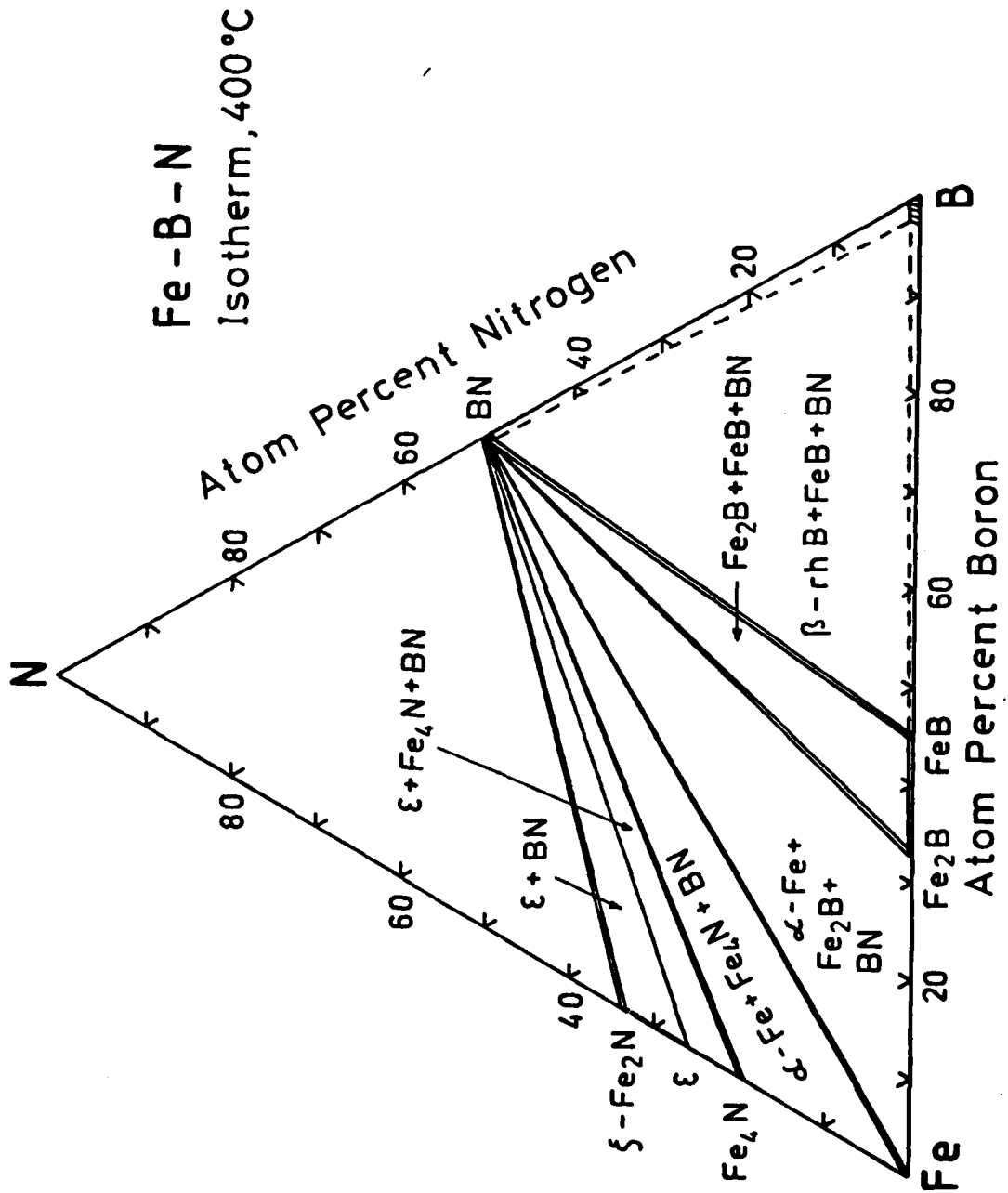
Fig.B.I.4 Phase equilibria in the ternary system Fe-B-N, isothermal section at 400°C derived from data by Kiessling and Liu,
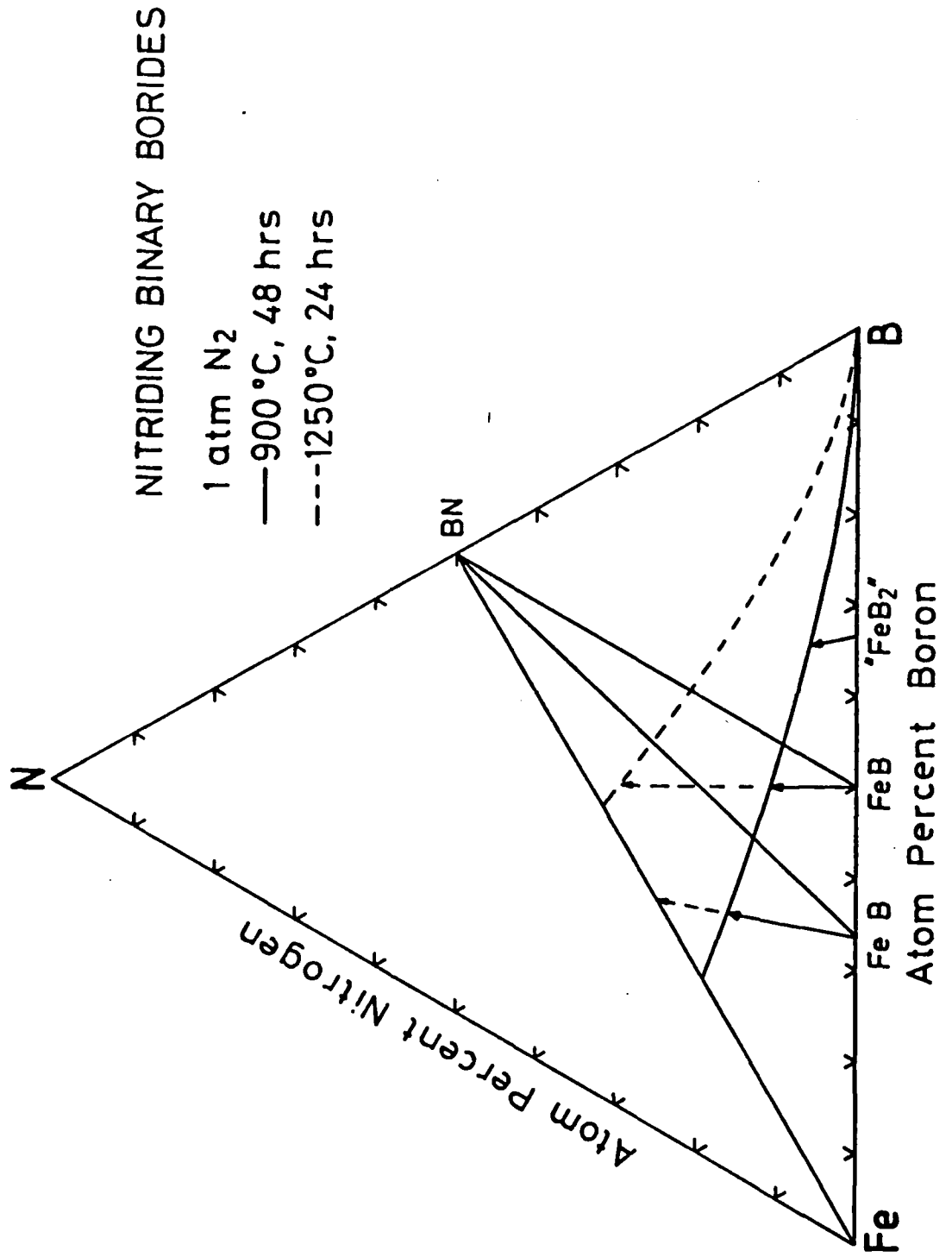
Fig.B.I.5 Nitriding of binary iron-borides under pure nitrogen;
arrows indicate amount of nitrogen take up.

II THE TERNARY SYSTEM COBALT-BORON-NITROGEN

a) CRITICAL LITERATURE REVIEW

No X-ray or phase diagram studies of the system cobalt-boron-nitrogen are known in the literature.

b) EXPERIMENTS AND RESULTS

Phase equilibria in the ternary system Co-B-N at 900°C (see Fig. $\overline{II}$,1) were determined by X-ray diffraction analysis of about 15 ternary alloys. For details of preparation see Fe-B-N.

The results of the X-ray phase analysis for a series of characteristic samples are presented in Table B,II,1. Similar to the system Fe-B-N and according to the phase relations obtained in Table B.II.1, Fig.II.1 cobalt and all binary cobalt-borides at 900°C are in stable thermodynamic equilibrium with hexagonal boronnitride. The formation of Co_3B in ternary alloys appears to be kinetically retarded as already the case in the Co-B binary.

The unit cell dimensions of the boundary phases in multiphase alloys obviously corresponds to the binary data within the error bars of the least squares extrapolation. It is thus concluded that practically no nitrogen (< 0.5 a/o N) is soluble in the binary cobalt borides. The crystalographic data of the hex-ss-BN (see Table B.II.1) as compared to pure BN (a= 2.505, c= 6.660 $\overset{o}{A}$) however indi_ate a small but significant solubility of cobalt between the covalently bonded graphite layers.

Phase equilibria at 1250°C remain unchanged except for the appearance of an extended liquid region adjacent to the low melting binary eutectic Co + Co_3B.

Thus from the above mentioned data, compatibility is observed between cobalt, the cobalt borides, and boronnitride with only a very limited mutual solid solubility.
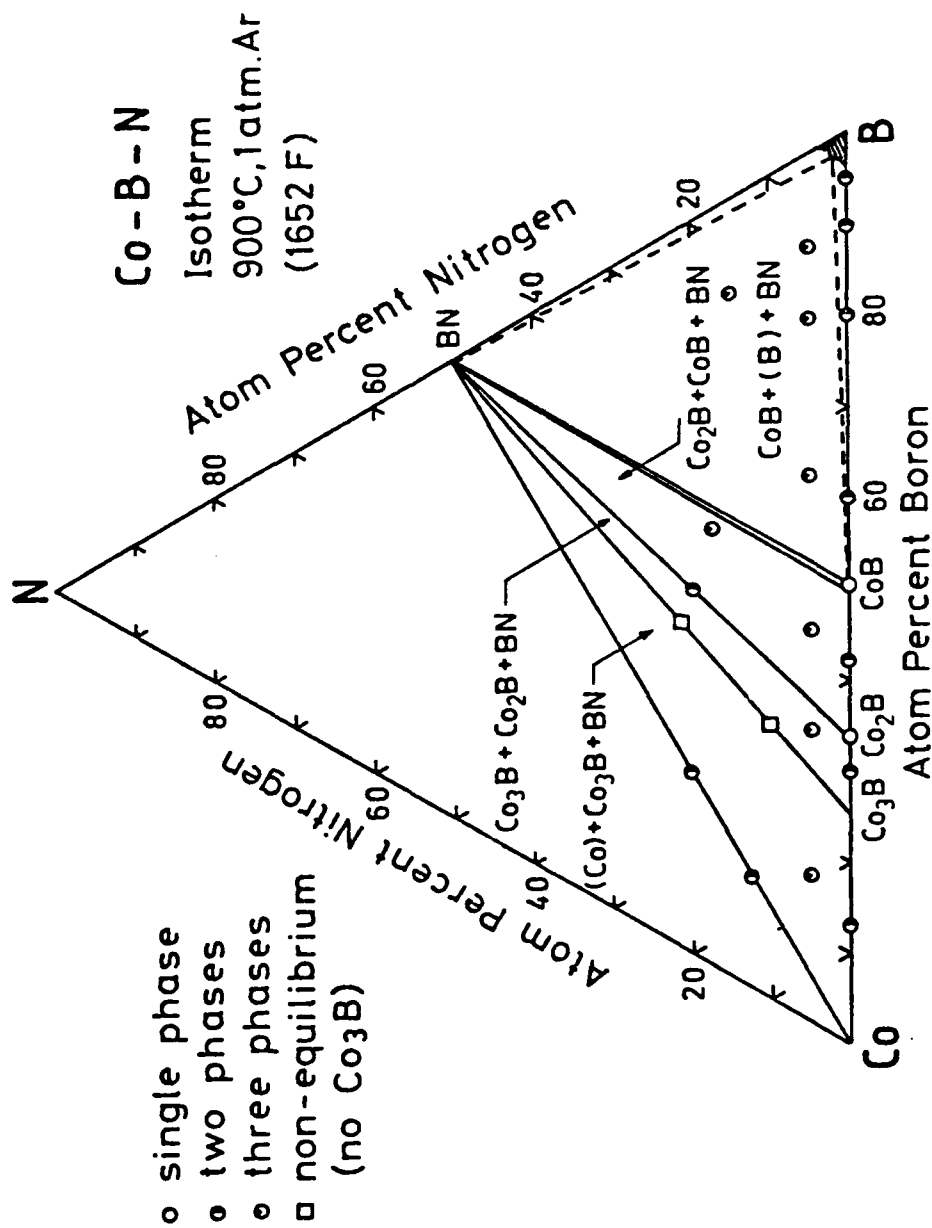
Fig.B.II.1 Phase equilibria in the ternary system Co-B-N, isothermal section at 900°C and 1 atm. argon.

Table B.II.1

Composition, Prepartion Techniques and Crystal Data of Ternary Allys: Cobalt-Boron-Nitrogen

Nominal Composition in at% Co - B - N	Preparation and Heat Treatment	X-ray Phase Analysis (*)	Structure Type	Space Group	Lattice Parameters (Å) a	b	c	Volume (Å³)
79 - 16 - 5	cold compacted heat/W-crucible Mo(Ar), 900°C, 72 h, B-amorph.	Co(cub.) + Co₃B	Cu-Type / Fe₃C	Fm3m / Pbnm	3.541(2) / 4.409(2)	- / 5.221(3)	- / 6.633(2)	44.41(6) / 152.71(11)
63 - 32 - 5	"	Co₃B + Co₂B	Fe₃C / CuAl₂	Pbnm / I4/mcm	4.408(1) / 5.013(1)	5.226(2) / -	6.624(1) / 4.219(1)	152.58(7) / 106.02(3)
52 - 43 - 5	"	Co₂B + CoB	CuAl₂ / FeB	I4/mcm / Pbnm	5.013(1) / 3.957(0)	- / 5.243(3)	4.217(1) / 3.041(1)	105.95(5) / 63.09(4)
35 - 60 - 5	"	CoB	FeB	Pbnm	3.954(1)	5.247(5)	3.040(1)	63.07(6)
18 - 77 - 5	"	CoB	FeB	Pbnm	3.954(1)	5.248(3)	3.041(1)	63.10(5)
10 - 85 - 5	"	CoB+ traces B	FeB	Pbnm	3.954(2)	5.250(2)	3.038(1)	63.06(4)
					n.d.			
10 - 75 -15	"	CoB+ traces B	FeB	Pbnm	3.954(1)	5.245(2)	3.044(1)	63.13(3)
					n.d.			

(*)   All samples contained small amounts of hex. BN in thermodynamic equilibrium (a= 2.505, c= 6.680)

n.d.   not determined

Alloys along the isopleth Co-BN with compositions from 20 to 50 mol% BN
appear in molten condition after heat treatment at 1250°C under 1 atom of
argon. Similar to the behavior in the Fe-B-N system, the reguli reveal a
phase separation of a metal rich liquid and a porous body of hex ss-BN.
Due to the rather high surface tension the metal-rich part is found to adopt
almost spherical shape when above or within the soft and porous substrate.
X-ray analysis of the powdered spherical droplets indicates the existence
of a cubic phase isotypic with the $Cr_{23}C_6$-type τ-boride in the Fe-B-N
ternary suggesting a formula $Co_{23}(B,N)_6$. Heat treatments at different
temperatures however do not produce this new compound in stable solid
state equilibrium. Thus the new compound is likely to be metastable and due
to this metastable character it is never encountered in single phase
condition but always observed in combination with various amounts of Co
and BN. The unit cell dimensions of $m\text{-}Co_{23}(B,N)_6$ are smaller than those
of binary metastable "$Co_{23}B_6$" and suggest a rather small amount of N only
if some at all is present (see also Table BI3). Identical quenching
(cooling) conditions for binary Co-B alloys however were not sufficient
to reveal binary $m\text{-}Co_{23}B_6$, as a proof for the stabilizing influence of
nitrogen in the ternary alloys.
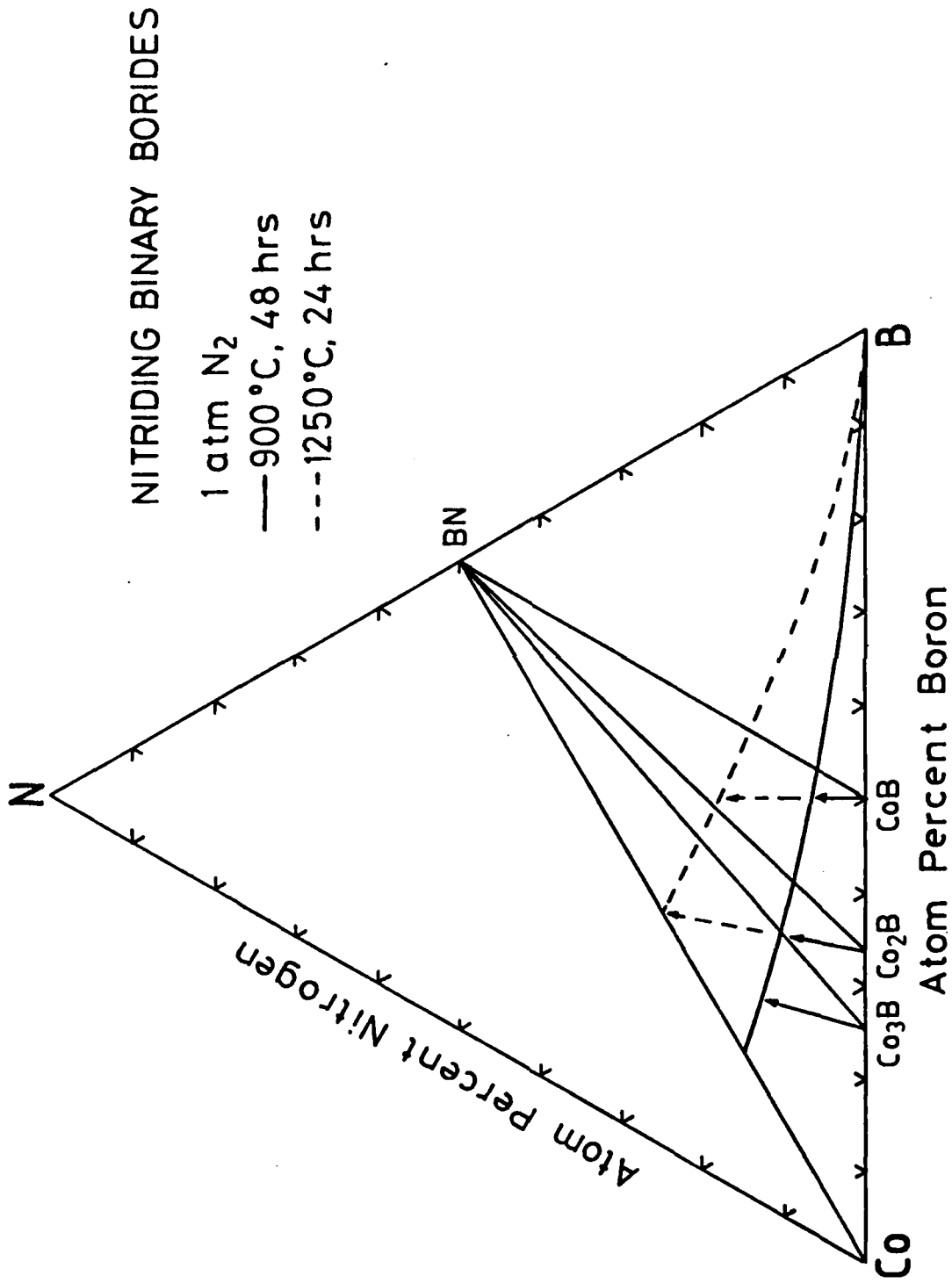
Fig.B.II.2 Nitriding of binary cobalt-borides, under pure nitrogen, arrows indicate amount of nitrogen take up.

III THE TERNARY SYSTEM NICKEL-BORON-NITROGEN

a) CRITICAL LITERATURE REVIEW

No X-ray or phase diagram studies of the system nickel-boron-nitrogen are known in the literature.

b) EXPERIMENTS AND RESULTS

Phase equilibria in the ternary system Ni-B-N at 900°C (see Fig.B.III.1 were determined by X-ray diffraction analysis of about 15 ternary alloys. For details of preparation and heat treatment see Fe-B-N. The results of the X-ray phase analysis for a series of characteristic samples are presented in Table B.III.1.

As typical for ironmetal-boron-nitrogen systems and according to the phase relations obtained in Table B.III.1 and Fig.B.III.1, nickel and all binary nickelborides at 900°C are found in stable thermodynamic equilibrium with hexagonal boronnitride. Both binary eutectic reaction isotherms Ni_2B + o-Ni_4B_3 (1018°C) and m-Ni_4B_3 + NiB (1018°C) seem to extend to lower temperatures into the ternary, as nickel-rich ternary samples already show signs of a liquid phase.

As already mentioned for the binary Ni-B system it appeared to be impossible to obtain the m-Ni_4B_3 + NiB + BN three phase equilibria free of o-Ni_4B_3. The unit cell dimensions of the boundary phases as analyzed from multiphase alloys correspond to the binary data within the error limits of the least squares extrapolation. This indicates that practically no nitrogen (< 0.5 a/o N) is soluble in the binary nickel borides. Lattice parameters of the hex-ss-BN however reveal a small but significant solubility of nickel (see Table BIII.1 and also Fe-B-N).
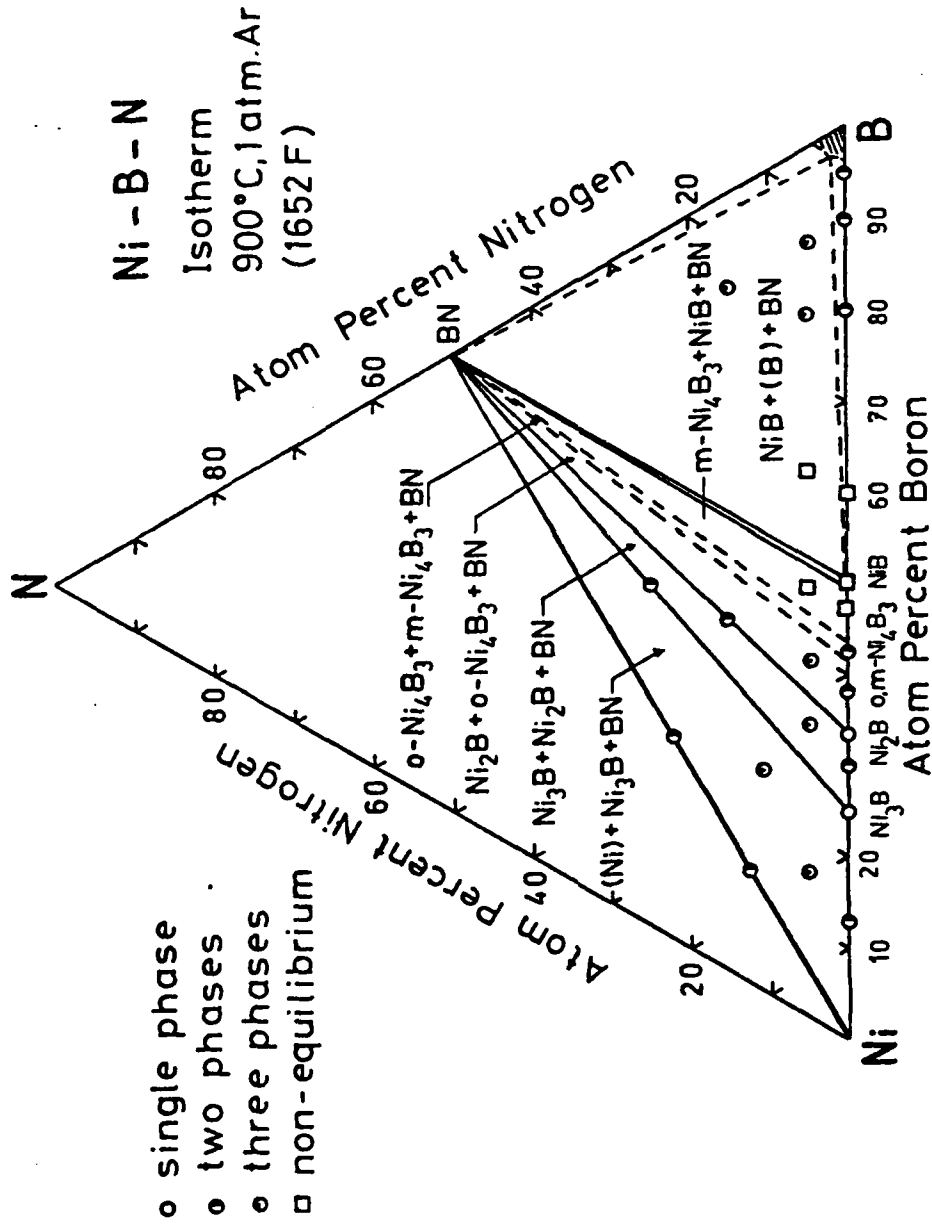
Fig.B.III.1 Phase equilibria in the ternary system Ni–B–N, isothermal section at 900°C and 1 atm. argon.

Due to the low melting temperatures of the Ni-B binary, no isothermal section was studied at 1250°C (wide areas of a ternary liquid phase). Ternary alloys Ni-BN with an approximate composition of 20 mol% BN which were shortly exposed to 1250°C and cooled by power shut off show a similar phase separation (liquid droplets plus a porous ss-BN substrate) as already encountered among similar Fe-B-N and Co-B-N alloys. X-ray analysis of the droplets is consistent with a multiphase composition of BN, Ni and a new tau phase τ-$Ni_{23}(B,N)_6$ which is likely to be metastable (see also Fe-B-N). The unit cell dimensions however are even smaller than those of binary m-$Ni_{23}B_6$ (see Table B,I.3) and nitrogen stabilization seems likely, as identical cooling conditions for binary Ni-B alloys were not sufficient to reveal m-$Ni_{23}B_6$.
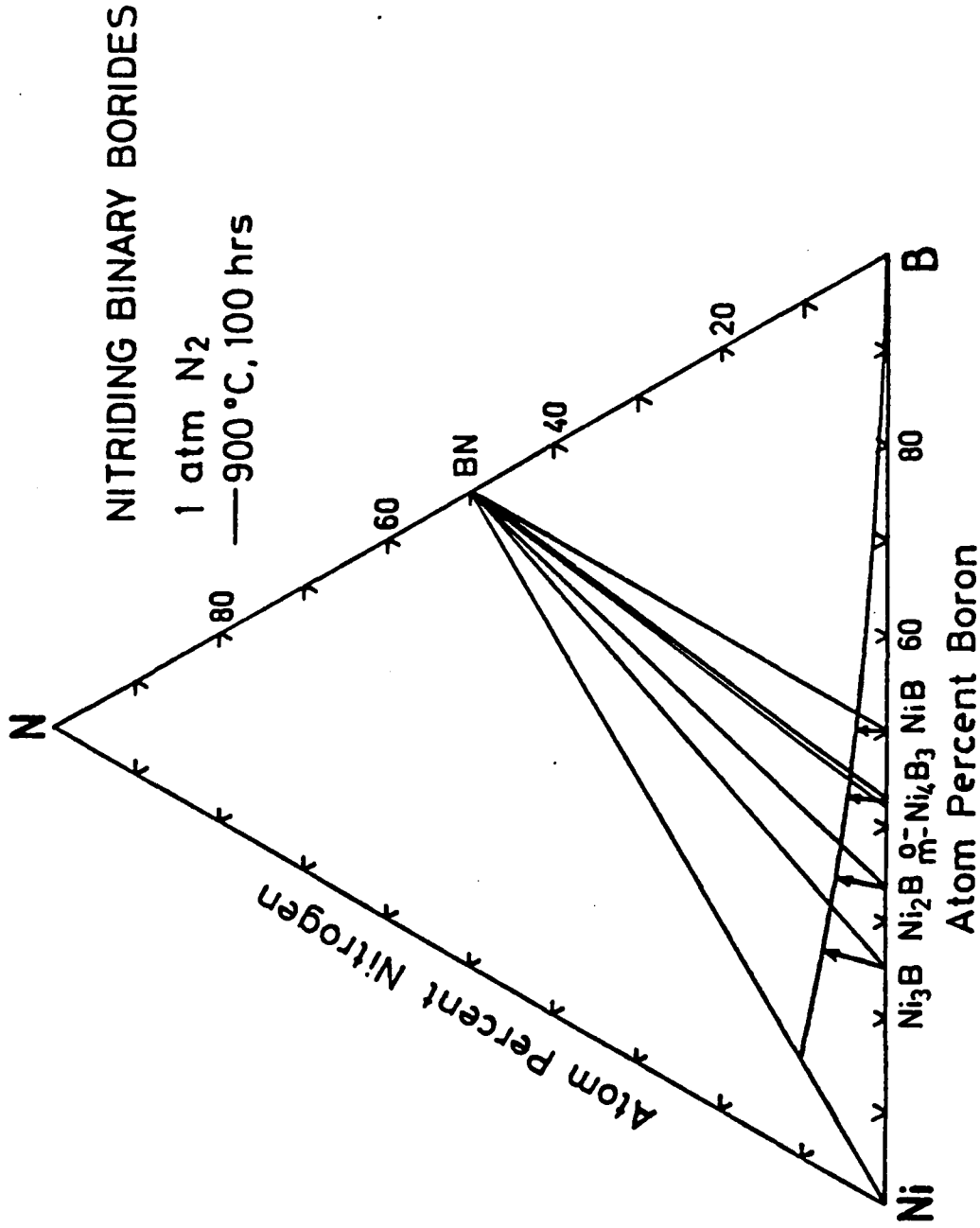
Fig.B.III.2 Nitriding of binary nickel borides under pure nitrogen, arrows indicate amount of nitrogen take up.

Table B.III.1

Composition, Preparation Techniques and Crystal Data of Ternary Alloys: Nickel-Boron-Nitrogen

Nominal Composition in at% Ni - B - N	Preparation and Heat Treatment	X-ray Phase Analysis (*)	Structure Type	Space Group	Lattice Parameters (Å) a	b	c	β	Volume (Å³)
79 - 16 - 5	cold compacted HF-treat/W-crucible Mo(Ar), 900°C 72 h, B-amorph.	Ni +	Cu-Type	Fm3m	3.5208(6)				43.645(14)
		Ni₃B	Fe₃C	Pbnm	4.3897(22)	5.2155(33)	6.618 (2)		151.52 (13)
63 - 32 - 5	"	Ni₃B +	Fe₃C	Pbnm	4.3915(17)	5.2222(19)	6.615 (2)		151.71 (10)
		Ni₂B	CuAl₂	I4/mcm	4.9893(6)	-	4.2462(4)		105.70 (3)
56 - 39 - 5	"	Ni₂B +	CuAl₂	I4/mcm	4.9912(7)	-	4.2478(5)		105.82 (3)
		o-Ni₄B₃	o-Ni₄B₃	Pnma	11.959 (3)	2.9824(6)	6.570 (5)		234.31 (18)
33 - 60 - 5	"	o-Ni₄B₃ +	o-Ni₄B₃	Pnma	11.963 (7)	2.9831(8)	6.577 (3)		234.71 (18)
		m-Ni₄B₃ +	m-Ni₄B₃	C2/c	6.433 (1)	4.8830(11)	7.824 (2)	103.30(2)	239.2 (1.1)
(**)		NiB	CrB	Cmcm	2.9281(3)	7.393 (3)	2.9668(7)		64.225(30)
10 - 85 - 5	(2x 900°C, 72 h)	NiB	CrB	Cmcm	2.9316(2)	7.390 (1)	2.9664(3)		64.269(11)
10 - 75 -15	+ 10 d 900°C in Ta (Quartz)	NiB	CrB	Cmcm	2.9281(7)	7.400 (2)	2.9674(3)		64.296(21)

(*) All samples contained small amounts of hex. BN in thermodynamic equilibrium (a= 2.506, c= 6.664)

(**) After heat treatment the composition appears to be shifted towards the nickel-rich side thermodynamic equilibrium was not attained.

C) Thermodynamic Data

I) The Iron-Boron -Nitrogen System

A thermodynamic description of the binary iron-boron system was earlier attempted by Kaufman (72) and by Hack (73). The latter reference also includes a detailed critical discussion of the thermodynamic data available at that time. In the meantime however, a new determination of the free enthalpy of formation by electromotive force measurements has been published (76) for the iron borides and for the temperature range of 1000 K to 1350 K. The new data are slightly more negative than those derived by (72-75).

With respect to the new thermodynamic data, and with respect to the new experimental phase diagram data assembled in this work (T_m(FeB)= 1588°C, T_E(FeB + ß-rhB)= 1450°C), a recalculation of the binary system seemed to be necessary. The experimental liquidus - and solidus- data were fitted using the least squares optimization program by Lukas (78) employing a polynomial expression for the Δ_fH- and S_E-values of the liquid phase:

$$X = x_A x_B [a_0 + a_1(x_A-x_B) + a_2(x_A-x_B)^2 + a_3(x_A-x_B)^3 + \ldots] \ .$$

The fusion data used for pure boron were 50.21 kJ mol^{-1} for the enthalpy and a melting temperature of T_m(B)= 2365 K, which then corresponds to an entropy of fusion of 21.33 J mol^{-1}K^{-1}; these data are in good agreement to experimental values (drop calorimetry) by Stout (77).

From a listing of the known heat and entropy of formation data for the binary iron borides in Table C.1., a large discrepancy is obvious for the ΔH_f-value of Fe$_2$B which therefore was used as a variable in the least squares optimization procedure. The final data according to our refinement are included in Table C.1. Calculated and observed data are in fine agreement; experimental and calculated curves are shown in Fig.I.3. on page 9.

In order to obtain information about the stability or "instability" of metastable "Fe_3B" and "$Fe_{23}B_6$", ternary phase equilibria data have been evaluated using phase diagram information (79). A listing of the (rather small) disproportionation energies of "Fe_3B" and "$Fe_{23}B_6$" is available from Table C.3. The low values of instability explain very well the formation of extended phase solutions $(Fe,M)_3(B,X)$ and $(Fe,M)_{23}(B,X)_6$ as well as the easy stabilization of the binary phases under nonequilibrium conditions.

Thermodynamic data for dilute solutions of boron in solid iron are scarce; data for ss-α Fe and ss-γ Fe have been estimated by Chart (73):

$$\frac{G(B\ in\ \gamma\text{-Fe})}{J\ mol^{-1}} = -26340 + 24.5\ T + 8.31\ T\ lnx_B \qquad (1150\text{-}1400\ K)$$

$$\frac{G(B\ in\ \alpha\text{-Fe})}{J\ mol^{-1}} = -37660 - 33.5\ T + 8.314\ T\ lnx_B \qquad (1000\text{-}1200\ K)$$

Fountain and Chipman (67) studied the conditions under which BN forms from dissolved N in Fe-B alloys; the solubility of N in Fe-B alloys (0.001 to 0.91 wt% B) was determined by the Sievert's-technique (950° to 1150°C) and the equilibrium constant, the free energy and heat of formation of BN from dissolved boron and gaseous nitrogen, and from dissolved boron and dissolved nitrogen, as well as for the formation of BN from Fe_2B and gaseous nitrogen, and from Fe_2B and dissolved nitrogen, was calculated. From these data, iso-thermal sections of the iron-corner of the Fe-B-N diagram were constructed (see Fig.B.I.1., p.58) revealing a small solubility of BN in iron and confirming the two phase equilibrium: Fe + BN.

An estimation of the free energy of the reaction $M + x\ BN \longrightarrow MB_x + \frac{x}{2}\ N_2$, using the optimized data for the iron borides and the thermodynamic values for hex-BN $\Delta H_f = -251.1$ kJ mol^{-1}, $\Delta S_f = 14.62$ J $mol^{-1}K^{-1}$ (80), revealed stable two-phase sections FeB_x-BN up to the melting range in excellent agreement

to the experimental data, which prove complete compatibility of (ss-Fe) and BN.

II) The Cobalt-Boron-System

Thermodynamic data for cobalt borides are listed in Table C.4. including data for the Co-B liquid according to a recent description by Kaufman (72). Agreement between calculated and observed phase diagram data (liquidus and solidus lines) is satisfactory: there is however a lack in precise thermodynamic data especially as far as Co_2B is concerned (see Table C.4.).

Similar to the Fe-B-N system, an estimation of the free energy of the reaction $M + x\ BN \longrightarrow MB_x + \frac{x}{2} N_2$ and using Kaufman's data (72) for the binary compounds, confirms the experimentally observed two-phase equilibria: Co-BN, CoB_x up to the melting range.

III) The Nickel-Boron System

Thermodynamic calculations of the constitutional diagram Ni-B have been presented by Kaufman (72) and Hack (73, includes also a critical assessment). Kaufman's data still include the compound "NiB_2" which has not been corroborated in this work and earlier. The agreement between calculated and observed phase diagram data (liquidus and solidus lines) according to (73) is fine (Table C.5.), despite discrepancies in the basic thermodynamic data of the compounds are unsatisfactory (see Table C.5.).

A thermodynamic estimation of the compatibility of Ni and nickelborides with hex. BN revealed stable two-phase equilibria $Ni + BN$, $NiB_x + BN$ up to the melting range in excellent agreement to the experimental observations.

A precise calculation of these compatibilities M-BN, MB_x-BN will be presented for all metal boronnitride systems in our final report.

Table C.1. Thermodynamic Data for Iron-Borides
Reference States are bcc-Iron and ß-rh Boron

Boride	x_B	$\dfrac{\Delta_f H}{kJmol^{-1}}$	$\dfrac{\Delta_f S}{Jmol^{-1}K^{-1}}$	Ref.
Fe$_2$B	0.3333	-30.00	-	(75)
		-33.78±3.2	-6.68	(76)
		-26.05	-3.81	(72)
		-34.15	-2.94	(73)
		-32.16(V)	-4.25(V)	this work
FeB	0.5000	-38.00	-	(75)
		-46.51±4.2	-12.02	(76)
		-35.04	-5.69	(72)
		-36.25	-1.05	(73)
		-46.51	-8.87(V)	this work

V means variable in the refinement

Table C.2. Polynomial coefficients of Excess Enthalpies and Entropies
of Formation of Liquid Fe-B Alloys. Values are in kJmol^{-1}
and JK^{-1}mol^{-1} respectively. (The reference states are the
pure liquid elements).

COEFF	a_o	a_1	a_2
$\Delta_f H$	-104.77	-67.34	56.04
S^E	-10.24	-36.47	17.45

Table C.3. Disproportionation Energies (J/gatom metal) for metastable iron-borides, derived from phase diagram data

Reaction	Free Enthalpy Change	Reference Diagram
$Fe_3B(Fe_3C\text{-type}) \rightarrow Fe + Fe_2B$	$\Delta G_{Z,Fe_3B}^{1273K} = -1463$	Fe-Co-B
	$\Delta G_{Z,Fe_3B}^{1073K} = -962$	Fe-Ni-B
$Fe_{23}B_6(\tau) \rightarrow Fe_3B(Ti_3P\text{-type}) + Fe$	$\Delta G_{Z,Fe_{23}B_6}^{1373K} = -2430$	Re-Fe-B

Table C.4. Thermodynamic Data for Cobalt Borides
Reference States are bcc Iron and ß-rh Boron

Boride	x_B	$\dfrac{\Delta_f H}{kJmol^{-1}}$	$\dfrac{\Delta_f S}{Jmol^{-1}K^{-1}}$	Ref
Co_3B	0.2500	-21.00	-	(75)
		-18.00	-4.239	(72)
		-26.39 ± 4.1	-4.995	(76)
Co_2B	0.3333	-28.00	-	(75)
		-19.40 ± 2.3		(74)
		-23.39	-3.741	(72)
		-57.63 ± 1.6	-26.74	(76)
CoB	0.5000	-34.00	-	(75)
		-34.80 ± 3.0		(74)
		-33.47	-0.669	(72)

Excess Terms for the Liquid Phase (after (72)):

Excess Enthalpy: $-x_{Co}\,x_B\,(x_{Co}\cdot 166.36 + x_B\cdot 128.70)$ in kJ gatom^{-1}

Excess Entropy : $-x_{Co}\,x_B\,\,21.255$ in J gatom^{-1}K^{-1}

Table C.5. Thermodynamic Data for Nickel-Borides
            Reference States are bcc-Iron and ß-rh Boron

Boride	x_B	$\dfrac{\Delta_f H}{.kJmol^{-1}}$	$\dfrac{\Delta_f S}{Jmol^{-1}K^{-1}}$	Ref.
Ni_3B	0.2500	-18.89	-2.78	(72)
		-22.24	-1.908	(73)
		-33.18±1.8	-11.05	(76)
Ni_2B	0.3333	-22.60±1.4		(74)
		-22.99	-4.281	(72)
		-21.24	+0.234	(73)
		-35.71±4.0	-10.10	(76)
$o-Ni_4P_3$	0.414	-25.60	-3.850	(73)
$"Ni_4B_3"$	0.429	-23.46	-4.58	(72)
$m-Ni_4B_3$	0.436	-25.65	-4.179	(73)
NiB	0.500	-23.47	-4.874	(72)
		-23.220	-3.665	(73)
		-20.10±2.8		(74)

Polynomial coefficients of Excess Enthalpies and Entropies of Formation
of Liquid Ni-B alloys; The reference states are the pure liquid elements.
After Hack and Chart (73).

COEFF	a_0	a_1	a_2	a_3	a_4
$\Delta_f H$	-150.72	-51.08	54.61	41.03	-36.28
S^E	-41.46	-8.50	38.10	4.34	-25.68

$$X = x_{Ni}x_B \left(a_0 + a_1(x_{Ni}-x_B) + a_2(x_{Ni}-x_B)^2 + a_3(x_{Ni}-x_B)^3 + a_4(x_{Ni}-x_B)^4 \right)$$

AD-A161 563   BORON NITRIDE AND SILICON NITRIDE SYSTEMS(U) WIEN UNIV   2/2
              (AUSTRIA) INST FUER PHYSIKALISCHE CHEMIE P ROGL ET AL
              SEP 85 DAJA45-84-C-0038

UNCLASSIFIED   F/G 7/4   NL

END
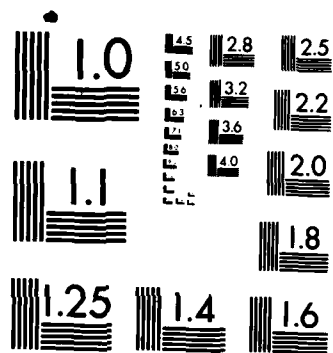
MICROCOPY RESOLUTION TEST CHART
NATIONAL BUREAU OF STANDARDS-1963-A

REFERENCES

1) H.Holleck; Chemiker-Zeitung 106 (1982) 213-224

2) Holocher-Ertl, H.Boller; Programm GITTER, version Ch.Horvath

   Institut für Physikalische Chemie, Universität Wien, 1983

3) H.Boller; Programm PULVER, Institut für Physikalische Chemie,

   Universität Wien, 1976

4) A.Cotton, G.Wilkinson; Anorganische Chemie, Verlag Chemie 1974

5) Holleman-Wiberg; Lehrbuch der Anorganischen Chemie, de Gruyter, 1976

6) Gmelin B, Boron Compounds-1st Suppl., Vol.2, Springer-Verlag 1980

7) H.J.Goldschmidt; Interstitital Alloys, Butterworths & Co.

   Publishers Ltd., 1967

8) G.Hägg; Nature 121 (1927) 826-827; 122 (1928) 314, 962

   Nova Acta Regiae Soc.Sci.Upsaliensis (4) 7, 1929, 6-22

   Z.physik.Chem. B8 (1930) 455-474

9) K.H.Jack; Proc.Roy.Soc. (London) A208 (1951) 200-215

10) V.G.Paranjpe, M.Cohen, M.B.Bever, C.Floe; Trans.AIME 188 (1950) 261-267

11) R.Juza und W.Sachsze; Z.anorg.Chemie 253 (1945) 95-108

12) R.Juza und W.Sachsze; Z.anorg.Chemie 251 (1943) 201-212

13) F.P.Bundy and R.H.Wentorf,Jr.; J.Chem.Phys. 38 (1963) 618, 631, 1144

14) O.Kubaschewski-von Goldbeck; Iron-Binary Phase Diagrams, Springer-Verlag

    1982

15) L.Kaufman, B.Uhrenius, D.Birnie, K.Taylor; Calphad 8(1)(1984), 25-66

16) R.Fruchart; Compt.Rend., 247 (1958) 1464 see also p.2367

17) T.Kanaizuka; J.Solid State Chem. 41 (1982) 195

18) D.Hohnke and E.Parthé, Acta Crystallogr. 20 (1966) 572

19) L.G.Voroshnin, L.S.Lyakhovich, G.G.Panich, and G.F.Protasevich;

    Metallov. i. Term.Obrab.Met. 9 (1970) 14

20) D.Armstrong; 7th Int.Symposium on Boron Uppsala, Sweden, June 9-12, 1981

21) K.I.Portnoi, M.Kh.Levinskaya, V.M.Romashov; Sov.Powder Metall.

Met.Ceram. 8 (1969) 657

22) B.Callmer, J.Lundström, J.Solid State Chem. 17 (1976) 165

23) Y.Khan, E.Kneller, M.Sostarich, Z.Metallkunde 73 (1982) 624-626

24) H.Brodowksy and H.J.Wernicke: Paper presented at Calphad XII

29.8.-2.9.83, 1983, Universite de Liège, Belgium

25) Y.Hayashi and T.Sugeno, J.Phys.Soc.Japan 19 (1964) 1251

26) W.B.Pearson; Handbook of Lattice Spacings and Structures of Metals and

Alloys, Pergamon Press, 1967, and references therein.

27) T.Swanson et al.; NBS Circular 539, vol.IV (1955) p.3

28) U.Herold und U.Köster; Z.Metallkunde 69 (1978) , 326-332

29) V.F.Bashev, I.S.Miroshnichenko, G.A.Sergeev; Russ.Metall, 17(7) (1981) 1206

30) O.T.Inal, L.Keller and F.G.Yost, J.Mat.Science 15 (1980) 1947-1961

31) P.Duhaj, F.Hanic, Phys.Stat.Sol. 62 (1980) 719

32) T.Bjurström and H.Arnfelt; Z.Physik.Chemie (B)4 (1929) 469-474

33) T.Bjurström, Arkiv.Kemi, Min. and Geol., K.Sv.Vetensk, Akad. 11A

(1973) No.5, 1-12

34) J.L.Walter, J.F.Bertram and R.R.Russel, Met.Trans. 9A (1978) 803

35) J.L.Walter, J.F.Bertram and I.Mellas, Mater.Sci.Eng. 36 (1978) 193

36) R.C.Ruhl, M.I.T. Thesis, 1967

37) M.Takahashi, M.Koshimura and T.Abuzuka, Jap.J.Appl.Phys. 20(10) (1981) 1821

38) M.L.Borlera and G.Pradelli, La Met.Italiana 11 (1967) 907

39) M.E.Nicholson, Trans.AIME 1, 209 (1957)

40) P.Rogl and H.Nowotny, Monatsh.Chemie 104 (1973) 943, see also P.Rogl,

J.C.Schuster and H.Nowotny, in: "Boron in Steel", Proc. of the Intern. Symp.

on Boron Steels, Eds. S.K.Banerji and J.E.Morral, AIME Milwaukee, Wi,

Sept. 18 (1979) p.33

41) S.Rundqvist, Acta Chem.Scand. 16 (1962) 1

42) G.Hägg and R.Kiessling, J.Inst.Met. 81 (1952) 57

43) G.T.Chart; Com.Communautes Europ.CECA No.7210-CA/3/303, Nov. 1981

44) J.O.Carlsson, T.Lundström; J.Less-Common Metals 22 (1970) 317-320

45) J.D.Schöbel, H.H.Stadelmaier; Z.Metallkunde 57 (1966) , 323-325

46) H.H.Stadelmaier, H.J.Lee; Z.Metallkunde 69 (1978)   , 685-689

47) P.T.Kolomytsev; Dokl.Akad.Nauk.SSSR, 124 (1959) 1247-1250

    Proc.Acad.Sci. USSR, Chem.Section 124-126 (1959) 151

48) J.A.Avlokhashvili, F.N.Tavadze, G.F.Tavadze, D.N.Tsikaridze,

    D.L.Gabunia, K.P.Tsomaya; J.Less-Common Metals 67 (1979) 367-373

49) S.Andersson, B.Callmer; J.Solid State Chem. 10 (1974) 210-231

50) S.Rundqvist; Acta Chem.Scand., 12 (1958) 658-662

51) S.Rundqvist; Nature, 181 (1958) 259-260

52) Havinga et al.; J.Less-Common Metals, 27 (1972) 169

53) J.D.Schöbel, H.H.Stadelmaier, Z.Metallkunde 56 (1965)   , 856-859

54) S.Rundqvist, Acta Chem.Scand. 13 (1959) 1193-1209

55) S.Rundqvist and S.Pramatus, Acta Chem.Scand. 21 (1967) 191

56) P.T.Kolomytsev; Isv.Akad.Nauk.SSSR, Otd.Techn.Nauk.Met. i. Topl.

    3 (1960) 83-85; engl.Transl.: Russ.Met.Fuels 3 (1960) 80-83

57) L.Shapiro and M.Ford, Trans.AIME 236 (1966) 536

58) R.Fruchart, A.Michel; Compt.Rend. 245 (1957) 171-172, and Bull.Soc.

    Chim.France 1959, 422-423

59) R.Kiessling, Y.H.Liu, Journal of Metals, N.Y. 3 (1951) 639-642

60) P.Blum; J.Phys.Radium 13 (1952) 430-431

61) ASTM-FILE, American Electro Metal Co., Yonkers, N.Y.

62) A.Brown, J.D.Garnish, R.W.K.Honeycombe; Met.Sci.J. 8 (1974) 317

63) W.Köster, W.Mulfinger; Z.Metallkunde, 30 (1938) 348-350

64) K.E.Spear, J.Less Common Metals 82 (1981) 237

65) P.Rogl, J.Less Common Metals, 1985, in press

66) H.Boller, W.Rieger and H.Nowotny, Mh.Chem. 95(6), 1497 (1964)

67) R.W.Fountain and J.Chipman, Trans. AIME 224 (1962) 599

68) R.S.Pease, Acta Crystallogr. 5 (1952) 356

69) R.P.Elliott; Constitution of Binary Alloys, 1st Suppl., New York,
    McGraw Hill, 1965

70) R.G.Blossey and R.D.Pehlke, Trans. AIME 236 (1966) 566

71) E.Fromm and E.Gebhardt, Gase und Kohlenstoff in Metallen,
    Springer, Heidelberg, N.Y., 1976

72) L.Kaufman, B.Uhrenius, D.Birnie and K.Taylor, Calphad 8(1) (1984) 25

73) K.Hack and T.G.Chart "Estimation and Critical Assessment of Thermodynamic
    Data for the Cr-B, Mn-B, Fe-B and Ni-B-Systems, NPL, Teddington, England
    (private commun), 1981

74) S.Sato and O.J.Kleppa, Met.Trans. 13B, (1982) 251

75) A.K.Niessen, F.R.de Boer; R.Boom, P.F.de Chatel, W.C.M. Mattens and
    A.R.Miedema, Calphad 7 (1983) 51

76) S.Ohmori, Y.Hashimoto and K.Koyama , 高温学会誌, Vol. 8. No. 6 (1982) 別刷

77) N.D.Stout, R.W.Mar and W.O.J.Boo, High Temp.Sci., 5 (1973) 241

78) H.L.Lukas, E.Th.Henig and B.Zimmermann, Calphad 1 (1977) 225

79) P.Rogl, J.C.Schuster and H.Nowotny in: Boron in Steel, Proc.Internat.Symp.
    on Boron Steels, TAIME, Milwaukee,Wisconsin, Sept. 18, 1979, p.33

80) A.Matuschka, Chemikerzeitung 98 (1974) 504

81) E.K.Storms and B.A.Mueller, NBS-Special Publ. 561, 1979, 143

SUMMARY

The existing literature data regarding the systems Fe-B-N, Co-B-N and Ni-B-N were critically assessed including the binary boundary systems. The thermodynamic phase equilibria at 900°C were reinvestigated for the binary systems Fe-B, Co-B and Ni-B using different methods of preparation and analysis. There were no indications for the existence of binary metal diborides "MB$_2$"; compounds "MB$_{\sim 20}$", as earlier reported in literature were successfully characterized with a rhombohedral unit cell and the crystal structure of β-rhombohedral boron with the transition metal atoms in the voids of the covalently bonded boron framework, i.e. ss-β-rh (B,M). A complete constitutional diagram Fe-B was established in the temperature range 600° < T < 1700°C using X-ray phase analysis, metallography, DTA and melting point analysis (automatic computer controlled three-colour pyrometry). Compounds "Fe$_3$B" with either the Ti$_3$P- or the Fe$_3$P-type as recently postulated, were not confirmed as thermodynamic stable equilibrium phases. Differential thermal analysis and melting point analysis revealed an eutectic reaction L $\rightleftharpoons$ FeB + ss-β-rh(B,Fe) at 1450 ± 3°C. The congruent melting point of the compound FeB was measured to be 1588 ± 8°C.

The phase diagram Fe-B was calculated thermodynamically with respect to the new experimental data established, and a complete set of parameters were obtained for the liquid phase.

The phase equilibria in the ternary systems Fe-B-N, Co-B-N and Ni-B-N were established mainly from X-ray powder diffraction data, and isothermal sections at 900°C and 1 bar Ar have been constructed. In all three systems the binary transition metal borides form two-phase equilibria with hexagonal boronnitride. There is practically no solubility of BN in the binary metal borides and no ternary equilibrium phases were observed. Melting in the concentrational sections M-BN, M= Fe,Co, occurs at ca. 1350°C; for the corresponding nickel-alloys the temperatures are somewhat lower. Up to these temperatures there is complete compatibility between metal, metal borides and BN; Alloys M-BN, melted and quenched reveal the formation of metastable compounds (Fe,Co,Ni)$_{23}$(B,N)$_6$ with the τ-Cr$_{23}$C$_6$-type of structure. Phase relations in the Fe-B-N system were also studied under technical conditions (900°C, technical argon, samples in a Mo-container within a graphite susceptor). Oxygen impurities via a gas phase transport reaction (carbonoxide) led to the formation of a ternary phase Fe$_3$(B,N,C) with cementite-structure.

The kinetic of nitriding was studied in all three systems from binary transition metal boride samples annealed at 900°C and 1200°C under 1 bar of high purity nitrogen.

Part II   TRANSITION METAL-SILICON-NITROGEN SYSTEMS

EXPERIMENTAL PROCEDURES

In order to identify all binary silicide phases and to obtain master alloys for further preparation binary metal-silicon alloys were prepared by arc melting under argon (99.999% pure) from powders or pieces of the constituting elements using the starting material listed in tab.1. Ternary compositions were prepared by mixing powders of these master alloys and binary nitride powders listed in tab.2. These ternary mixtures were cold pressed and sintered under pure argon in an RF-furnace at $1300^{\circ}C$ (Ti-Si-N, Zr-Si-N) or at $1500^{\circ}C$ (V-Si-N, Nb-Si-N, Ta-Si-N) for 48 h. Heat treatment at temperatures up to $1000^{\circ}C$ was performed in evacuated quartz tubes lined with Mo or Ta foil.

X-ray diffraction (CuK_{α}-radiation) was performed on all alloys using Guinier or 114mm Debye-Scherrer cameras.

Tab.1: Metallic Starting Materials

Silicon   powder, purity: m 99,9%, from Alpha Div., Ventron Corp., USA

Silicon   lump, purity: m 99,9999%, from Alpha Div., Ventron Corp., USA

Titanium   powder, purity: m 99%, impurities (in ppm): Ca 4000, Al 3500, Fe 1000, C 150, Si 30, other 30; from Alpha Div., Ventron Corp., USA.

Titanium   rod, purity: + t 99,9%, impurities (in ppm): O 100, Fe 70; kindly supplied by Dr.Bauer, INSA, Rennes,France

Zirconium   powder, purity 99.9%, from Alpha Div., Ventron Corp., USA

Zirconium   bar, purity: t99,9%, impurities (in ppm): O 450, H 260, Hf < 200, C < 200, N 45, Si 45, Al 52, Cr 60, other < 30; from Cezus Puk Ugine, France; kindly supplied by Dr.Bauer, INSA, Rennes, France

Vanadium   powder, purity: 99,5%, impurities (in ppm): C 9 1, : 800, Cr 600, Fe 500, Al 200, others < 100; from Alpha Div., Ventron Corp., USA

Niobium   powder, purity: 99,8%, impurities (in ppm): Ta 800, Ti 100, Fe 80, O 80, C 50, W 50 others < 10; from Alpha Div., Ventron Corp. USA.

Tantalum   powder, purity: 99,6%, impurities (in ppm): O 1700, Fe 150, Nb 100, other < 10; from Alpha Div., Ventron Corp. USA.

Tab.2: Ceramic Starting Materials

Silicon nitride (mixture of α-Si$_3$N$_4$ and β-Si$_3$N$_4$), powder
58% Si; from Alpha Div., Ventron Corp. USA

Titanium nitride (TiN) powder, purity 99%, from Alpha Div., Ventron
Corp. USA

Zirconium nitride (ZrN), powder, purity: 99%, from Materials Research
Corp., USA

Vanadium nitride (VN), powder, purity 99%, from Materials Research
Corp., USA

Niobium nitride (δ-NbN), powder, purity 99.9%, from Alpha Div., Ventron
Corp., USA

Tantalum nitride (ϵ-TaN), powder, purity 99,9%, from Alpha Div., Ventron
Corp., USA

BINARY SYSTEM TITANIUM-SILICON

Experimental Results

All phases and crystal structures reported[1] could be corroborated and are confirmed with the exception of L.T.-Ti_5Si_4 which might form at lower temperatures than the annealing temperature chosen (tab.3). All lattice parameters found are close or identical to literature values. Only for Ti_5Si_3 a homogeneity range is observed. The lattice parameters at the Ti-rich phase boundary (in equilibrium with α-Ti) a= 0.74506 nm, c= 0.51407 nm decrease to a= 0.74220 nm, c= 0.51293 nm at the Si-rich phase boundary. The ratio c/a remains remarkably constant over the entire homogeneity range. α-Ti coexisting with Ti_5Si_3 has lattice parameters decreased to a= 0.29403 nm, c= 0.46746 nm from a= 0.295 nm, c= 0.4682 nm for pure α-Ti[2] due to formation of solid solution with silicon.

References

1) P.Rogl and J.C.Schuster, 1st Semiannual Report under Contract DAJA45-84-C-0038 (March, 1985)

2) J.P.Bars, D.David, E.Etchessahar and J.Debuigne, Met.Trans. A14 (1983) 1537

Tab.3. Results of X-ray analysis of binary Ti-Si alloys

at% Ti	as cast	annealed, 1000°C, 550h
33,3	$TiSi_2$ + trace TiSi	$TiSi_2$
50.0	TiSi + H.T.-Ti_5Si_4	TiSi
55.5	TiSi + H.T.-Ti_5Si_4	H.T.-Ti_5Si_4 + trace TiSi
62.5	Ti_5Si_3	Ti_5Si_3
75.0	Ti_5Si_3+α-Ti(S.S.)	Ti_5Si_3 + Ti_3Si

TERNARY SYSTEM TITANIUM-SILICON-NITROGEN

Literature Review

For the temperature range 700-1000°C isothermal sections for the system Ti-Si-N were calculated from thermochemical data by Krilov and Bronnikov[1] as well as Beyers et al.[2] (fig.1). Their results are supported by experimental results with respect to the compatibility of Si_3N_4 with TiN (between 1050°C and 1650°C [3-5]), of Ti_5Si_3 with TiN (at 1100°C [6]) and of $TiSi_2$ with TiN (at 600°C [7]). The tieline TiN-Si is not supported by experimental data: TiN is reported to react with liquid S: [8]. This is in agreement with the appearent compatibility of Si_3N_4 with $TiSi_2$ at 1500°C [9].

At temperatures as low as 500°C Si_3N_4 reacts with Ti to form TiN and Ti-silicides[10]. At 2200°C the reaction products of Si_3N_4 + 5.5Ti, 7Ti and 9Ti resp. were reported to be TiN + $TiSi_2$, TiSi and Ti_5Si_3 resp.[11] Nitriding Ti_5Si_3 at 2109 K led to the formation of TiN [12]. Based on these experimental data an isothermal section for 1300°C was compiled [13].

Experimental results

At 1000°C Si_3N_4 coexists with TiN_{1-x} but reacts with up to 47 at% Ti to form TiN_{1-x} (a= 0.4237 nm) and $TiSi_2$. The lattice parameters for Si_3N_4 and $TiSi_2$ are identical with binary values Si_3N_4 + 52 to 65 at% Ti react to TiN_{1-x} (a= 0.4234 nm) and $D8_8$-type phase with slightly but significantly higher c/a lattice parameter ratio than for binary Ti_5Si_3 alloys. This indicates that Ti_5Si_3 dissolves some nitrogen. In addition specimens initially consisting of TiN and TiSi or Ti_5Si_4 resp. reacted to form this $D8_8$-type phase with increased c/a-ratio.It is therefore concluded

that contrary to preliminary results [13] TiN_{1-x} does not coexist with TiSi or Ti_5Si_4 but rather a three phase field TiN_{1-x} + $TiSi_2$ + $D8_8$-$Ti_5Si_3N_{1-x}$ exist. The alloy Si_3N_4 + 80 at% Ti reacted to $D8_8$-type $Ti_5Si_3N_{1-x}$ and α-Ti (solid solution), with a= 0.29713 nm, c= 0.47796 nm) which corresponds to 15 at% nitrogen. Lattice parameters, c/a-ratios and unit cell volumes of the $D8_8$-type phase field homogenity limits are shown in fig.2.

In stoichiometric TiN no solubility for Si was found at 1000°C. Assuming this evidence to hold for the entire binary homogeneity range of TiN_{1-x} comparison of the measured lattice parameters for TiN_{1-x} with literature values [14] permit to estimate the composition of TiN_{1-x}: coexisting with Si_3N_4 + $TiSi_2$ to be 46 at% nitrogen; coexisting with $TiSi_2$ + $D8_8$-type $Ti_5Si_3N_{1-x}$ to be 45 at% nitrogen; and coexisting with $D8_8$-type $Ti_5Si_3N_{1-x}$ and α-Ti (solid solution) to be 38 at% N.

Since ε-Ti_2N is not observed in ternary alloys it is concluded that phase fields containing ε-Ti_2N are confined to compositions close to the Ti-N binary by a tie line TiN_{1-x} + α-Ti (S.S.) analogous to the system Ti-Al-N [15].

No detailed investigation of the α-Ti phase field was made. However from the observed lattice parameters, which do not deviate substantially from binary α-Ti (solid solution with N) no considerable solubility for Si is to be expected in that phase.

A complete isothermal section at 1000°C is proposed (fig.3).

References

1) Yu.I.Krilov, and V.A.Bronnikov, Porosh.Met. (1) 52 (1976).

2) R.Beyers, R.Sinclair and M.E.Thomas, J.Vac.Sci. Technol. B2, (1984) 781.

3) S.Somiya, M.Yoshimura and N.Shinohara, Rep.Res.Lab.Eng.Mater., Tokyo Inst.Technol. (6) (1981) 107.

4) T.Hirai and S.Hayashi, J.Mater.Sci. 17, (1982) 1320

5) S.Hayashi, T.Hirai, K.Hiraga and M.Hirabayashi, J.Mater.Sci. 17, (1982) 3336.

6) M.Kabbaj, A.Galerie and M.Caillet, Proc. 10th Int.Symp.Reactivity of Solids, Dijon, France, 1984.

7) H.Norström, T.Donchev, M.Östling and C.S.Peterson, Physica Scripta 28, (1983) 633

8) G.A.Yashinskaya, Porosh.Met. (7) (1966) 53.

9) J.A.Champion, B.J.Keene and S.Allen, J.Mater.Sci. 8, (1973) 423

10) T.W.Orent and R.A.Wagner, J.Vac.Sci.Technol. B1, (1983) 844

11) Yu.S.Borisov, A.L.Borisova, Yu.A.Kocherzhinski and E.A.Shishkin, Porosh.Met. (3) (1978) 63

12) L.Brewer and O.Krikorian, J.Electrochem.Soc. 103 (1956) 38

13) J.C.Schuster and H.Nowotny, Proc.11th Int.Plansee Seminar, Reutte, Austria,1985

14) A.N.Christensen and S.Fregerslev, Acta Chem.Scand. $\underline{A31}$ (1977) 861

15) J.C.Schuster and J.Bauer, J.Solid State Chem. $\underline{53}$ (1984) 260
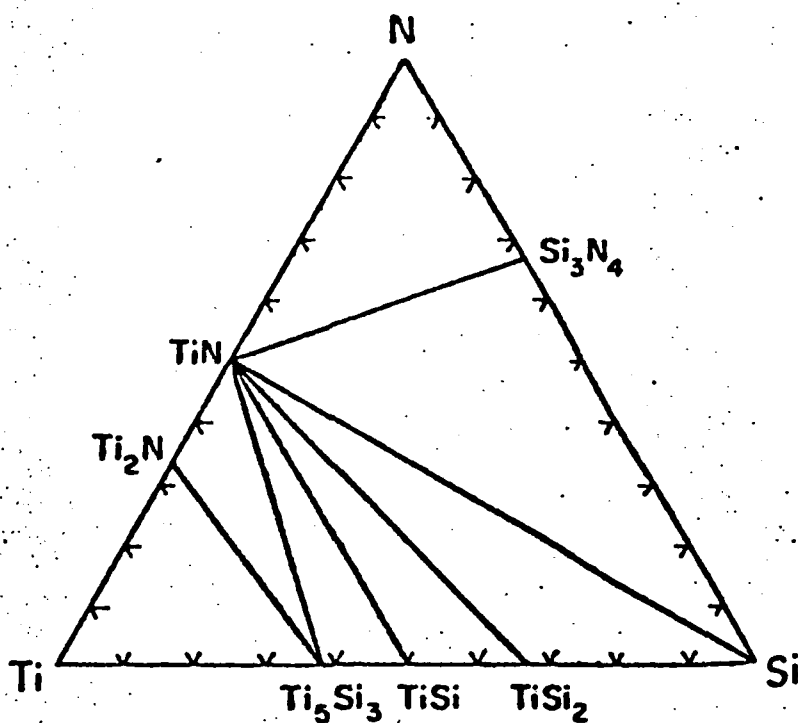
Fig. 1 Phase equilibria in the system Ti-Si-N
calculated from binary thermochemical data
(R.Beyers, R.Sinclair and M.E.Thomas,
J.Vac.Sci.Technol., B2 (1984) 781
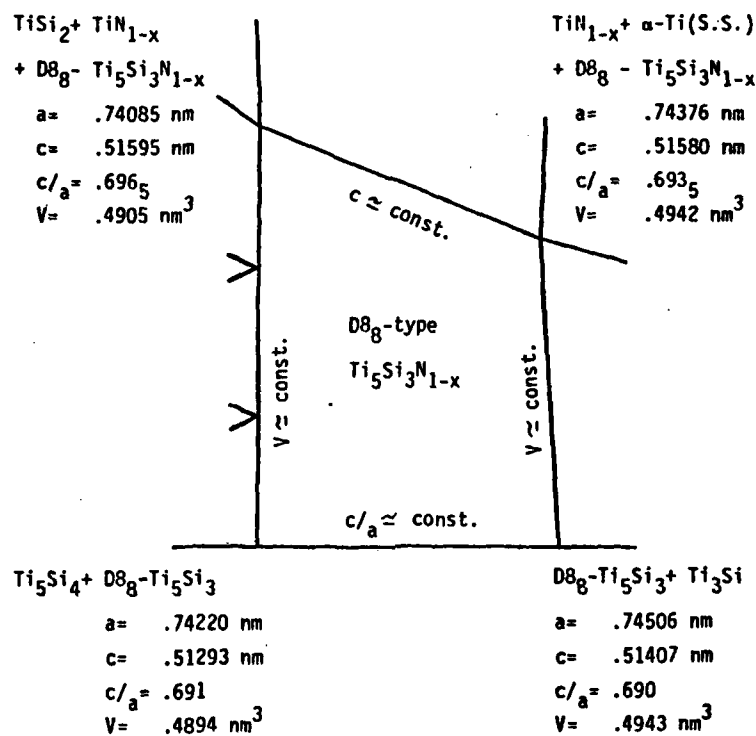
Fig. 2   Lattice parameters, c/a ratios and unit cell
volumes of the $D8_8$-type $Ti_5Si_3N_{1-x}$ phase field
homogeneity limits at 1000°C
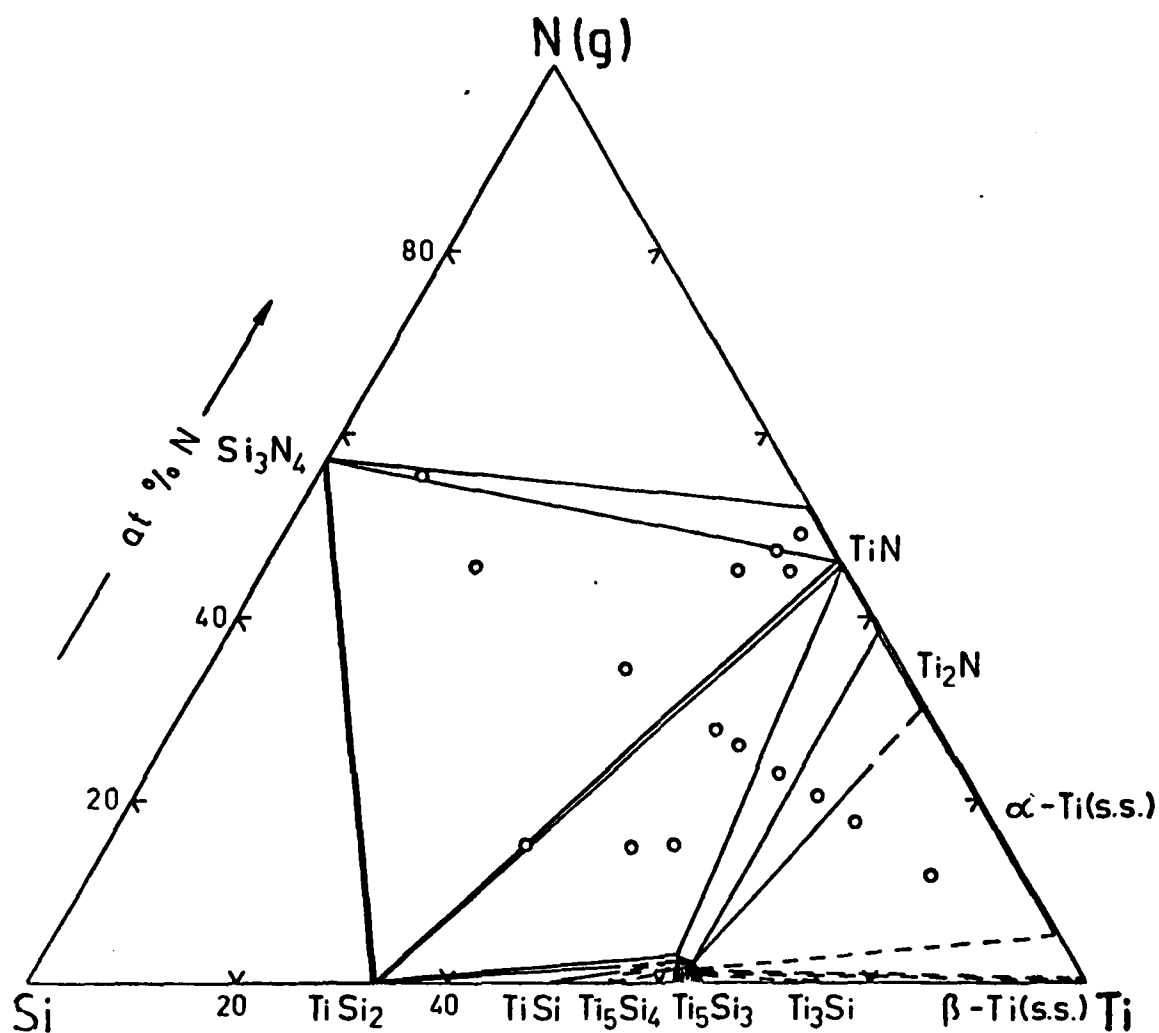
Fig. 3a   Isothermal section of the ternary system Ti-Si-N at 1000°C
(in the absence of external nitrogen pressure)
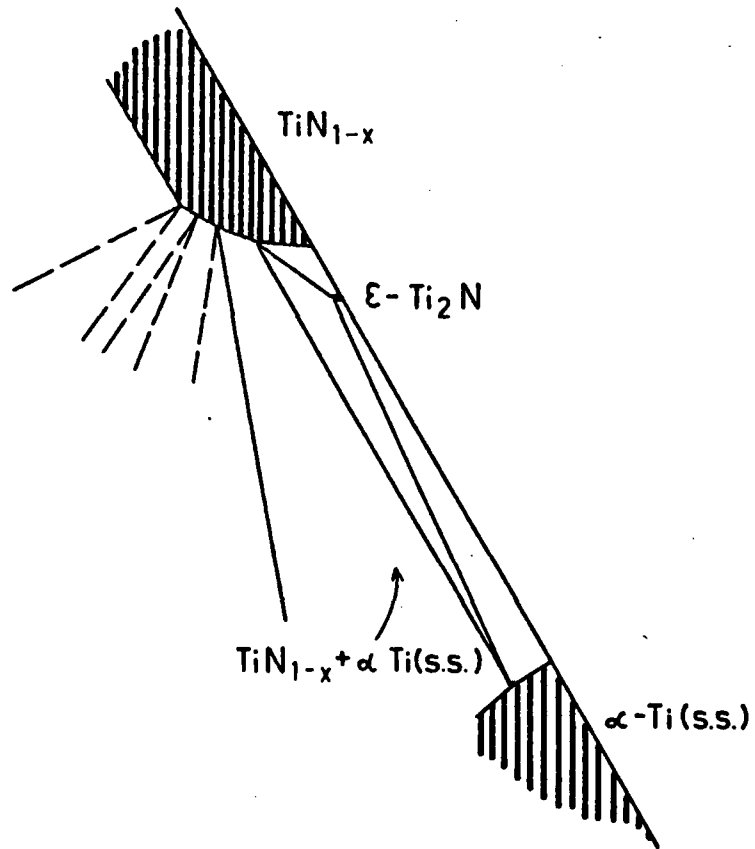
Fig. 3b Detail of the isothermal phase partition at
1000°C: The phase equilibria at compositions
close to the binary Ti-N (schematic)

BINARY SYSTEM ZIRCONIUM-SILICON

Experimental Results

The phases $ZrSi_2$, H.T.-ZrSi (CrB-type structure), L.T.-ZrSi (FeB-type structure), Zr_5Si_4, Zr_3Si_2 and Zr_2Si are corroborated and their crystal structures are confirmed. Lattice parameters observed are close to reference data [1].

In addition a $D8_8$-type phase forms in an arc melted alloy $Zr_{62.5}Si_{37.5}$ even when ultrapure materials and processing conditions are applied. This Zr_5Si_3 phase decomposes upon annealing at 1000°C for 550 h to a considerable extent into Zr_3Si_2 and Zr_2Si. Zr_5Si_3 is therefore an equilibrium phase in the binary system Zr-Si at high temperatures. This is in agreement with the phase diagram (fig.4) by Kochershinskii et al [2] (reproduced by Moffatt [3]) but not with the one by Rudy [4] (reproduced in ref.1). Lattice parameters are given in tab.4.

Zr_5Si_4 melts congruently. This is again in agreement with the phase diagram by Kochershinskii et al. but not the one by Rudy. However no phase transformation of Zr_5Si_4 was observed in our specimen.

The transformation of ZrSi from the CrB-type structure (H.T.-ZrSi) to the FeB-type structure (L.T.-ZrSi) has been found to be not only temperature dependent but also to be sensitive to small changes in composition: ZrSi with CrB-type structure in an alloy with a composition at the Zr-rich phase limit (traces of Zr_5Si_4 present) does not transform into the FeB-type structure after anneal at 1000°C for 550 h. However at the Si-rich phase limit (traces of $ZrSi_2$ present) the FeB-type modification of ZrSi is

observed in the as cast and the heat treated specimen. The amount of the
FeB-type modification increases during annealing. The volumes of the
unit cells of the two modifications of ZrSi were found to be identical
(CrB-type: a= 0.37629 nm, b= 0.99191 nm, c= 0.37451 nm, V= 0.1398 nm^3;
FeB-type: a= 0.69821 nm, b= 0.37856, c= 0.52901 nm, V= 0.1398 nm^3).

The phase Zr_3Si [5,6] was not observed in the present investigation.
This might be due to a possibly very slow rate of formation of that
phase at the annealing temperature chosen (1000°C).

References

1) P.Rogl and J.C.Schuster, 1st Semiannual Report under Contract DAJA 45-
   84-C-0038, March 1985.

2) Yu.A.Kochershinskii, O.G.Kulik and G.A.Shishkin, Metallofizika 64 (1976) 48

3) W.G.Moffatt, "Handbook of Binary Phase Diagrams" (General Electric Comp.,
   Schenectady   N.Y., 1976)

4) E.Rudy, "Compendium   of Phase Diagram Data", Report under Contract
   AFML-TR-65-2, Part V (Wright-Patterson AFB, OH., 1969)

5) K.Schubert, A.Raman and W.Rossteutscher, Naturwiss. 51 (1964) 506

6) W.Rossteutscher and K.Schubert, Z.Metallk. 56 (1965) 813

7) H.Schachner, H.Nowotny and R.Machenschalk, Mh.Chem. 84 (1953) 677

8) F.A.Shunk, "Constitution of Binary Alloys, Second Supplement",
   (McCraw-Hill, .Y., 1967)

Tab.4 Lattice parameters for Zr_5Si_3 (hexagonal, $P6_{3/mmm}$, $D8_8$-type, Mn_5Si_3-type structure)

			comment	reference
a= 0.7886 nm	c= 0.5558 nm	c/a= 0.705	impure	7
a= 0.7945 nm	c= 0.5559 nm	c/a= 0.700		8
a= 0.79488 nm	c= 0.55588 nm	c/a= 0.699	Si-rich	this work
a= 0.79551 nm	c= 0.55617 nm	c/a= 0.699	Zr-rich	this work

Fig. 4 The binary system Zr-Si (according to Kochershinskii et al., Metallofizika 64 (1976) 48
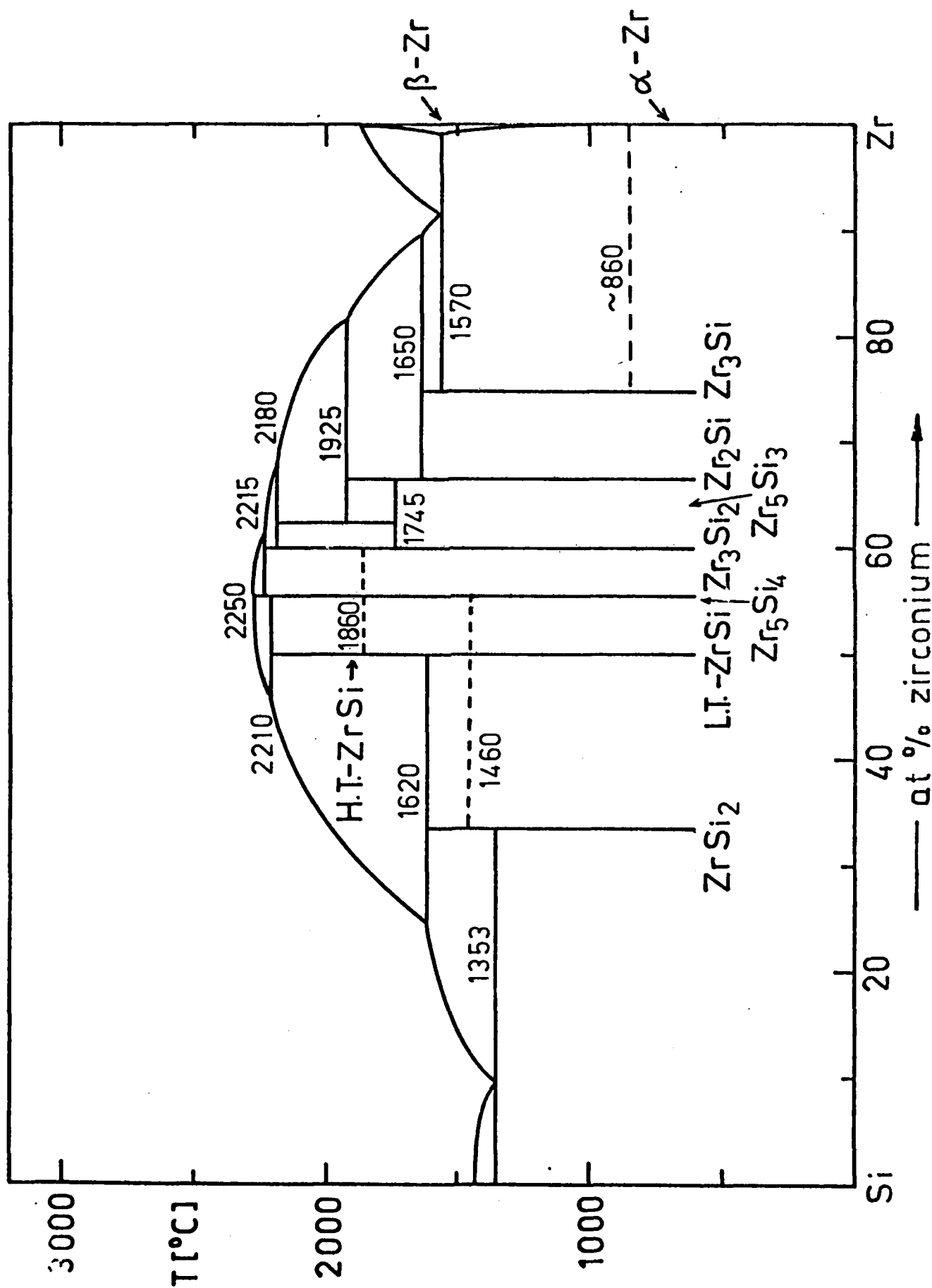
TERNARY SYSTEM ZIRCONIUM-SILICON-NITROGEN

Literature Review

Nowotny et al.[1] investigated the section Zr_5Si_3-N of the system Zr-Si-N at 1600°C under argon by adding ZrN to a mixture $Zr_{62.5}Si_{37.5}$. At very low nitrogen contents $D8_8$-type $Zr_5Si_3N_{1-x}$ was observed to coexist with Zr_3Si_2 ("U_I"). At nominally 5 at% nitrogen they observed single phase $D8_8$-$Zr_5Si_3N_{1-x}$. At nominally 10 at% nitrogen they found $D8_8$-$Zr_5Si_3N_{1-x}$ in equilibrium with ZrSi and ZrN. Nitriding Zr_5Si_3 at 1400°C or 1800°C with NH_3 yields ZrN. A phase field partition of the $D8_8$-phase is given for the system Zr-Si-C (fig.5) and it is claimed that the analogous equilibria exist in the system Zr-Si-N.

ZrN is reported to react with Si[2]. Si_3N_4 is decomposed by Zr[3]. The reaction products were not identified. Krilov and Bronnikov[4] calculated from binary thermochemical data the reaction products to be ZrN, Zr_2Si, Zr_5Si_3, $ZrSi_2$, $ZrSi_3$(!), Si and N_2 for temperature up to 1000°C.

References

1) H.Nowotny, B.Lux and H.Kudielka, Mh.Chem. 87 (1956) 447

2) G.A.Yashinskaya, Porosh.Met. (7) (1966) 53

3) L.Brewer and O.Krikorian, J.Electrochem.Soc. 103 (1956) 43

4) Yu.I.Krilov and V.A.Bronnikov, Porosh.Met. (1) (1976) 52

Experimental Results

At 1000°C all solid state reactions in the system Zr-Si-N proceed very slowly. In order to reach equilibrium multiple annealing with intermediate powderisation of the pellets was necessary.

Neither at 1000°C nor at 1300°C the $D8_8$-type phase Zr_5Si_3 is stable in the binary system Zr-Si but exists stabilized by nitrogen as a ternary phase $Zr_5Si_3N_{1-x}$. It coexists at both temperatures with ZrN, Zr_2Si, Zr_3Si_2, Zr_5Si_4 and ZrSi (CrB-type). The lattice parameters found are a= 0.78922 nm, c= 0.56251 nm (coexisting at 1000°C with ZrSi + ZrN) and a= 0.78922 nm, c= 0.56477 nm (coexisting at 1000°C with ZrN). The solution of nitrogen increases the ratio c/a from 0.699 for the binary Zr-Si alloy up to 0.716 for the composition most rich in nitrogen. No other ternary phase is observed (tab.5).

Si_3N_4 coexist at 1000°C with ZrN and ZrSi (FeB-type) and at 1300°C with ZrN and $ZrSi_2$ (fig.6a and b).

Tab.5: Solid state reaction products observed in the system Zr-Si-N
upon annealing at 1000°C (evacuated quartz tube)

$ZrN + 58$ at% Si $\xrightarrow{500 \text{ h}}$ $Si_3N_4 + ZrSi_2$

$Si_3N_4 + 20$ at% Zr $\xrightarrow{400 \text{ h}}$ $Si_3N_4 + ZrN + ZrSi$ (FeB-type)

$Si_3N_4 + 40$ at% Zr $\xrightarrow{400 \text{ h}}$ $Si_3N_4 + ZrN + ZrSi$ (FeB-type)

$Si_3N_4 + 52$ at% Zr $\xrightarrow{600+300\text{h}}$ $ZrSi$ (CrB-type) $+ Zr_5Si_3N_{1-x} + ZrN$

$Si_3N_4 + 56$ at% Zr $\xrightarrow{240+120\text{h}}$ $Zr_5Si_3N_{1-x} + ZrN$ (+ traces of Si_3N_4 and Zr)

$Si_3N_4 + 58$ at% Zr $\xrightarrow{400 \text{ h}}$ $Zr_5Si_3N_{1-x} + Zr_2Si + ZrN$

$Si_3N_4 + 80$ at% Zr $\xrightarrow{400 \text{ h}}$ $Zr_2Si + \alpha\text{-Zr}$ (S.S.) $+ ZrN$
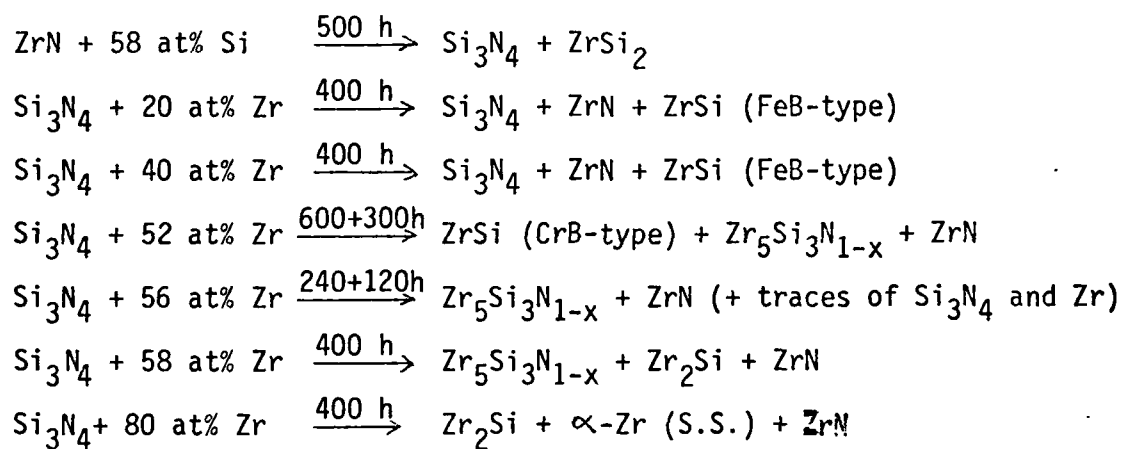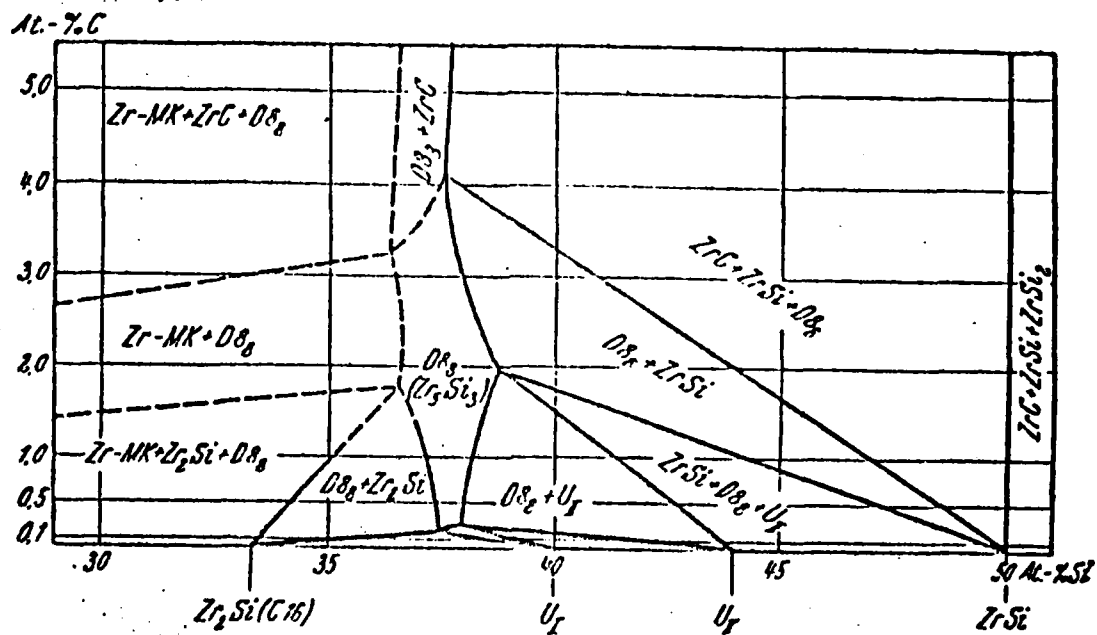
Fig. 5 Phase field partition in the system Zr-Si-C at 1400°C
(H.Nowotny, B.Lux and H.Kudielka, Mh.Chem. 87 (1956) 447
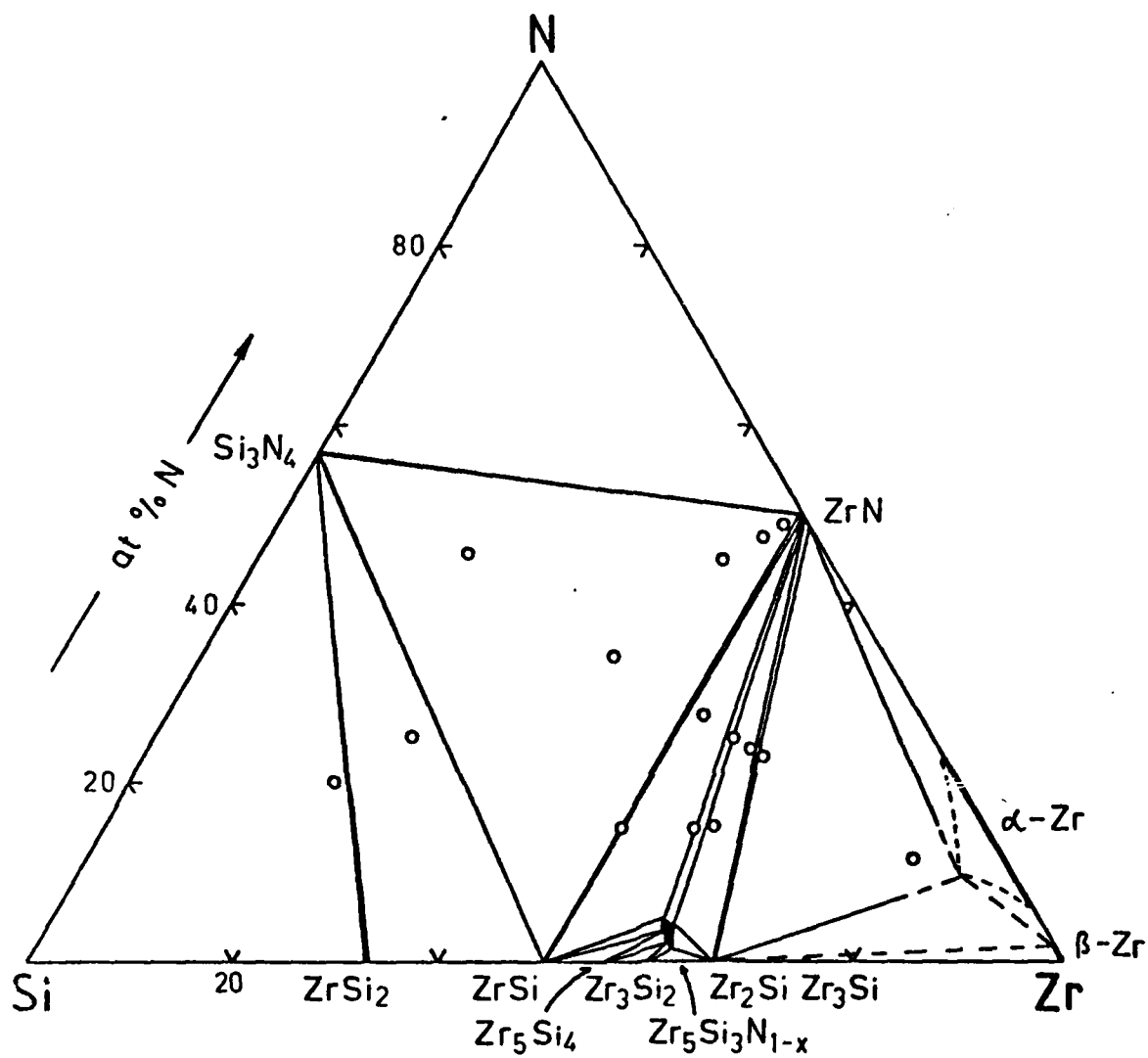
Fig. 6a   Isothermal section of the ternary system Zr-Si-N at 1000°C
           (in the absence of external nitrogen pressure)
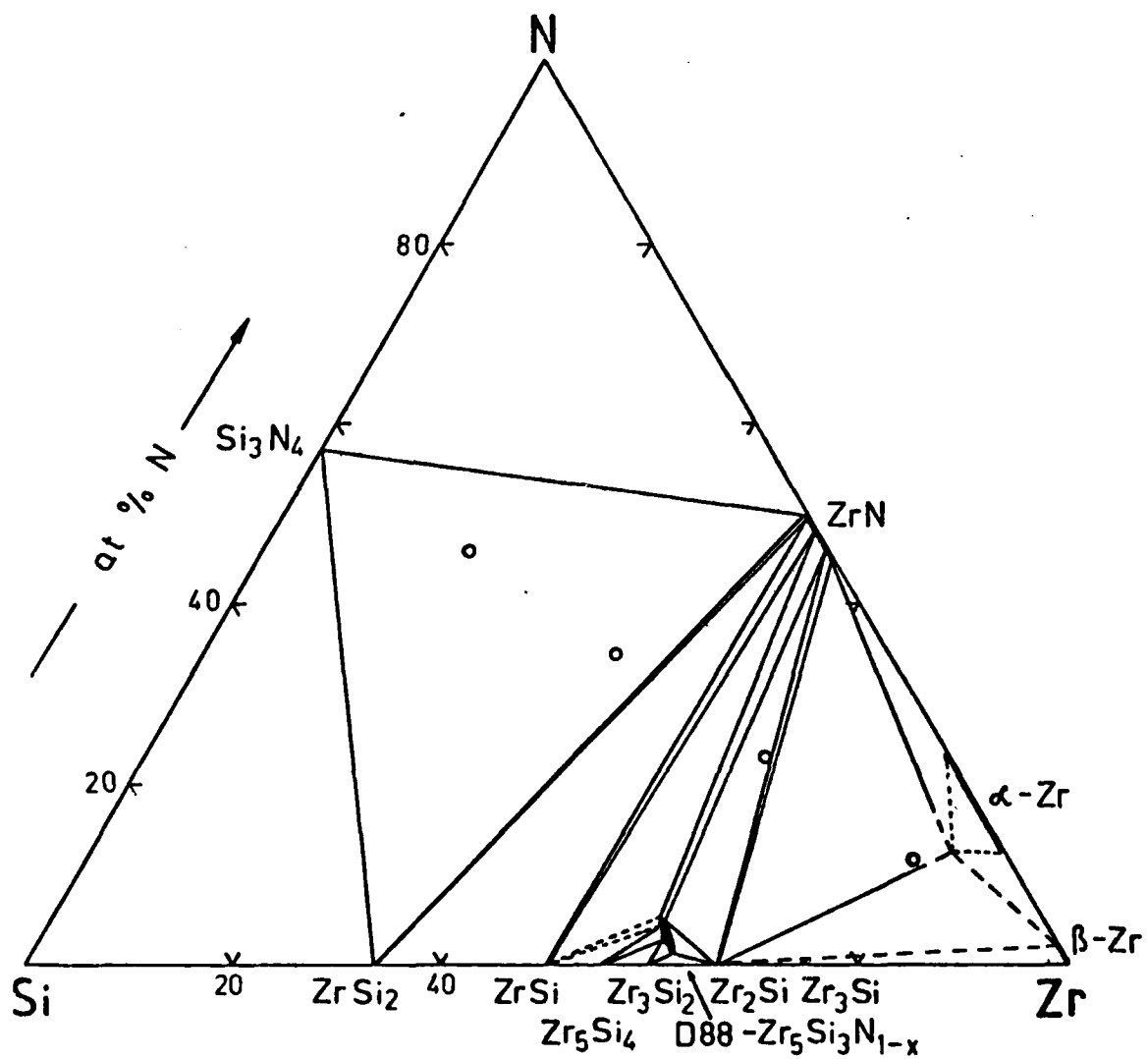
Fig. 6b Isothermal section of the ternary system Zr-Si-N at 1300°C
(in the absence of external nitrogen pressure)

BINARY SYSTEM VANADIUM-SILICON

Experimental Results

All intermediate phases reported in the literature[1] are corroborated and confirmed with respéct to crystal structure. The lattice parameters found are in close agreement with literature values. No discrepancy to the established phase diagram is detected (tab.6).

References

1) P.Rogl and J.C.Schuster, 1st Semiannual Report under Contract
   DAJA45-84-C-0038 (March 1985)

Tab.6. Results of X-ray analysis of binary V-Si alloys

at% V	as cast	annealed, 1500°C, 48h
33	VSi_2	VSi_2
50	$VSi_2 + V_6Si_5$	V_6Si_5 + trace VSi_2
55	V_6Si_5 + trace VSi_2	V_6Si_5
57	$V_6Si_5 + V_5Si_3$	$V_6Si_5 + V_5Si_3$
60	$V_5Si_3 + V_6Si_5$	V_5Si_3
62,5	V_5Si_3	V_5Si_3
75	V_3Si	V_3Si

BINARY SYSTEM VANDIUM-NITROGEN

Experimental Results

Specimen with compositions ranging from 5 to 45 at% nitrogen were annealed at temperatures between 1000°C and 1750°C under pure argon. The results of X-ray analysis (tab.7) agree with the data compiled in ref.1. Attempts to confirm the peritectic nature of the decomposition mode of V_2N by optical or electron microscopy led to inconclusive results, since the cast specimen were too porous due to nitrogen gas evolution during melting.

Reference

1) P.Rogl, J.C.Schuster, 1st Semiannual Report under Contract
   DAJA45-84-C-0038 (March 1985)

Tab.7. Results of X-ray analysis of binary V-N alloys (sintered under 10^5Pa of argon)

nominal composition		annealed at	annealed at	annealed at
at%V	at%N	1000°C, 300h	1200°C, 30h	1750°C, 2h
95	5	$V + V_9N_4$	$V + V_9N_4$	
90	10	$V + V_9N_4$	$V + V_9N_4$	V_9N_4
85	15	$V + V_9N_4$	$V + V_9N_4$	V_9N_4
80	20	$V + V_9N_4$	$V + V_9N_4$	V_9N_4
75	25	$V_9N_4 + VN$	V_9N_4	V_9N_4
70	30	$V_9N_4 + VN$	V_9N_4	V_9N_4
65	35	$V_9N_4 + VN$	V_9N_4	V_9N_4
60	40	$V_9N_4 + VN$	V_9N_4	V_9N_4
55	55	$V_9N_4 + VN$	V_9N_4	V_9N_4

TERNARY SYSTEM VANADIUM-SILICON-NITROGEN

Literature Review

Nowotny et al.[1] prepared specimen along the section $V_{.625}Si_{.375}$-N. Compacted powder mixtures of silicon and vanadium were heated under NH_3 gas. This led to the formation of a $D8_8$-type ternary phase $V_5Si_3N_{1-x}$ and VN.

H.Feld et al.[2] reported that Si_3N_4 reacts at 1730°C under vacuum or inert gas within 5 minutes.

Experimental Results

Isothermal sections at 1000°C and 1500°C are investigated. Si_3N_4 reacts with vanadium to form binary and ternary phases (tab.8). The only ternary phase observed is $V_5Si_3N_{1-x}$ with $D8_8$-type structure. This phase coexists at 1000°C with Si_3N_4, all binary vanadium silicides and V_9N_4 (fig.7a). Since Si_3N_4 decomposes under 10^5Pa argon at temperatures below 1500°C a tieline exists between the $D8_8$-type $V_5Si_3N_{1-x}$ phase and nitrogen gas at 1500°C (fig.7b). The lattice parameters of $V_5Si_3N_{1-x}$ coexisting at 1000°C with V_3Si and V_9N_4 as well as coexisting with Si_3N_4 were found to be a= 0.7121 nm and c= 0.48473 nm, c/a= 0.681. At 1500°C the lattice parameters are increased to a= 0.71554 and c= 0.48521, c/a= 0.678 for $V_5Si_3N_{1-x}$ coexisting with either VSi_2 or V_9N_4. Chemical analysis of the alloy $[Si_3N_4 + 40\ at\%\ V]$ which was single phase according to X-ray data after anneal at 1500°C for 30h under argon yielded 15,1 at% nitrogen indicating complete filling of the octahedral voids in the $D8_8$ structure by nitrogen at this temperature.

Annealing $V_{.625}Si_{.375}$ under 10^6Pa nitrogen at 1400°C led to the formation of VN.

References

1) H.Nowotny, B.Lux and H.Kudielka, Mh.Chem. 87 (1956) 447

2) H.Feld, E.Gugel and H.G.Nitzsche, Werkstoffe u. Korrosion, 20 (1969) 571

Tab.8 Solid state reaction products observed in the system V-Si-N

a) upon annealing at 1000°C for 600h (evacuated quartz tube)

Si_3N_4 + 20 at% V $\longrightarrow$ Si_3N_4 + V_9N_4

Si_3N_4 + 40 at% V $\longrightarrow$ Si_3N_4 + V_9N_4

Si_3N_4 + 80 at% V $\longrightarrow$ V_3Si + V_9N_4

Si_3N_4 + 90 at% V $\longrightarrow$ V_3Si + V + V_9N_4

$V_{.33}Si_{.67}$ + Si_3N_4(10 at% N) $\longrightarrow$ Si_3N_4 + VSi_2

$V_{.33}Si_{.67}$ + VN (10 at% N) $\longrightarrow$ Si_3N_4 + VSi_2 + $V_5Si_3N_{1-x}$

$V_{.33}Si_{.67}$ + VN (15 at% N) $\longrightarrow$ Si_3N_4 + VSi_2 + $V_5Si_3N_{1-x}$

$V_{.33}Si_{.67}$ + VN (20 at% N) $\longrightarrow$ Si_3N_4 + $V_5Si_3N_{1-x}$

$V_{.675}Si_{.375}$ + Si_3N_4(10 at% N) $\longrightarrow$ Si_3N_4 + $V_5Si_3N_{1-x}$

$V_{.75}Si_{.25}$ + Si_3N_4(10 at% N) $\longrightarrow$ $V_5Si_3N_{1-x}$ + V_9N_4

b) upon annealing at 1500°C for 30h (RF-furnace, 10^5Pa argon)

Si_3N_4 + 20 at% V $\longrightarrow$ VSi_2 + $V_5Si_3N_{1-x}$

Si_3N_4 + 30 at% V $\longrightarrow$ $V_5Si_3N_{1-x}$ + trace VSi_2

Si_3N_4 + 40 at% V $\longrightarrow$ $V_5Si_3N_{1-x}$

Si_3N_4 + 50 at% V $\longrightarrow$ $V_5Si_3N_{1-x}$ + V_9N_4

Si_3N_4 + 60 at% V $\longrightarrow$ $V_5Si_3N_{1-x}$ + V_9N_4

Si_3N_4 + 85 at% V $\longrightarrow$ V_3Si + V_9N_4

$V_{.60}Si_{.40}$ + VN(30 at% N) $\longrightarrow$ $V_5Si_3N_{1-x}$

$V_{.50}Si_{.50}$ + VN(3 at% N) $\longrightarrow$ $V_5Si_3N_{1-x}$ + VSi_2

$V_{.50}Si_{.50}$ + VN(25 at% N) $\longrightarrow$ $V_5Si_3N_{1-x}$ + V_9N_4

$V_{.75}Si_{.25}$ + VN(5 at% N) $\longrightarrow$ $V_5Si_3N_{1-x}$ + V_9N_4

Fig. 7a   Isothermal section of the ternary system V-Si-N at 1000°C
(in the absence of external nitrogen pressure)
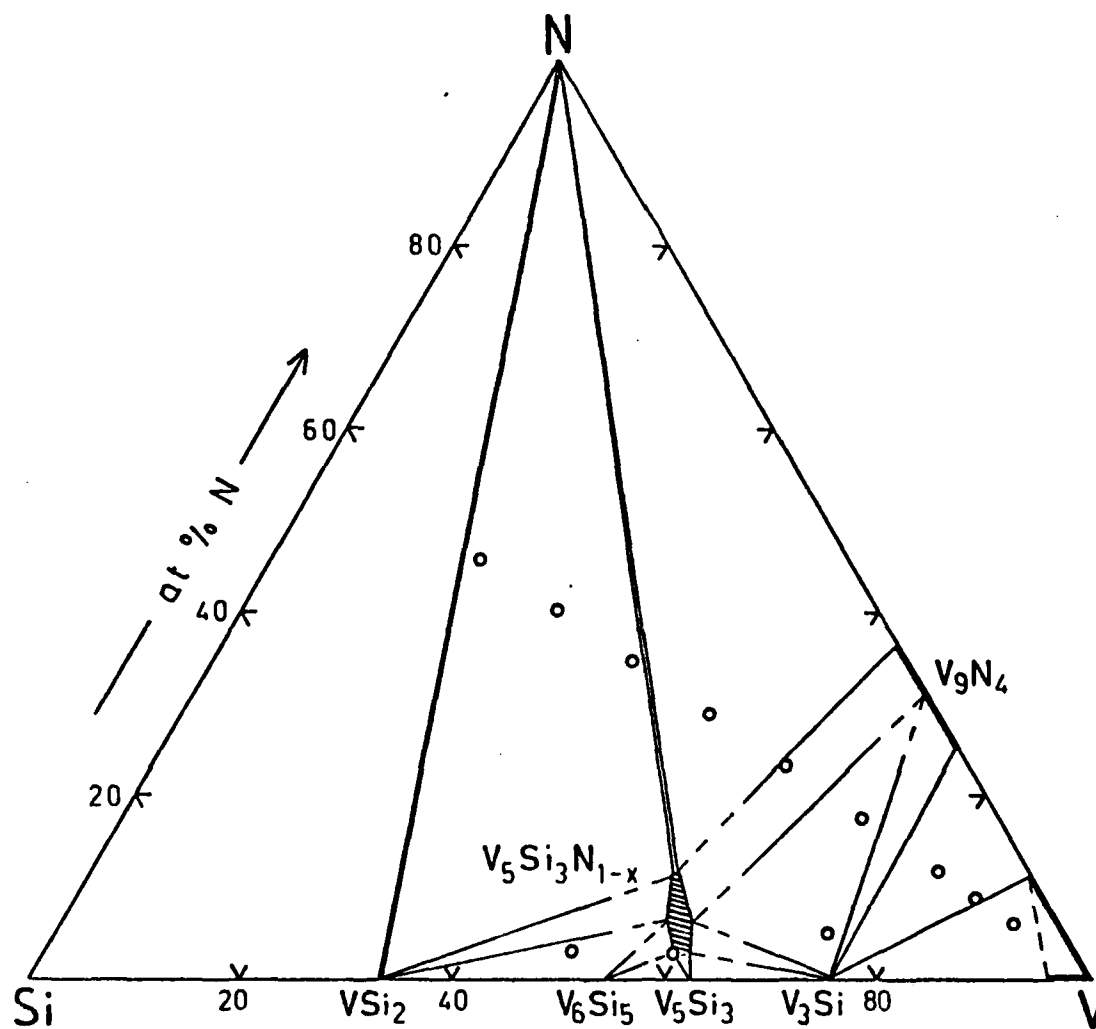
Fig. 7b Isothermal section of the ternary system V-Si-N at 1500°C
(in the absence of external nitrogen pressure)

THE BINARY SYSTEM NIOBIUM-SILICON

Experimental Results

All intermediate phases reported in the literature[1] are corroborated and confirmed with respect to crystal structure. The lattice parameters found are close to literature values. The results of X-ray analysis (tab.9) and optical micrographs agree with the established phase diagram.

Reference

1) P.Rogl and J.C.Schuster, 1st Semiannual Report under Contract
   DAJA45-84-C-0038 (March 1985)

Tab.9 Results of X-ray analysis of binary Nb-Si alloys

at% Nb	as cast	annealed, 1500°, 30h
33	$NbSi_2$	
50	$NbSi_2 + Nb_5Si_3(W_5Si_3$-type)	
55	$NbSi_2 + Nb_5Si_3(W_5Si_3$-type)	
57	$NbSi_2 + Nb_5Si_3(W_5Si_3$-type)	$NbSi_2 + Nb_5Si_3$ (Cr_5B_3type)
62.5	$Nb_5Si_3(W_5Si_3$-type)	$NbSi_3(Cr_5B_3$-type)
67	$Nb_5Si_3(W_5Si_3$-type) + Nb_5Si_3 (Cr_5B_3-type)	$Nb + Nb_5Si_3$ (Cr_5B_3-type)
75	$Nb_5Si_3(Cr_5B_3$-type) + Nb_3Si	$Nb + Nb_5Si_3(Cr_5B_3$-type)
80	Nb_3Si + trace Nb	
81.8	$Nb_3Si + Nb$	

TERNARY SYSTEM NIOBIUM-SILICON-NITROGEN

Literature Review

For temperature up to 1000°C Krylov and Bronnikov[1] calculated from thermochemical data that Si_3N_4 reacts with niobium to form Nb_5Si_3 and Nb_2N. This was confirmed by the same authors by experimental results. They found Nb_5Si_3, $NbSi_2$, Nb_2N and NbN to be the solid state reaction products.

For temperatures of 1400°C and higher H.Nowotny et al.[2] as well as Brewer and Krikorian[3] reported the formation of a ternary phase $Nb_5Si_3N_{1-x}$ with $D8_8$-type structure upon nitriding an alloy $Nb_{.625}Si_{.375}$. Using ammonia for nitridization instead of nitrogen gas cubic δ-NbN with lattice parameters of a= 0.441-0.444 nm was formed in addition to $Nb_5Si_3N_{1-x}$. δ-NbN was the main reaction product at 1800°C[2].

Experimental Results

The phase equilibria at 1000°C (fig.8a) found by X-ray analysis of a limited number of alloys (tab.10a) confirm the results of Krilov and Bronnikov[1]. Si_3N_4 is found to coexist with ε-NbN, γ-Nb_4N_3, β-Nb_2N, Nb_5Si_3 (Cr_5B_3-type) and $NbSi_2$ but not with Nb. No change of lattice parameters for binary phases in ternary alloys is observed. Thus one can assume negligible solubility of the respective third component in these phases.

In alloys annealed at 1500°C the $D8_8$-type phase $Nb_5Si_3N_{1-x}$ occurs (tab.10b). The solid phases found to coexist with $Nb_5Si_3N_{1-x}$ at this temperature are $NbSi_2$, Nb_5Si_3 (Cr_5B_3-type), β-Nb_2N and δ-NbN (fig.8b). In perfect agreement with earlier results[2] we find the lattice parameter c of $Nb_5Si_3N_{1-x}$ to increase with nitrogen content from c= 0.52487 nm to 0.53103 nm while the value for a remains constant at a= 0.75169 nm. The nitrogen content in the alloy $[Si_3N_4 + 20$ at% $Nb]$ after annealing at 1500°C under argon for 30h was found to be 0.19 wt%. Considering the fact that besides $Nb_5Si_3N_{1-x}$ minor amounts of $NbSi_2$ were present in the sample this nitrogen content indicates complete or almost complete filling of the octahedral voids in the $D8_8$-type structure by

nitrogen atoms.

Nitriding $Nb_{.625}Si_{.375}$ at 1400°C under 10^6 Pa nitrogen results in the formation of δ-NbN.

References

1) Yu.I.Krilov and V.A.Bronnikov, Porosh.Met. (1)   (1976) 52

2) H.Nowotny, B.Lux and H.Kudielka, Mh.Chem. 87 (1956) 447

3) L.Brewer and O.Krikorian, J.Electrochem.Soc. 103 (1956) 38

Tab.10. Solid state reaction products observed in the system Nb-Si-N

a) upon annealing at 1000°C for 600h (evacuated quartz tube)

$Si_3N_4^- + \delta\text{-NbN}$ $\longrightarrow$ $Si_3N_4 + \epsilon\text{-NbN} + \gamma\text{-Nb}_4N_3$

$Si_3N_4 + 20$ at% Nb $\longrightarrow$ $Si_3N_4 + \beta\text{-Nb}_2N + Nb_5Si_3(Cr_5B_3\text{-type})$

$Si_3N_4 + 55$ at% Nb $\longrightarrow$ $Si_3N_4 + \beta\text{-Nb}_2N + Nb_5Si_3(Cr_5B_3\text{-type})$

$Si_3N_4 + 75$ at% Nb $\longrightarrow$ $\beta\text{-Nb}_2N + Nb_5Si_3(Cr_5B_3\text{-type})$

$Nb_{.50}Si_{.50} + Si_3N_4(10$ at% N$)$ $\longrightarrow$ $Si_3N_4 + NbSi_2 + Nb_5Si_3(Cr_5B_3\text{-type})$

b) upon annealing at 1500°C for 30h (RF-furnace, 10^5Pa, argon)

$Si_3N_4 + 20$ at% Nb $\longrightarrow$ $Nb_5Si_3N_{1-x} + NbSi_2$

$Nb_{.50}Si_{.50} + \delta\text{-NbN}(5$ at% N$)$ $\longrightarrow$ $Nb_5Si_3N_{1-x} + NbSi_2$

$Si_3N_4 + 55$ at% Nb $\longrightarrow$ $Nb_5Si_3N_{1-x} + \zeta\text{-NbN}$

$Nb_{.625}Si_{.375} + \delta\text{-NbN}(5$ at% N$)$ $\longrightarrow$ $Nb_5Si_3N_{1-x} + \beta\text{-Nb}_2N$
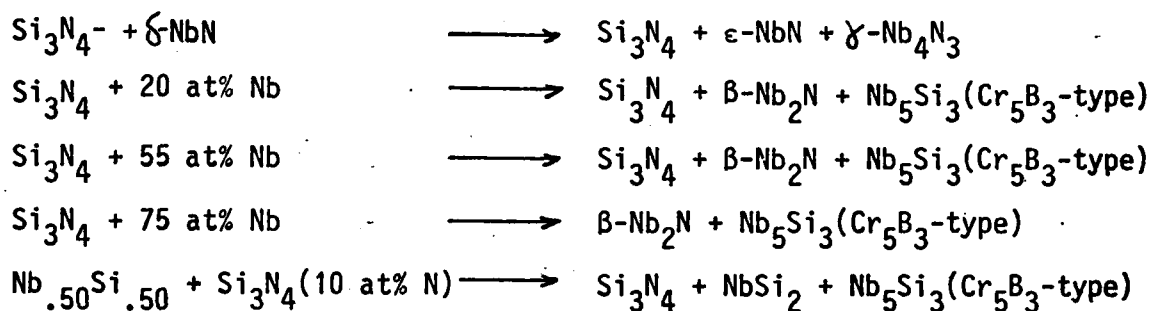
$Nb_{.75}Si_{.25} + \delta\text{-NbN}(5$ at% N$)$ $\longrightarrow$ $Nb_5Si_3N_{1-x} + \beta\text{-Nb}_2N$
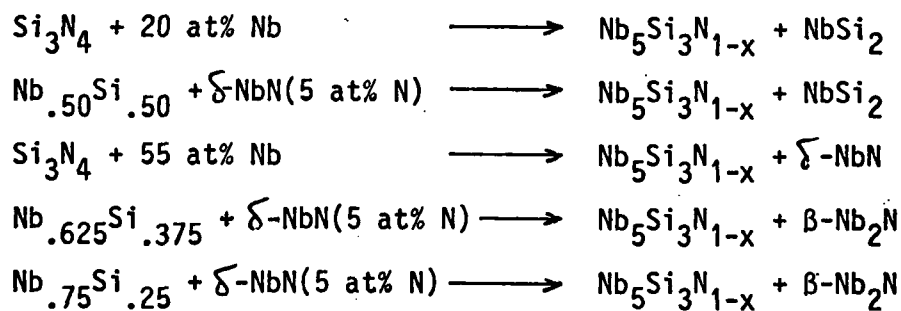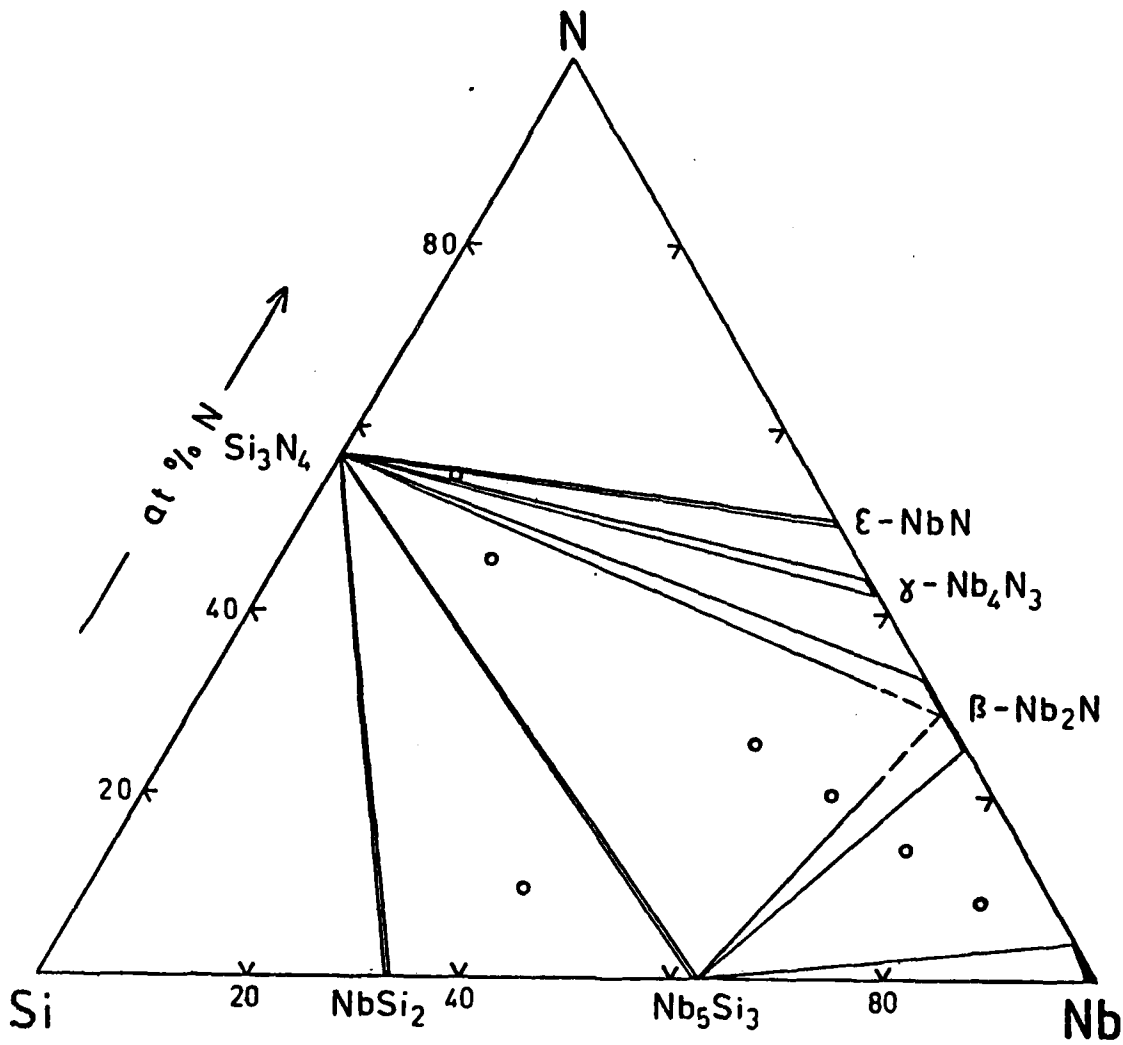
Fig. 8a   Isothermal section of the ternary system Nb-Si-N at 1000°C
(in the absence of external nitrogen pressure)
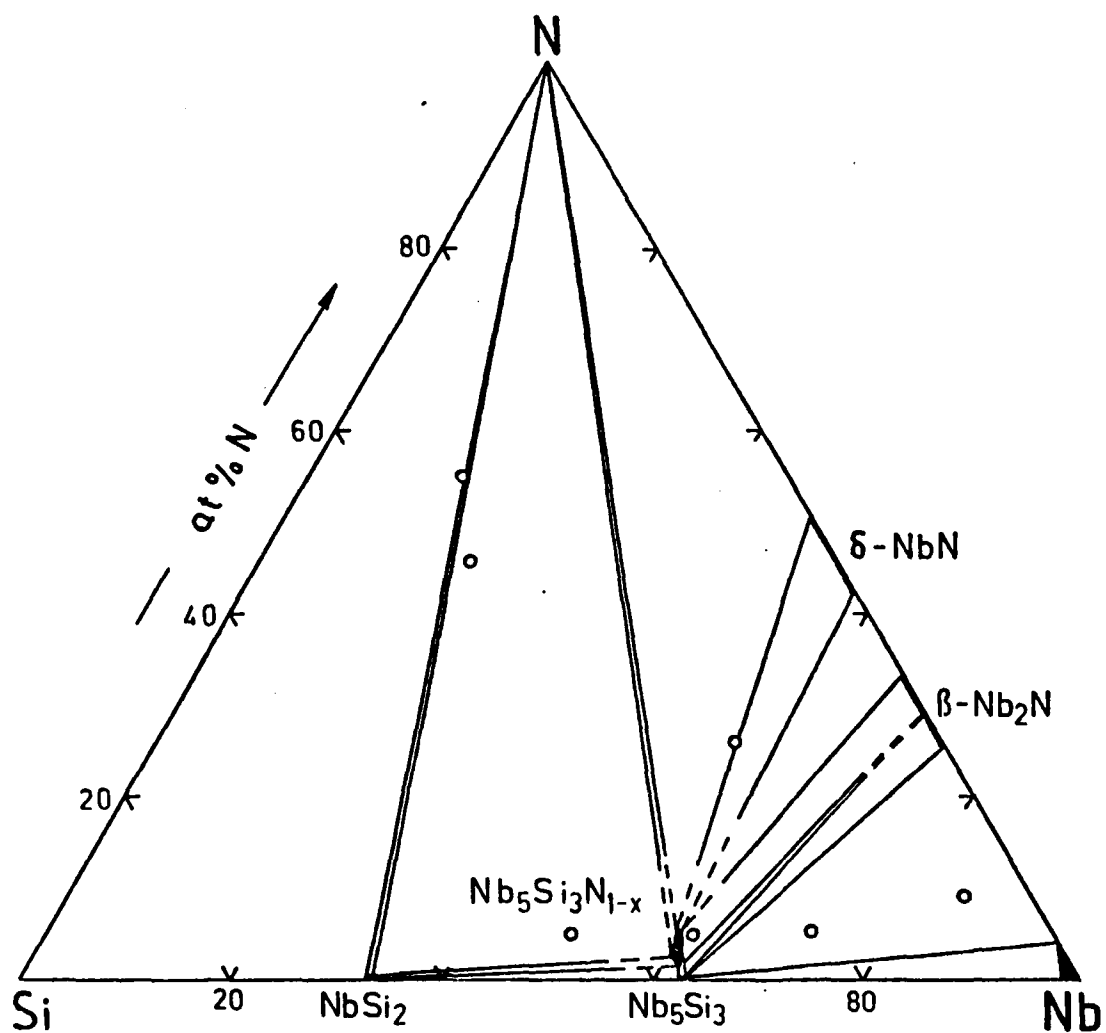
Fig. 8b Isothermal section of the ternary system Nb-Si-N at 1500°C
(in the absence of external nitrogen pressure)

BINARY SYSTEM TANTALUM-SILICON

Experimental Results

All intermediate phases reported in the literature[1] are corroborated and confirmed with respect to crystal structure. The lattice parameters found are in close agreement with literature values. No discrepancy to the established phase diagram is detected (tab.11).

Reference

1) P.Rogl and J.C.Schuster, 1st Semiannual Report under Contract
   DAJA45-84-C-0038 (March 1985)

Tab.11. Results of X-ray analysis of binary Ta-Si alloys

at% Ta	as cast	annealed, 1500°C, 30h
33,3	$TaSi_2$	
50	$TaSi_2 + Ta_5Si_3$	
62,5	Ta_5Si_3 + trace $TaSi_2$	Ta_5Si_3 + trace $TaSi_2$
67	Ta_2Si	Ta_2Si
75	Ta_3Si	
80	Ta_3Si + trace Ta	Ta_3Si + trace Ta
81.8	Ta_3Si + Ta	Ta_3Si + Ta
83.3	Ta_3Si + Ta	Ta_3Si + Ta
95	Ta + trace Ta_3Si	

TERNARY SYSTEM TANTALUM-SILICON-NITROGEN

Literature Review

Due to considerable interest in technological applications such as metal-ceramic joints[1], Si_3N_4 enforced Ta-wire[2] or the use of Si_3N_4 layers as dielectrics[3] this ternary system was studied in more detail. Brewer and Krikorian[4] reported an isothermal section for 1600K under an atmosphere of 7.5×10^4 Pa nitrogen (fig.9). It shows a ternary phase, $Ta_5Si_3N_{1-x}$ with $D8_8$-type structure in equilibrium with Ta_2N, TaN, nitrogen gas, Si_3N_4, $TaSi_2$ and Ta_5Si_3. No information on the Ta-rich region of the system is given. Nowotny et al.[5] observed at 1400°C the formation of $D8_8$-$Ta_5Si_3N_{1-x}$ upon nitriding $Ta_{.625}Si_{.375}$ using ammonia or nitrogen gas as nitriding agent. Recently Tamari and Toibana[6] reported the results of the reaction between Si_3N_4 and tantalum (60 mol%) at temperatures between 1000°C and 1700°C. Although equilibrium was not reached the data demonstrate the sequence of reactions taking place at 1400°C under argon (fig.10). First Si_3N_4 is decomposed under formation of β-Ta_2N. Then silicides form with increasing amount of silicon (freed from Si_3N_4) according to the sequence $Ta_2Si \longrightarrow Ta_5Si_3 \longrightarrow TaSi_2$. Finally the disilicide reacts with the initially formed β-Ta_2N yielding the $D8_8$-type phase $Ta_5Si_3N_{1-x}$. Under nitrogen atmosphere of 10^5 Pa the formation of TaN is observed additionally.

Experimental Results

To complement these data isothermal sections at 1000°C and 1500°C (fig.11) were prepared. At the lower temperature no ternary phase exists. Si_3N_4 reacts to form Ta_5Si_3 and β-Ta_2N (tab.12a). The reaction proceeds very slowly; extremly long annealing times are necessary to reach equilibrium. At 1500°C the ternary

phase $Ta_5Si_3N_{1-x}$ with $D8_8$-type structure forms (tab.12b). $Ta_5Si_3N_{1-x}$ coexists with $TaSi_2$, nitrogen gas, β-Ta_2N and Ta_5Si_3. Si_3N_4 is not stable under argon at this temperature. The lattice parameters of the $D8_8$-phase in equilibrium with $TaSi_2$ and Ta_5Si_3 are found to be a= 0.75008 nm and c= 0.52288 nm. The c parameter increases to c= 0.52457 nm at the nitrogen rich stability limit of the phase field. All lattice parameters of the binary phases remain unaltered in ternary alloys indicating negligible solubility for the respective third component.

Nitriding $Ta_{.625}Si_{.375}$ at 1400°C under 10^6Pa nitrogen results in the formation of δ-TaN and ϵ-TaN.

References

1) United Kingdom Patent No. 993443 (1965)

2) United Kingdom Patent No. 947271 (1964)

3) J.J.Brennan, Spec.Ceramics 6 (1975) 123

4) L.Brewer and O.Krikorian, J.Electrochem.Soc. 103 (1956) 38

5) H.Nowotny, B.Lux and H.Kudielka, Mh.Chem. 87 (1956) 447

6) N.Tamari and Y.Toibana, Osaka Kogyo Gijutsu Shikensho Kiho 32 (1981) 126

Tab.12. Solid state reaction products observed in the ternary system Ta-Si-N

a) upon annealing at 1000°C for 600h (evacuated quartz tubes)

Si_3N_4 + ϵ-TaN $\longrightarrow$ Si_3N_4 + ϵ-TaN + β-Ta_2N

Si_3N_4 + 20 at% Ta $\longrightarrow$ Si_3N_4 + Ta_5Si_3 + β-Ta_2N

Si_3N_4 + 55 at% Ta $\longrightarrow$ Ta_5Si_3 + Ta_2Si + β-Ta_2N

Si_3N_4 + 75 at% Ta $\longrightarrow$ Ta_2Si + Ta_3Si + β-Ta_2N

Si_3N_4 + 85 at% Ta $\longrightarrow$ Ta_3Si + Ta + β-Ta_2N

b) upon annealing at 1500°C for 30h (RF-furnace, 10^5Pa, argon)

Si_3N_4 + 20 at% Ta $\longrightarrow$ $Ta_5Si_3N_{1-x}$

Si_3N_4 + 55 at% Ta $\longrightarrow$ $Ta_5Si_3N_{1-x}$ + β-Ta_2N

Si_3N_4 + 64 at% Ta $\longrightarrow$ $Ta_5Si_3N_{1-x}$ + β-Ta_2N

Si_3N_4 + 85 at% Ta $\longrightarrow$ Ta_3Si + β-Ta_2N + Ta

$Ta_{.33}Si_{.67}$ + ϵ-TaN(5 at% N) $\longrightarrow$ $Ta_5Si_3N_{1-x}$ + $TaSi_2$

$Ta_{.50}Si_{.50}$ + ϵ-TaN(5 at% N) $\longrightarrow$ $Ta_5Si_3N_{1-x}$ + $TaSi_2$ + Ta_5Si_3
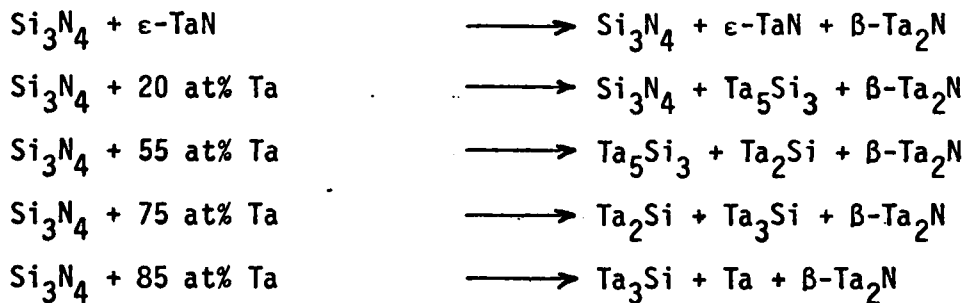
$Ta_{.67}Si_{.33}$ + ϵ-TaN(5 at% N) $\longrightarrow$ Ta_5Si_3 + trace β-Ta_2N
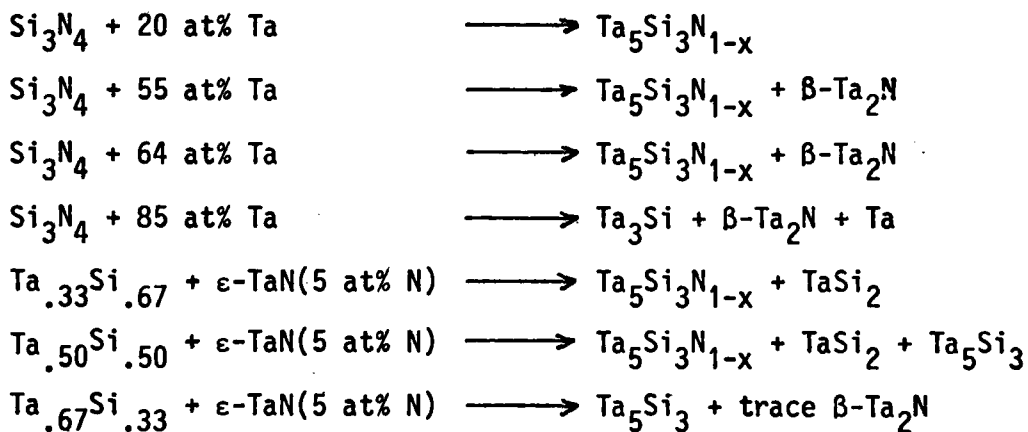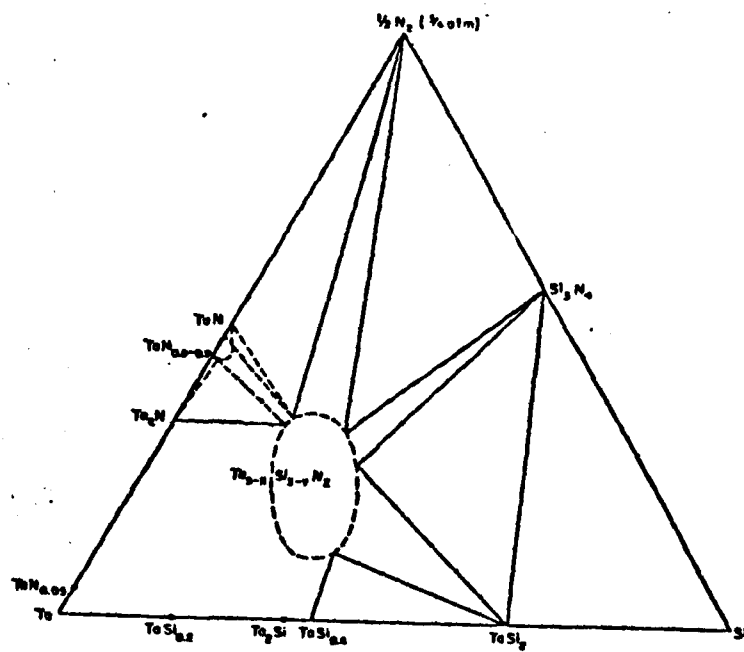
Fig. 9   Isothermal section of the ternary system Ta-Si-N
at 1600 K (under 7.5 x 10^4Pa nitrogen)
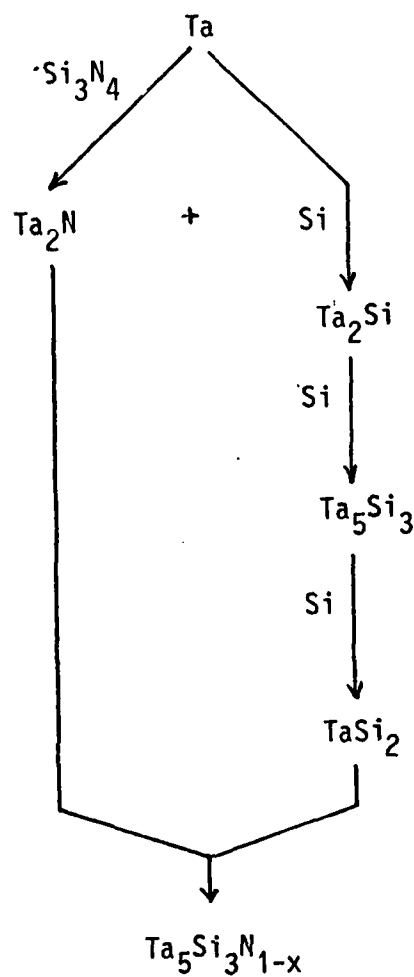
Fig. 10 Sequence of reactions taking place between
Si_3N_4 and Ta upon heating to 1400°C (according
to Tamari and Toibana, Osaka Kogyo Gijutsu
Shikensho 32 (1981) 126)
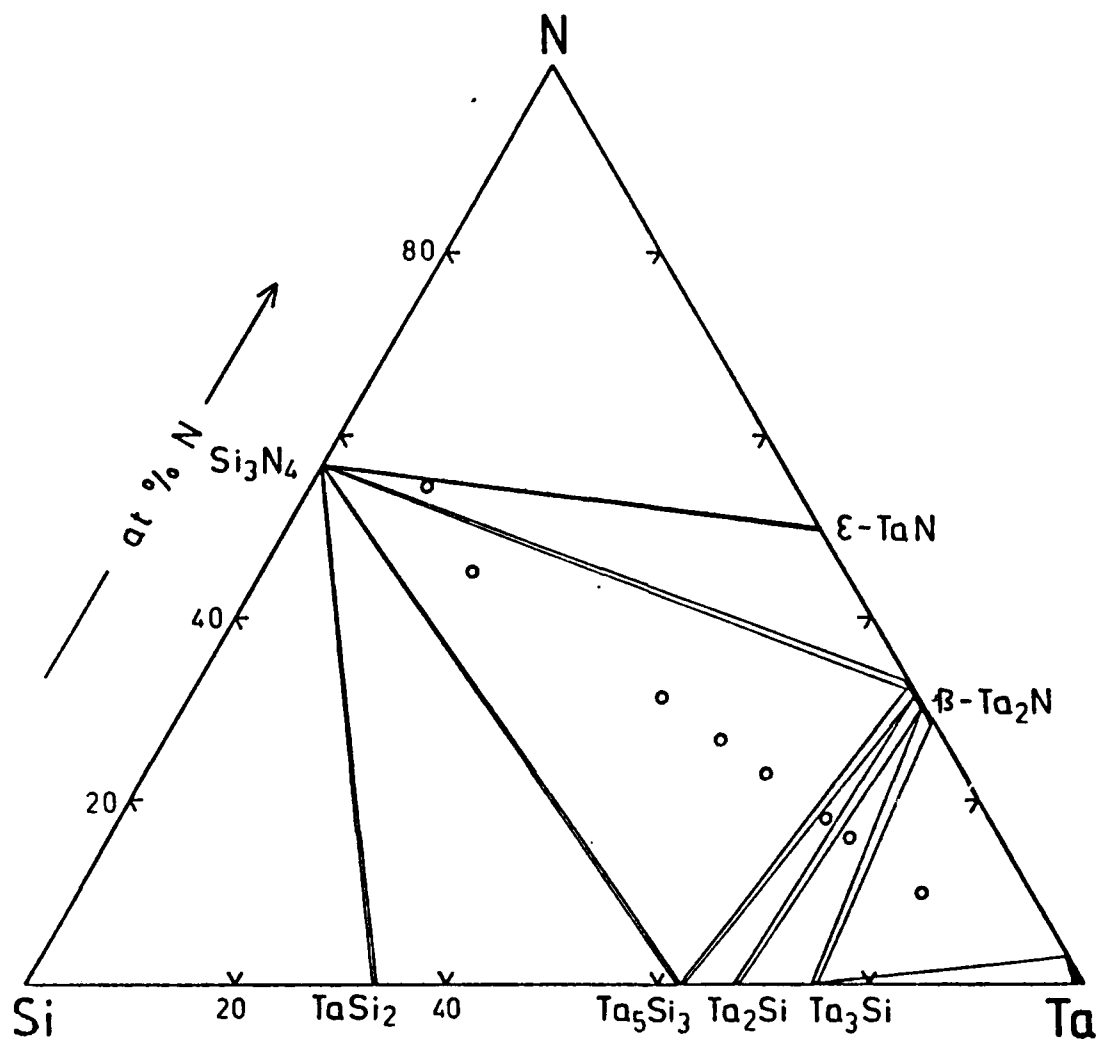
Fig. 11a   Isothermal section of the ternary system Ta-Si-N at 1000°C
   (in the absence of external nitrogen pressure)

Fig. 11b Isothermal section of the ternary system Ta-Si-N at 1500°C
(in the absence of external nitrogen pressure)

Part III Automatic Pyrometry - Pirani Furnace

The new automatic three-colour pyrometer has been tested against a series
of high precision DTA-runs in the binary system Fe-B. The pyrometer was first
calibrated to the melting point of NBS-standard copper (T_M= 1083.3°C) which
was melted in a newly assembled Thermolyne heater with a graphite holder
for the copper bar, ensuring a black body condition. Heating and cooling cycles
were precise as to $\pm$0.2°C. Precise melting point data in the Fe-B system
were collected from the $Fe_{50}B_{50}$- and $Fe_{35}B_{65}$-compositions. 10g-samples were
first remelted a few times to ensure homogeneity. At this stage of the
project a HF-furnace was used and power was controlled manually. There was
excellent agreement between DTA and 3-colour pyrometry T_E(FeB,ß)= 1450$\pm$2°C
(Pyr.) against 1452$\pm$3°C (DTA). Both values are lower than the values
assessed in literature (1497°C, ref.(14)). The melting point of congruent
melting FeB was observed at T_m(FeB)= 1588$\pm$5°C; again this value is quite
different from those experimentally observed earlier but is close to their
average of 1590°C as estimated by (14). These two values were used as fixed
points in our thermodynamic modelling of the Fe-B phase diagram; see
also Part I.C.1.

END

FILMED

1-86

DTIC